Review

Not peer-reviewed version

Unmanned Aerial Geophysical Remote Sensing: A Survey

Farzaneh Dadrass Javan *, Farhad Samadzadegan, Ahmad Toosi, Mark van der Meijde

Posted Date: 1 November 2024

doi: 10.20944/preprints202411.0058.v1

Keywords: Geophysical survey; Remote sensing; Unmanned Aerial Vehicle; Magnetometry; Gravimetry; Ground penetrating radar; Electromagnetic survey; Spectrometry and radiometry; LiDAR; UAV photogrammetry.

Review

Unmanned Aerial Geophysical Remote Sensing: A Survey

Farzaneh Dadrass Javan [1,*], Farhad Samadzadegan [2], Ahmad Toosi [2] and Mark van der Meijde [1]

[1] University of Twente, The Netherlands
[2] University of Tehran, Iran
* Correspondence: f.dadrassjavan@utwente.nl

Abstract: Geophysical surveys, a conventional means of analyzing the Earth and its environs, have traditionally relied on ground-based methodologies. However, up-to-date approaches encompass remote sensing (RS) techniques, employing both spaceborne and airborne platforms. The emergence of Unmanned Aerial Vehicles (UAVs) has notably catalyzed interest in UAV-borne geophysical RS. This study comprehensively reviews the state-of-the-art UAV-based geophysical methods, encompassing magnetometry, gravimetry, gamma-ray spectrometry/radiometry, electromagnetic (EM) surveys, ground penetrating radar (GPR), traditional UAV RS methods (i.e., photogrammetry and LiDARgrammetry), and integrated approaches. Each method is scrutinized concerning essential aspects such as sensors, platforms, challenges, applications, etc. Drawing upon an extensive review of over 435 scholarly works, our analysis reveals the versatility of these systems, ranging from geophysical development to applications over various geoscientific domains. The reviewed studies unanimously highlight the advantages of UAV RS in geophysical surveys. UAV geophysical RS effectively balances the benefits of ground-based and traditional RS methods regarding cost, resolution, accuracy, and other factors. Integrating multiple sensors on a single platform and fusion of multi-source data enhance efficiency in geoscientific analysis. However, implementing geophysical methods on UAVs poses challenges, prompting ongoing research and development efforts worldwide to find optimal solutions from both hardware and software perspectives.

Keywords: Geophysical survey; Remote sensing; Unmanned Aerial Vehicle; Magnetometry; Gravimetry; Ground penetrating radar; Electromagnetic survey; Spectrometry and radiometry; LiDAR; UAV photogrammetry

---

1. Introduction

Geoscience, which is also referred to as Earth science, includes a wide array of natural sciences focused on studying the Earth [1]. These fields include geophysics, geology, geodesy, geography, and others [2–5]. Within geoscience, geophysics specifically investigates the physical phenomena and characteristics of Earth and its surrounding spatial environment. It combines the fields of geology, physics, and mathematics in a single approach. It uses quantitative methods to analyze these phenomena. In essence, geophysics offers a means to describe various aspects of the subsurface environment, such as composition and structure thereby providing information on, e.g., objects, geological features, groundwater conditions, or pollution levels, through non-invasive techniques [6]. The term "non-invasive" indicates that these methods do not damage the Earth's crust due to drilling or excavation. Geophysical methods include, among others, magnetic survey (magnetometry) [7], gravity survey (gravimetry) [8], electromagnetic (EM) survey [9,10], gamma-ray spectrometry (GRS)/radiometry [11], ground penetrating radar (GPR) [12], seismic tomography [13], electrical resistivity tomography (ERT) [14], and others.

Geophysical methods fall into two main categories: traditional close-range methods and modern remote sensing (RS)-based methods [15–17]. Close-range methods involve surveys conducted with equipment positioned as close to the Earth's surface as possible, covering both terrestrial and aquatic

 doi:10.20944/preprints202411.0058.v1

environments. On the other hand, RS-based techniques utilize platforms and instruments situated at a considerable distance from the Earth's surface [16,18]. These RS-based methods can be either spaceborne, employing satellites as platforms, or airborne, utilizing various manned and unmanned aerial platforms.

The increasing popularity of Unmanned Aerial Vehicles (UAVs) in the last decade, along with ongoing efforts by universities and industries to develop UAV-compatible devices and payloads, has profoundly impacted geophysics [19]. UAVs offer several advantages for geophysical surveys, including cost-effectiveness, ability to cover larger areas, lightweight design for easy transport, autonomous flying capability (which eliminates potential risks for onboard pilots in manned aircraft), and low-flying capability, all among its favorable features. These characteristics establish UAV-borne geophysical survey methods as a balanced compromise between traditional airborne and ground-based approaches, effectively combining the strengths of both methods simultaneously.

An extensive examination of literature concerning UAV-based geophysical methods, drawing from both scholarly research and corporate endeavors, reveals that these methods encompass traditional manned airborne techniques and introduce innovative additions such as seismic surveys [20,21]. This evolution has led to the development of UAV-based magnetometry [22], gravimetry [23], EM surveys [10], GPR [24], gamma-ray spectrometry/radiometry [25], as well as seismic surveys [26]. In addition to these basic geophysical methods, UAV photogrammetry [27] and LiDARgrammetry [28], while not traditionally considered geophysical techniques, hold applicability across various geoscientific domains [29,30].

The growing trend of UAV-based geophysical surveys in recent years and the increasing volume of research and papers published annually highlight a gap for a comprehensive review of UAV-based geophysical surveys. Existing research tends to focus on specific aspects of UAV-based geophysical surveys, as exemplified by the works of [22,24], which review UAV-based magnetometry or GPR, respectively. However, a comprehensive review paper, similar to a handbook, covering all feasible UAV-based geophysical survey methods remains needed. To address this gap, we aim to thoroughly review all methods feasibly developed for geophysical (or other geoscientific) surveys using UAVs.

To the best of our knowledge, no prior work has comprehensively compiled and reviewed all the methods mentioned. Thus, the novelty of our work is in collecting all standard UAV-based geophysical methods and providing new insights into methods that may initially not be recognized as geophysical techniques but can be applied effectively in this domain.

2. Research Methodology

A comprehensive search across different databases and sources has been done to address our research objectives. Our search comprises two methods: systematic querying in Scopus and manual search in Google Scholar, ResearchGate, etc. Although it is challenging to determine the definitive superior database for scientometrics, Scopus has been chosen as the foundation for our systematic querying. This decision is based on previous studies that have analyzed bibliometric bases, including [31,32].

Initially, relevant and similar terms were selected in an automated search strategy, and a query was made in Scopus using the filtering possibilities available there. The query for keyword search was as follows: TITLE-ABS-KEY (uav AND geophysics) OR TITLE-ABS-KEY (uav AND magnetic AND survey) OR TITLE-ABS-KEY (uav AND gravity AND survey) OR TITLE-ABS-KEY (uav AND ground AND penetrating AND radar) OR TITLE-ABS-KEY (uav AND gamma AND spectrometry) OR TITLE-ABS-KEY (uav AND gamma AND radiometry) OR TITLE-ABS-KEY (uav AND electromagnetic AND survey). Various word forms were examined and compared to ensure no significant articles were missed in our collection. For instance, in some cases, along with the commonly used term "UAV", terms like "unmanned aerial vehicle" or "drone" were also used.

In addition to the automated query, a manual searching approach was also employed in the other resources above to address any deficits in studies that might not have been identified in the automated search. These deficits primarily pertain to UAV-borne RS methods such as photogrammetry and LiDARgrammetry, which are not typically considered geophysical methods and may not be easily identified through automated searches[1]. Relevant studies in manual searches were finalized by reading the papers' text. Various word forms were examined to ensure that no significant documents were lost. The joint search returned a total of 587 studies, characterized by the word cloud shown in Figure 1. The word cloud offers a visual representation of the interdisciplinary nature of UAV-borne geophysical RS, bridging concepts from both the geoscience discipline and RS technology. The words presented in the cloud provide insight into the research landscape and the various themes explored within this field.

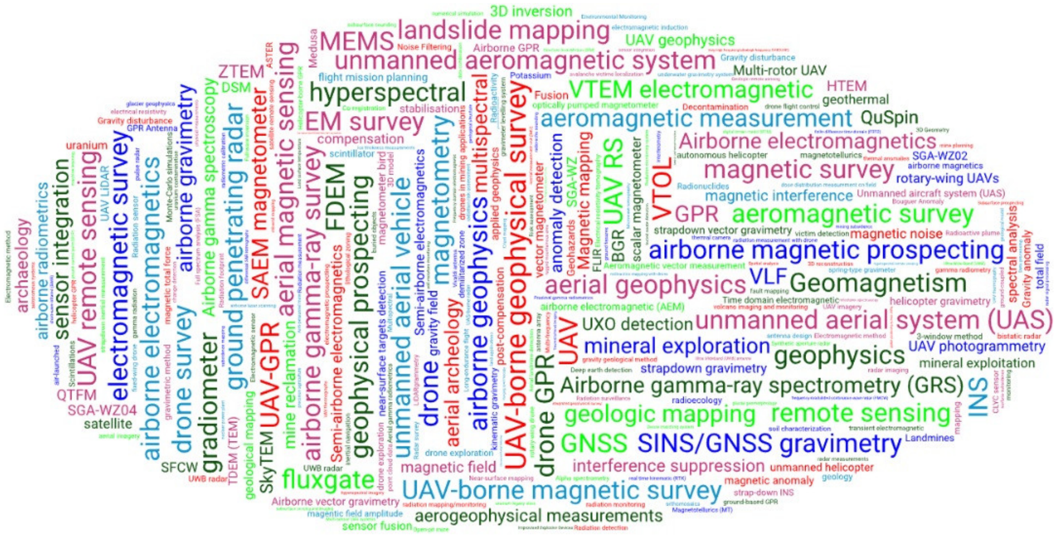

Figure 1. Word cloud presenting the keywords in the domain of UAV-borne geophysical RS (the words were collected from the "Keywords" section of each scientific article).

Moreover, an overview of the gathered publications is presented in Figure 2. There is an increase in publications (Figure 2a). This emerging topic is mainly developing through articles in journals and presentations at conferences, with no dedicated books yet available (Figure 2b). The impact of this topic extends across various disciplines, including computer science and environmental science (Figure 2c). Figure 2d illustrates that both developed and developing countries have begun to delve into the domain of UAV-borne geophysical RS, indicating its widespread relevance. Notably, universities and research centers, predominantly from developed countries, are leading in this field (Figure 2e). Furthermore, Figure 2f reveals that research is published in various journals, ranging from geosciences to RS technology, underscoring the interdisciplinary nature of this topic. Following the PRISMA flowchart [33] In Figure 3, the gathered documents were refined (containing three steps: identification, screening, and eligibility). Ultimately, 435 papers were considered eligible for review.

[1] We refer to geoscientific studies such as soil mapping, crust deformation mapping/monitoring, and similar applications.

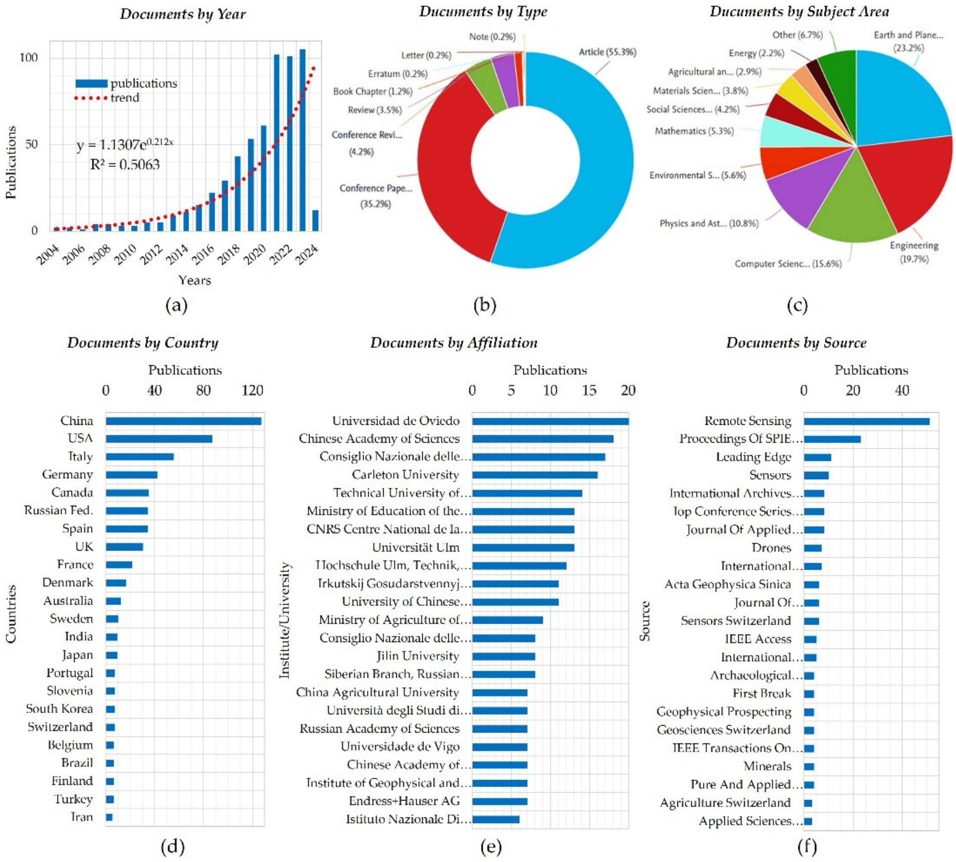

Figure 2. A review of the collected publications by (**a**) year (**b**) type, (**c**) subject area, (**d**) country (first author), (**e**) affiliation (first author), and (**f**) source.

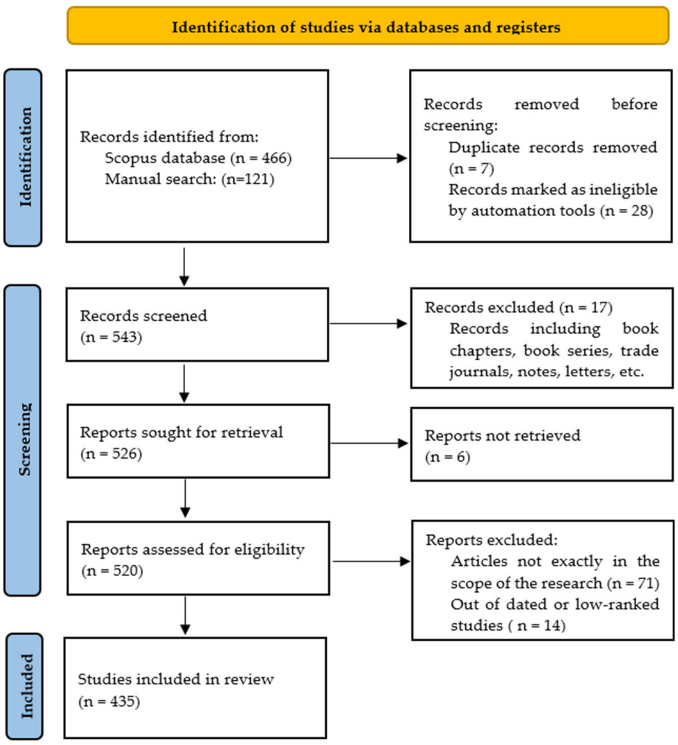

Figure 3. Refinement of studies based on the PRISMA workflow.

Preprints.org (www.preprints.org) | NOT PEER-REVIEWED | Posted: 1 November 2024 doi:10.20944/preprints202411.0058.v1

3. UAV-Borne Geophysical Survey Methods

Geophysical methods are classified into two primary categories based on sensor operation: those employing passive sensors and those using active sensors. For detailed information on passive and active sensors and their operation, refer to [34]. Additionally, a third category considers methods that integrate sensors and fuse data. Figure 4 illustrates this categorization. Note that "active/passive methods" indicate whether the method utilizes an active or passive sensor.

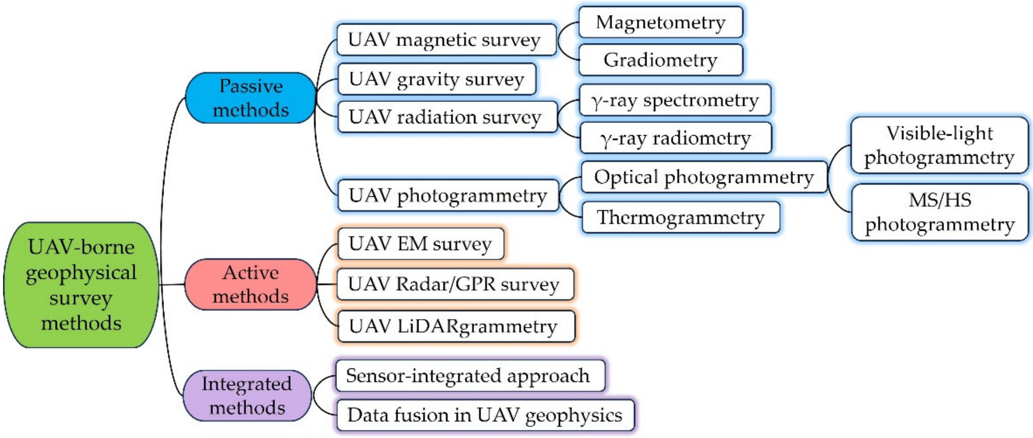

Figure 4. Categorization of geophysical methods applicable to UAVs.

3.1. UAV-Borne Geophysical Survey: Passive Methods

3.1.1. Unmanned Aerial Magnetometry

The introduction of UAVs in geophysics, especially in airborne magnetometry, has driven notable global academic and technological progress [35]. UAV-borne magnetometry offers safety, cost-efficiency [22], and prolonged flight endurance, facilitating low-altitude flights and high-resolution magnetic data collection [36–38], compared to traditional ground-based or airborne surveys using a low-flying airplane. There is a noticeable trend towards the adoption of UAV-borne magnetometry, with universities and companies actively engaging in pioneering research [39].

Reliable surveying systems on lightweight UAV platforms address the limitations of traditional terrestrial and aerial magnetometry [22,40]. These systems efficiently collect high-quality magnetic data, enhancing spatial resolution at low altitudes [41]. They extend operations to previously inaccessible areas, reducing costs and offering flexibility [42,43]. UAV-based surveys bridge the gap between terrestrial and airborne methods, enhancing detectability [44]. Challenges include ensuring data quality comparable to manned aerial systems and developing lightweight magnetometers for small UAV platforms. Figure 5 depicts a UAV-based magnetometer system, with subsystems detailed in [22].

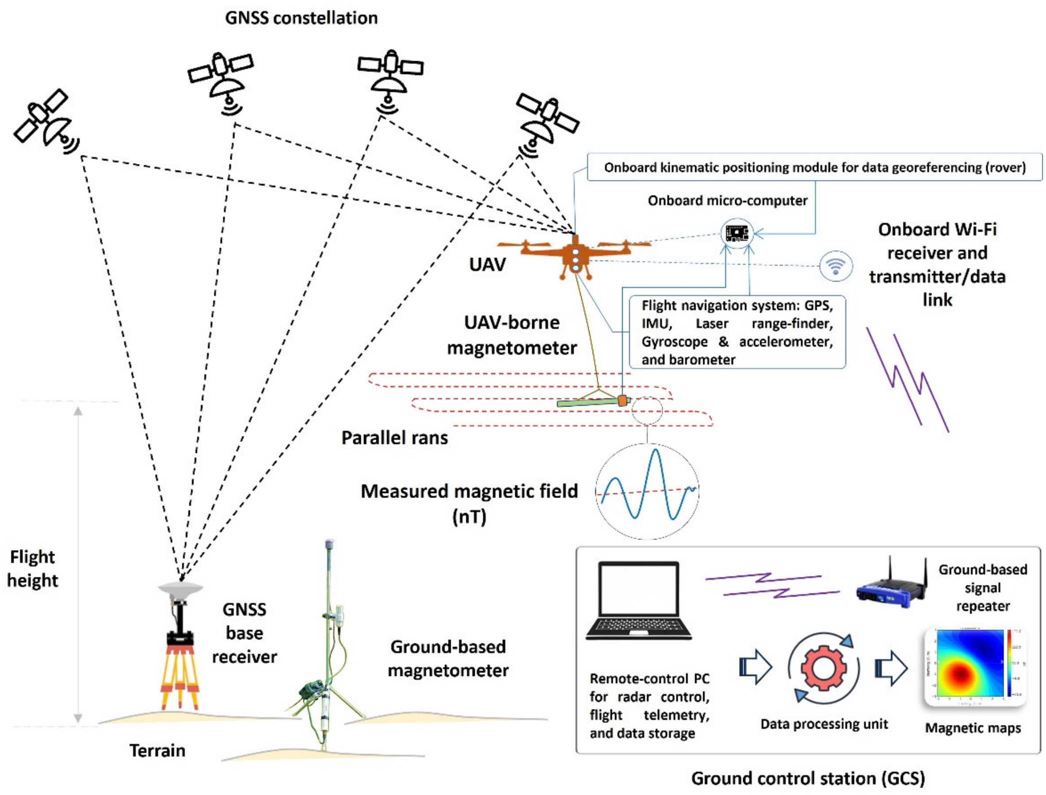

Figure 5. UAV-borne magnetometry system[2].

Different manufacturers offer a variety of magnetic sensors (magnetometers) compatible with UAVs [41]. Table 1 overviews the most widely available cutting-edge options, with confirmed quality and reliability.

Table 1. Review of the cutting-edge UAV-compatible magnetometers (building on [22]).

Spc. / Mag.	GSMP-35U/25U	MFAM	QTFM	MG01	G823A
Figure		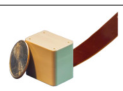			
Type	Potassium vapor	Caesium vapor	Rubidium vapor	3-axis solid state	Cesium vapor
Manufacturer	Gemsystems (GEM)	Geometrics	QuSpin Ltd.	UAV Navigatio n	Geometrics
Sensitivity	0.0002/0.022 nT @ 1 Hz	7 nT @ 1 Hz	1 nT @ 1 Hz	-	0.0004 nT @ 1 Hz
Resolution/Accurac y	0.0001 nT/± 0.1 nT	0.0001 nT	-	27 µG/±1 G	-
Heading Error	± 0.05 nT	± 7.5 nT	± 1.5 nT	-	± 0.15 nT

[2] A ground-based magnetometer is typically used in extended aerial operations where the diurnal variations of the Earth's magnetic field are significant. The data from this base station is essential for modeling these variations and correcting the data captured by the aerial method.

Preprints.org (www.preprints.org) | NOT PEER-REVIEWED | Posted: 1 November 2024 doi:10.20944/preprints202411.0058.v1

Dynamic Range	15,000 to 120,000 nT	20,000 to 100,000 nT	1,000 to 100,000 nT	±2 G	-
Gradient Tolerance	50,000 nT/m	-	10,000 nT/m	-	500 nT/in
Sampling Intervals	1, 2, 5, 10, 20 Hz	1,000 Hz	400 Hz	5,000 Hz	20 Hz
Temperature Operating Range	-40 to +55 °C	-35 to +50 °C	-30 to +60 °C	-40 to+85 °C	-35 to +50 °C
Power Consumption	12 W	1-2 W	2 W	0.5 W	24-32 W
Head/Control box dimension	16.1×6.4/23.6×5.6×3.9 cm	3.3×2.5×3.2/12×5.2×2.2 cm	1.9×1.9×4.7/1.9×3.5×8.9 cm	-	6×14.6/51×51×53 cm
Weight	1 kg	0.23 kg	0.15 kg	0.15 kg	14 kg

Table 2 presents an examination of diverse cutting-edge UAV-borne magnetometry systems currently accessible worldwide, including both commercial options and those developed through scientific research and development (R&D).

Table 2. Review of UAV-borne magnetometry systems.

Sys.	**Manufacturer**	**Platform Type**	**Magnetometer**	**Specifications**	**References**
AirBird/ GradBird	Geosystems (GEM)	Suitable for rotary-wing drone	Single/double sensor GSMP-35U/25U	Weight: 3.5 kg; Speed: > 10 m/s; Endurance: 1.5 h; Tow cable length: 10 m; Sensor shell: fiberglass; Components: GPS, IMU, laser altimeter, data acquisition module, etc.	[45]
MagArrow	Geometrics	Any enterprise UAVs	Two MFAM sensors	Weight: > 2 kg; Speed: 10 m/s; Endurance: 2 h; Positioning: from UAV's GNSS; Sensor shell: carbon fiber; Components: GPS, IMU, etc.; Sampling rate: every 1 cm.	[46]
MagDrone	Geometrics	Theolog Tho-R-PX8-12 octocopter	MFAM and fluxgate	Weight: 10 kg; Speed: 40 km/h; Endurance: 25 min; Positioning: onboard GPS; Sensor shell: fiberglass; Payload: 4.5 kg.	[41,47]
MG-1P	DJI, Lab of EM Radiation, and Sensing Tech.	Rotary-wing (octocopter) MG-1P	Cesium OPM (CAS-18-VL)	Total/take-off weights: 9.8/13.7 kg; Endurance: 20 min; Speed: 7 m/s; Payload: 10kg; Outline dimension: 1.4×1.4×0.5 m.	[48]
CMAGTRES-S100	DJI	DJI M210 and Wind-4 rotary wing drones	Optically pumped scalar magnetometer	Weight: 6-7 kg; Survey speed: ~14 m/s; Sensor type: scalar total-field; Sampling rate: 10-20 Hz.	[41]

Geoscan-401	Geo Matching	Rotary-wing (quadcopter)	Quantum magnetometer	Speed: 50 km/h; Endurance: 40 min with a 2.5 kg load.	[49]
Tholeg tho-R-PX-12	Tholeg	Rotary-wing (octocopter)	Fluxgate	Endurance: 25 min with a 4.5 kg load; Max speed: 40 km/h.	[47]
3DR X8+	Not specified	Rotary-wing (octocopter)	Fluxgate	Weight: 2.56 kg; Endurance: 15 min with a 1 kg load; Max speed: 90 km/h.	[50]
S1000	DJI	Rotary-wing (multi-rotor)	Overhauser	Endurance: 20 min with a 2 kg load; Max speed: 64.8 km/h.	[51]
Matrice 600	DJI	Rotary-wing (multi-rotor)	MFAM	Endurance: 18 min with a 5.5 kg load; Max speed: 64.8 km/h.	[52]
Heavyweight	Not specified	Rotary-wing (hexacopter)	MMPOS-1 Quantum magnetometer	Take-off weight: 15 kg; Speed: 7-10 m/s.	[53]
Skylance 6200	Stratus Aeronautics	Rotary-wing (octocopter)	Cesium vapor magnetometer	Endurance: 30 min with a 5 kg load; Cruise speed: 37 km/h.	[54,55]
UAV-Mag	Pioneer Exploration	Rotary-wing (quadcopter)	GEM GSMP35-A	Sensitivity: 0.3 pT@1Hz; Resolution: 0.0001 nT; Accuracy: ± 0.1 nT; Sampling rate: 20 Hz.	[56]
IT180-120	Sterna	Mini multirotor	Not specified	Engine type: gasoline power	[57]
MD4-1000	Microdrones, Germany	Rotary-wing (quadcopter)	Fluxgate	Length: 1.03 m; Payload capacity: 1.2 kg; Endurance: 1 h with a 1 kg load.	[58]
Single/Dual Mag	Mobile Geophysical Technology (MGT)	Multi-rotor (hexacopter)	Fluxgate magnetometers	Endurance: 20 (15) min with Single (Dual) Mag Payloads; Speed: 15 m/s; Resolution: 10 pT; Sampling rate: 1, 10, 50, 100 Hz.	[59]
Wind 4 and Spreading Wings S900	DJI	Multi-rotor (hexacopter)	Potassium vapor magnetometer	Total weight: 3.3 kg; Endurance: 5-7 min with a 2 kg load; Speed: 57.6 m/s.	[60]
MG-1P	DJI	Multi-rotor (octacopter)	CAS-L3 Cesium OPM	Endurance: 20 min; Speed: ~43 km/h; Sensitivity: 0.6 pTrmsp $Hz^{0.5}$@1 Hz.	[40]
MAG-DN20G4	Zhejiang Danian Tech. Co.	Multi-rotor	Fluxgate	Endurance: 25 min with a 7 kg load; Speed: 28.8 km/h.	[61]
UMT Cicada	Not specified	Multi-rotor (hexacopter)	Geometrics MFAM	Endurance: 1 h with a 2.5 kg load; Engine type: hybrid gas-electric.	[62,63]

Preprints.org (www.preprints.org) | NOT PEER-REVIEWED | Posted: 1 November 2024 doi:10.20944/preprints202411.0058.v1

Matrice M210	DJI	Multi-rotor (quadcopter)	Fluxgate	Endurance: 27 min; Platform weight: 2.3 kg; Payload weight: 0.484 kg; Speed: 61.2 km/h.	[64]
FY680	Tarot company	Multi-rotor (hexacopter)	Magneto-inductive magnetometer	Platform weight: 0.6 kg; Endurance: 30 min; Speed: ~47 km/h; Type: carbon-fiber.	[35]
Mavic Pro2	DJI	Mini multi-rotor (quadcopter)	Geometrics QTFM	Endurance: 31 min; Speed: 72 km/h.	[65]
Phantom 4	DJI	Quadcopter	Fluxgate	Endurance: 28 min; Speed: 72 km/h.	[66]
GJI S900	Queen's University	Multi-rotor	GSMP-35U	Endurance: 18 min; Payload: 2.2 kg.	[67]
GeoRanger	Fugro/CGG, the Netherland	Fixed-wing (GeoRangerTM)	Cesium vapor magnetometer	Endurance: 15 h; Cruise speed: 75 km/h; Max payload: 5.4 kg.	[22,54,68]
AeroVision	Abitibi Geophysics and GEM Systems	Fixed-wing (AeroVision)	Cesium vapor magnetometer	Endurance: 10 h; Cruise speed: 120 km/h; Max payload: 8.2 kg.	[54,69]
Venturer	Stratus Aeronautics Inc.	Fixed-wing (Venturer)	Fluxgate and two Geometrics G-823A cesium vapor magnetometers	Endurance: 9-10 h; Speed: 95 km/h; Sensor shell: carbon fiber & fiberglass; Engine: gasoline-powered; Components: IMU, DGPS, altimeter, autopilot, etc.; Payload: 8.2 kg.	[54]
ScanEagle	Insitu & Boeing	Fixed-wing drone	OP magnetometer	Weight: 12 kg; Wingspan: 3.1 m; Length: 1.2; Engine: fuel-based; Endurance: ~22 h; Components: GPS, gyros, accelerometers, magnetometer, etc.	[70]
Ant-Plane series	Not specified	Ant-Plane 1, 2, 3, 3-2, 3-4, 4-1, 5, 6-3 fixed wings	Magneto-resistant magnetometer	Endurance: 1.5-10 h; Cruise speed: 70-150 km/h; Payloads: 0.8-2 kg.	[71,72]
Prion	Magsurvey, UK	Fixed wing	G822 cesium vapor	Cruise speed: 90 km/h; Payload: 9 kg.	[73]
GeoSurv II	Sander Geophysics & Carleton University	Fixed-wing	Cesium G822A and fluxgate magnetometers	Endurance: 8 h; Cruise speed: 111 km/h; Payload: 9.1 kg.	[36]
SIERRA	NASA	Fixed-wing	Cesium vapor sensor	Endurance: 8 h; Speed: 117 km/h; Payload: ~28 kg.	[74]

Preprints.org (www.preprints.org) | NOT PEER-REVIEWED | Posted: 1 November 2024 doi:10.20944/preprints202411.0058.v1

Cai Hong-3 (CH-3)	IGGE & CAAA*	Fixed-wing	CS-VL cesium vapor sensor	Endurance: 10 h; Cruise speed: 180 km/h; Payload: 145 kg.	[75]
Albatros VT2	Radai Oy, Finland	Radai Albatros VT fixed wing	Fluxgate	Take-off weight: 5 kg; Endurance: 3 h; Speed: 50-110 km/h; Resolution: 0.5 nT; Sampling range: ± 10^5 nT; Engine: electric-1000 W; Payload: 2 kg.	[47,76,77]
Cai Hong-4 (CH-4)	Chinese CAAA	Fixed-wing	Cesium fluxgate sensor	Endurance: 12 h; Cruise speed: 150 km/h; Payload: 345 kg.	[78]
MONARCH	GEM Systems	CTOL/VTOL fixed-wing	GSMP-35U/25U potassium magneto/gradio-meters	Endurance: 1.5-hour range with 70 km/h cruise speed; Cruise speed: 70 km/h; Payloads: 4 kg.	[79]
Skywalker X8	Skywalker	VTOL fixed-wing	3-axis Fluxgate (FGM3D100 sensor)	Weight of magnetometer: 0.18 kg; Endurance: 25 min; Air speed: 65-70 km/h; Max flying altitude: 200 m; Sampling rate: 10-20 Hz.	[80]
Brican TD100	Brican	VTOL fixed-wing	MAD-XR sensor unit (a 3-axis vector and three scalar magnetometers)	Engine type: electric motor; Max payload: 8.2 kg; Max flight altitude: 91 m.	[81,82]
Nebula N1	Nebula UAV Systems	VTOL fixed-wing	Not specified	Cruise Speed: 50 km/h; Engine type: electric motor.	[81]
JOUAV CW-25E	JOUAV UAS	VTOL fixed-wing	Rubidium and Cesium OP magnetometers	Endurance: 4 h (240 km); Engine: electric motor; Cruise speed: 20 m/s; Payload: 4 kg.	[83]
RMAX-G1	Japanese Yamaha-Motor Co.	Unmanned helicopter	Cesium OPM	Endurance: 1.5 h; Max speed: 20 m/s; Max payload: 10 kg; Platform's total weight: 1.2 kg; Towing cable length: 4.5 m.	[84,85]
V750	Weifang Freesky Aviation Ind. Co.	Unmanned helicopter	Helium OPM and fluxgate magnetometers	Endurance: >4 h; Payload: 80 kg; Overall length: 6.6 m.	[86]
Z3	Nanjing Research Inst. on Simulation Technique	Unmanned helicopter	Helium OPM and fluxgate magnetometers	Payload weight: 25 kg; On-load endurance: ≥1.5 h; Overall length: 2.7 m.	[86]

Preprints.org (www.preprints.org) | NOT PEER-REVIEWED | Posted: 1 November 2024 doi:10.20944/preprints202411.0058.v1

Scout B1-100	Aeroscout, Switzerland	Unmanned helicopter	Fluxgate	Endurance: 1.5 h (with 10 liters of fuel); Max speed: 110 km/h; Payload: 18 kg.	[58,87]
GEM Hawk	GEM Systems	Unmanned helicopter	Potassium magnetometers (GEM Airbird)	Takeoff weight: 16.4 kg; Endurance: 50 min; Speed: 50 km/h; Payload: 4 kg; Resolution: 0.0001 nT; Sensitivity: 0.0003 nT@ 1 Hz.	[88]
AutoCopter (XL), Bergen, & RaptorCam	INEEL	Unmanned helicopter	G823A magnetometer	Endurances: 35, 30, and 20 min; Payloads: 6.8, 4.5, and 0.9 kg; Engine types: 120 cc Gas, 28 cc Gas, and 8cc Nitro.	[89]
Maxi-Joker	DJI	Unmanned helicopter	G823A magnetometer	Endurance: 15 min; Payload: 4 kg.	[90]
SICX-12 Mongoose	Not specified	Unmanned helicopter	G823A magnetometer	No information was released.	[90]
WH-110A	China	Unmanned helicopter	CS-VL cesium and fluxgate magnetometers	Endurance: 3 h; Speed: 60 km/h; Payload: 35 kg.	[91,92]
Unmanned flying object (UFO)-H	China	Unmanned helicopter	Cesium fluxgate magnetometer	Endurance: 180 min; Speed: 43 km/h; Payload: 35 kg.	[93]
SU-H2M	China	Unmanned helicopter	Potassium (GSMPc35U) and fluxgate (TFM100-G2) magnetometers	Endurance and battery life: 3 h; Speed: 60 km/h; Payload: 45 kg; Engine type: oil-powered.	[39]

In the domain of UAV magnetometry, one of the critical issues is EM interference. Mounting magnetic sensors on aerial vehicles poses challenges due to magnetic interference from propulsion and flight control systems. This interference originates from both the environment and onboard systems, diminishing sensor sensitivity and detection ranges [39,81,87,94]. Environmental factors include anything in the UAV's surroundings that impacts the magnetic survey, while onboard factors pertain to various UAV components with magnetic characteristics. Due to these magnetic components, UAVs may compromise the accuracy of total magnetic field measurements [60]. Advances in magnetometer technology enable increased use in small to medium UAVs, but miniature UAVs face challenges due to their compact size and shorter distances between interference sources and sensors [22,43,49,81]. Addressing magnetic interference is a paramount challenge in aerial magnetometry development [39,49,94–96]. This section explores solutions to counter magnetic interference, considering both active and passive approaches.

- *Active Solution:* Post-compensation addresses UAV magnetic interference [22,39,96], utilizing calibration flights to gather high-altitude data and calculate compensation coefficients using a model (Equation (1)) [97].

$$H_T = C_1 Cos\alpha + C_2 Cos\beta + C_3 Cos\gamma + H_G\{C_4 Cos^2\alpha + C_5 Cos\alpha Cos\beta + C_6 Cos\alpha Cos\gamma + C_7 Cos^2\beta + C_8 Cos\beta Cos\gamma + C_9 Cos^2\gamma\} + H_G\{C_{10} Cos\alpha (Cos\alpha)' + C_{11} Cos\alpha (Cos\beta)' + C_{12} Cos\alpha (Cos\gamma)' + C_{13} Cos\beta (Cos\alpha)' + C_{14} Cos\beta (Cos\beta)' + C_{15} Cos\beta (Cos\gamma)' + C_{16} Cos\gamma (Cos\alpha)' + C_{17} Cos\gamma (Cos\beta)' + C_{18} Cos\gamma (Cos\gamma)'\} = \sum_{i=1}^{18} C_i A_i \quad (1)$$

Preprints.org (www.preprints.org) | NOT PEER-REVIEWED | Posted: 1 November 2024 doi:10.20944/preprints202411.0058.v1

Where H_T is the total interference field intensity, and H_G represents the geomagnetic field. Cosα, cosβ, and cosγ are the directional cosines of the geomagnetic field vector with respect to the UAV's axes. Cj ($1 \leq j \leq 18$) are compensation coefficients aimed at mitigating magnetic interference effects.

Compensation coefficients (Cj) are estimated using magnetometer data (α, β, γ) through the least squares method according to Equation (2). These coefficients, along with the model, mitigate aircraft interferences during magnetic surveys.

$$C = (A^T A)^{-1} A^T H_{int} \qquad (2)$$

Where H_{int} and C are column vectors representing H_T and Cj, respectively, and A is the design matrix [22,39].

To evaluate compensation, the "improvement ratio" and the "fourth-difference" metrics are used [22,98]. Calibration flights correlate UAV maneuvers with magnetic field changes for compensation. Flight of maneuver data should mirror UAV behavior, ideally collected at high altitudes. Post-compensation is not suitable for low-altitude flights, especially for multi-rotor UAVs due to instability. Yet, during high-altitude operations, post-compensation can be applied with magnetometers placed away from the UAV's platform [22,39].

- *Passive Solution:* Post-compensation may not suffice for UAV magnetometry, necessitating an alternative approach by placing the magnetic sensor away from the aerial platform. Methods include suspending it beneath the UAV with a semi-rigid tether or affixing it to the UAV frame with a rigid bar. Various sensor attachment configurations are illustrated in Figure 6, accommodating different UAV types [41,99–101]. Placing the magnetometer away from the aerial platform can lead to sensor errors and fluctuations due to vibrations. Firmly affixing it to the airframe or using an extended boom may compromise flight stability, especially for fixed-wing UAVs [22,43,60,96,98]. Comparative studies suggest optimal sensor-platform distances of 3 to 5 meters to minimize interference [22,43,49,56,66,81,96,102]. For VTOL fixed-wing systems, mounting sensors at the winglets or nose-tip via a fixed-boom configuration is effective [80].

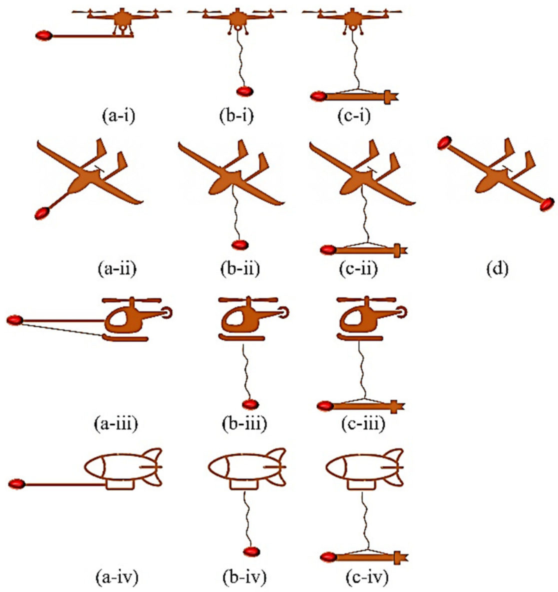

Figure 6. Different arrangements for mounting magnetometers on UAVs: (**a-i** to **a-iv**) fixed-boom design for rotary-wings, fixed-wings, helicopters, and airships, respectively; (**b-i** to **b-iv**) towed sensor design for the mentioned UAV types; (**c-i** to **c-iv**) towed bird design for the mentioned UAV types; and (**d**) fixed wing-tip design for fixed-wing UAV.

Table 3 presents a comprehensive compilation of studies conducted in the field of UAV-borne magnetometry, with a specific emphasis on applications.

Preprints.org (www.preprints.org) | NOT PEER-REVIEWED | Posted: 1 November 2024 doi:10.20944/preprints202411.0058.v1

Table 3. Review of UAV-borne magnetometry applications.

Application/Aim of Study	Platform Type	UAV Name/Model	Magnetic Sensor(s)	References
Offshore geophysical surveying	Fixed-wing	GeoRanger	Cesium vapor	[103]
Beach-shallow sea transition area magnetic surveying	Unmanned helicopter	Z3 and V750	Helium OPM and fluxgate	[86]
UAV magnetometry feasibility study	Unmanned helicopter	RMAX, AutoCopter, Bergen R/C, and RaptorCam	Geometrics G823A	[89]
Geomagnetic field variations mapping	Fixed-wing	GeoRanger	Cesium vapor	[104]
Volcanology using UAV magnetometry	Unmanned helicopter	RMAX-G1 (in [84,85])	Cesium OPM (in [84,85])	[84,85,105]
Volcanology (assessing geohazards associated with volcanic activity)	Multi-rotor	DJI Mavic 2	QTFM	[65]
UAV magnetometry for antarctic studies	Fixed-wing	The Ant-Plane generation (e.g., Ant-Plane 6-3)	Magneto-resistant and fluxgate	[71,72]
Geophysical fault mapping	Unmanned helicopter	Bell 206B3 helicopter	Cesium OPM	[106]
Geophysical exploration	Fixed-wing	SIERRA	Cesium vapor	[74]
Geophysical/archeological exploration and UXO/pipeline detection	Fixed-wing and multi-rotor	Single/Dual Mag	Fluxgate	MGT
Anti-submarine warfare system	Unmanned helicopter	MQ-8 Fire Scout and Brican TD100	Not specified	[81]
Integrated geophysical survey	Fixed-wing	CH-3	Cesium vapor	[75]
UAV magnetometry for general purpose	Fixed-wing	Venturer	Cesium vapor	[101]
UAV magnetometry for general purpose	Multi-rotor	3DR X8+	fluxgate	[50]
UAV magnetometry for general purpose	Unmanned helicopter	Scout B1-100	Fluxgate	[87]
UAV magnetometry for general purpose	Fixed-wing	GeoSurv II	Cesium vapor and fluxgate	[36,107,108]
UAV magnetometry for general purpose	Multi-rotor	Hexacopter	Fluxgate	[109]
Investigate mineral prospects, delineate UXOs, and survey archaeological sites	Fixed-wing UAV	The MONARCH	Potassium vapor	GEM Systems
Low-altitude geophysical magnetic prospecting	Multi-rotor	Heavyweight	Quantum Overhauser	[53]
Geophysical exploration	Unmanned helicopter	WH-110A and UFO-H	Cesium OPM and Fluxgate	[91–93]
Aeromagnetic survey and assessing the magnetization of a dipole	Multi-rotor	STERNA and IT180-120	Not specified	[110]
Gas and oil infrastructure mapping	Multi-rotor	Octocopter	Cesium and Rubidium vapor	[111]
Orphaned gas and oil wells locating	Multi-rotor	UMT Cicada and DJI Matrice 600	MFAM	[52,62,112,113]
Subsurface geophysical exploration	Multi-rotor	DJI Matrice 600 Pro	Fluxgate	[114]
Aeromagnetic mapping of regional scale	Multi-rotor	DJI M210	Fluxgate	[64]
Mapping geological and geophysical features of surface outcrops	Fixed-wing	Albatros VT2	Fluxgate	[47]
Flight safety test and data acquisition	Fixed-wing	CH-4	Fluxgate and Cesium vapor	[78]
Planetary exploration	Multi-rotor	DJI Matrice 600 Pro	Vector magnetometer	[115]
Archeological survey	Multi-rotor	DJI Phantom 4 and S1000+	Fluxgate and Cesium vapor	[66,116]
Mineral exploration/ minning applications	Multi-rotor	DJI S1000, S900, and Matrice 600 Pro	Overhauser and Potassium vapor (e.g., GSMP-35U)	[51,60,67,117]

Application/Aim of Study	Platform Type	UAV Name/Model	Magnetic Sensor(s)	References
Mineral exploration	Multi-rotor and fixed-wing	SkyLance, Venturer, and The Prion	Cesium vapor	[54,55,73]
Mineral exploration	Multi-rotor	Geoscan 401	Quantum magnetometer	[49]
Mineral exploration	Multi-rotor	Tholeg and MAG-DN20G4	Fluxgate	[47,61]
Mineral exploration	Unmanned helicopter	SU-H2M	Potassium OPM (GSMPc35U) and fluxgate (TFM100-G2)	[39]
Mineral exploration	Multi-rotor	FY680	Magneto-inductive	[35]
Mineral exploration	Multi-rotor	DJI M210	Scalar magnetometer	[118]
Mineral exploration	VTOL fixed-wing	Not specified	GSMP-35U Potassium, GSM-19 Overhauser	[119]
Mineral (Chromite) exploration	Multi-rotor	Pioneer UAV-MAG	Potassium vapor	[56,120]
Mineral (Gold) exploration	Multi-rotor	SkyLance 6200	Cesium vapor	[121]
Target detection and identification	Fixed-wing	GeoRanger	Not specified	[68]
Near-surface target detection	Multi-rotor	DJI MG-1P octocopter	Cesium OPM (CAS-18-VL)	[48]
Near-surface ferrous objects (e.g., ordnance) detection	Unmanned helicopter amd multi-rotor	Scout B1-100 and MD4-1000	Fluxgate	[58]
UXO detection	Unmanned helicopter	Maxi-Jocker and Mongoose	Geometrics G823A	[90]
UXO detection	Multi-rotor	DJI MG-1P	Cesium OPMs	[40]
UXO detection	Multi-rotor	An Octocopter	Fluxgate	[122]
UXO detection	Multi-rotor	DJI Wind 4 quadcopter	QTFM	[123]

3.1.2. Unmanned Aerial Gravimetry

Integrating UAV-borne gravity surveys with ground-based methods aids subsurface resource exploration, enhancing gravity field determination for diverse applications [124]. The UAV-based gravimetry system, depicted in Figure 7, includes a ground base station and an airborne gravimetry system. The ground base station comprises components like a ground control/command station (GCS), ground data transmission (GDT) station, and ground support equipment (GSE). The GCS facilitates real-time transmission of gravimeter data via satellite links. The airborne gravimetry system consists of an unmanned vehicle, UAV-compatible gravimeter, data-transferring computer, GNSS signal recorder, and uninterruptible power supply (UPS). The UAV, central to any unmanned aerial system (UAS), can take various forms, including airships, helicopters, fixed-wing, and multirotors, with no usage restrictions [23].

Two main operational modes of UAV-based gravimetry exist: continuous-flight and grasshopper (see Figure 8). Continuous-flight mode entails the drone collecting data while traversing an assigned area, ideal for large surveys such as those in the petrochemical industry. Challenges include distinguishing between platform and gravitational accelerations, often addressed using isolation platforms and gimbals. Grasshopper mode involves the UAV landing at specific points for data collection before taking off again. This mode, suitable for rotary-wing drones, collects data during stationary periods. Challenges in this mode include aligning the gravimeter's axis and sensitivity to angular errors. Grasshopper mode typically requires more time for gravimetry due to flight and landing [125]. Further details and comparisons are available in the cited reference. The successful integration of UAV-compatible gravimeters onto unmanned platforms for continuous-flight and grasshopper mode operations requires several auxiliary systems. These include isolation (self-leveling) platforms, gimbals, and differential GPS capabilities [125,126].

Preprints.org (www.preprints.org) | NOT PEER-REVIEWED | Posted: 1 November 2024 doi:10.20944/preprints202411.0058.v1

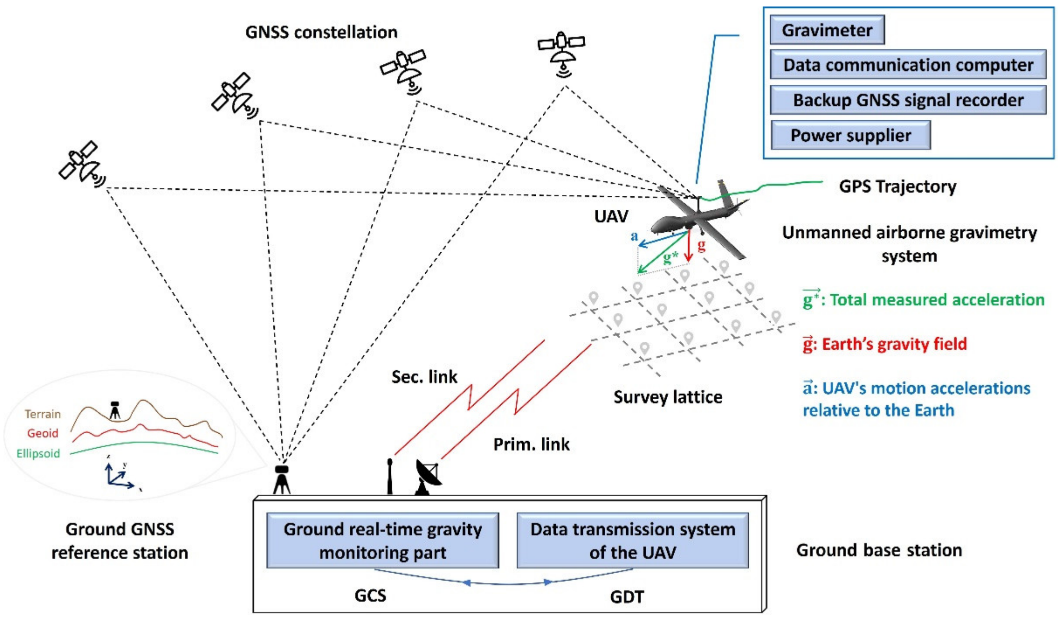

Figure 7. UAV-based gravimetry system (the scheme was depicted based on [23,127,128]).

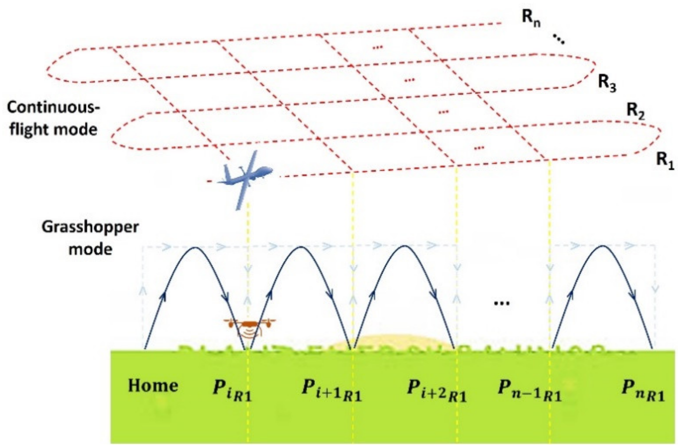

Figure 8. Operational modes in UAV-borne gravimetry (R: flight rans, P: sampling points).

Various corrections must be applied during gravity data collection, particularly in airborne gravimetry operations, including UAV-borne methods. These corrections include latitude correction, free-air (elevation) correction, Bouguer correction, topography (terrain) correction, Earth tides, Eötvös correction, and low-frequency translation correction, among others [23,129–131]. For brevity, readers seeking more detailed insights into these corrections are referred to the cited references.

This section provides a concise overview of gravity sensors compatible with UAVs. Miniature gravity sensors are designed for UAV integration, considering the payload capacity of UAVs. These sensors fall into two main categories: strapdown systems and Micro-Electro-Mechanical-Systems (MEMS) accelerometers. In strapdown configuration, a triad of accelerometers is directly affixed to the airborne vehicle. MEMS accelerometers offer a lightweight solution for UAV-based gravimetry. Triaxial MEMS devices have been successfully deployed in various UAV-based gravimetry operations. Table 4 lists advanced UAV-compatible gravimeters along with additional details. These are among the most widely available options, and their quality has been confirmed.

Table 4. Review of the cutting-edge UAV-compatible gravimeters.

Categories	Strapdown gravimeter			MEMS gravimeter				
Name/model	Light-weight iCorus	iMAR iNAV-RQH	Wee-g	Imperial College's MEMS-based devices	HUST's MEMS device	Silicon Micro Gravity	FG5-L	Scintrex RG1*
Figures			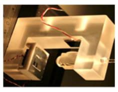			-		
References	[132–134]	[135]	[125,136–138]	[139]	[140]	[141,142]	[143,144]	[125,145]

* Despite being primarily designed for underwater operations, they can also be used in UAV gravimetry [125].

This section reviews the state-of-the-art UAV-borne gravimetry systems developed to date. Table 5 provides a comprehensive list of these advanced drone-deployed systems, along with relevant information for each.

Table 5. Review of state-of-the-art UAV-borne gravimetry systems.

Sys.	Manufacturer/Funder	Platform	Gravity Sensor	Specifications	Reference
1	Portuguese Ministry of Defence	CASA C212, Litton LN-200, and Crossbow AHRS440	Strapdown gravimeter	UAV power consumption: <3 W, Gravimetry system: Strapdown, Aim: developed for the PITVANT project.	[146]
2	Self-developed	Autonomous cruise-type unmanned helicopter	Not specified	Not specified	[147]
3	Geological Survey of Japan	Unmanned helicopter	Not specified	Not specified	[148]
4	Self-developed	Penguin-B miniature drone	Strapdown gravimeter	Engine: combustion, Wingspan: 3.3 m, Payload: 10 kg, Flight altitude: 4,500 m, Endurance: 20 h, Cruise speed: 120 m/s, Max range: 1,400 km.	[149]
5	University of Glasgow	A type of UAV	Miniaturized chip-based gravimeter	Not specified	[150]
6	Self-developed	VTOL unmanned helicopter	IMU iNAV RQH/RQT for coupled navigation, coupled with GNSS receiver.	Resolution: 0.5 km, Accuracy: 4-11 mGal, Navigation modes: DGPS and PPP, Syetem name: INS/DGNSS UAV gravimeter	[135,151]
7	National Oceanic and Atmospheric Administration (NOAA)	Aurora Centaur OPA fixed-wing UAV	Micro-g LaCoste TAGS-7 gravimeter	Control type: optionally piloted aircraft, endurance: 16 h at 25,000 ft.	[152]

Preprints.org (www.preprints.org) | NOT PEER-REVIEWED | Posted: 1 November 2024 doi:10.20944/preprints202411.0058.v1

Sys.	Manufacturer/Funder	Platform	Gravity Sensor	Specifications	Reference
8	Self-developed	Long-endurance Boreal drone	Gravimeter and GNSS antenna	Weight: 20 kg, Endurance: 10 h, Stabilization: robust to flight turbulent conditions	[153]
9	UK-funded project	Fixed-wing Prion Mk3	Not specified	Endurance: ~2h, Payload: 15kg, Cruising speed for surveying: 80 km/h, Note: BP proof of principle demonstrated its feasibility.	[154]
10	University of Glasgow	A drone with an isolation platform and active stabilization	Wee-g MEMs gravimeter	Not specified	[137]
11	National University of Defense Technology (NUDT), China	CH-4 medium-range fixed-wing UAV	SGA-WZ04 strapdown gravimeter	Endurance: 21 h, Range: 2,712 km, Gravimeter weight: < 50 kg, Max. takeoff weight: 1,330 kg, Gravimetry accuracy: > 0.6 mGal	[23]
12	Proje[158–160ct team: UAVE, DTU, and iMAR's joint UAV gravimetry system Sponsor: bp and New Resolution Geophysics (NRG)	The long-endurance Prion Mk3 fixed-wing UAV	iMAR's iCORUS SISG	Gravimeter weight: 6.8 kg, Endurance: 2.5 h, UAV Dimension (length×wingspan): 4×3 m	[134]
13	Self-developed	A type of UAV	Strapdown gravimeter	Max. accuracy: 0.47 mGal, Configuration: strapdown	[155]
14	The Russian Helicopters holding (the Rostec State Corporation)	The unmanned helicopter-type BAS-200	A modern 31 kg UAV-borne gravimeter	Payload: 50 kg, Endurance: 4 h, Flight altitude: 3,900 m, Dim.: 3.9×1.2 m, Range: 100 km.	[156,157]
15	EIT Raw Materials, Geological Survey of Finland, RADAI Oy, Technical University of Denmark, and Beak Consultants GmbH	Long-range fixed-wing drone	UAV-borne gravity and EM sensors	The system was used for Drone Geophysics and Self-Organizing Maps (DroneSOM) project	[158–160]

Table 6 offers a comprehensive examination of the literature on UAV-borne gravimetry, emphasizing its applications. In contrast to magnetometry, the range of applications is currently restricted due to the emerging status of the field, with most studies focused on system R&D.

Table 6. Review of UAV-borne gravimetry applications.

Aim of the study/Application	Platform	Gravity Sensor	Reference
System R&D: Assessment of affordable IMUs for UAV-based gravimetry to estimate gravity disturbances	UAVs developed within PITVANT and different regular aircraft (CASA C212, Litton LN-200, and Crossbow AHRS440)	Strapdown gravimeter	[146]
System R&D: Development of UAV gravimetry system	Unmanned helicopter	A type of drone-deployed gravimeter	[148]
System R&D: Developing a drone-borne gravimeter for geophysics surveying purposes	Not specified (any kind of drone can be utilized).	Miniaturized chip-based gravimeter	[150]
System R&D: Analyzing the performance of the UAV-based vector gravimetry system by surveying the gravity disturbance vector	Unmanned helicopter	A navigation grade IMU iNAV-RQH/RQT and a GNSS receiver	[151]
System R&D: Developing an INS/GNSS UAV-based vector gravimetry system	Unmanned helicopter	iMAR iNAV-RQH and NovAtel GNSS receiver	[135]
System R&D	Long-endurance Boreal drone	Gravimeter and GNSS antenna	[153]
System R&D: Developing a miniature UAV-borne gravimetry system	A drone with an isolation platform and active stabilization	Wee-g MEMs gravimeter	[137]
System R&D: Developing a UAV-borne gravimetry system	CH-4 medium-range fixed-wing UAV	SGA-WZ04 stap-down gravimeter	[23]
Datum definition: NOAA's Centaur program for conducting gravimetry across the US and redefining the American vertical datum (GRAV-D)	Aurora Centaur OPA fixed-wing UAV	Micro-g LaCoste TAGS-7 gravimeter	[152]
Proposal for 100 km line survey of gravimeter/gradiometer on drone-based platforms	Fixed-wing Prion Mk3	A type of UAV-compatible gravimeter	[154]
Earthquake study: Quick survey of gravity and magnetic data for earthquake ground motion prediction	Autonomous cruise-type unmanned helicopter	A type of UAV-compatible gravimeter	[147]
Mineral exploration	Any possible type of UAV in continuous flight and grasshopper modes	Any possible type of UAV-borne gravimeter	[125]
System R&D: Flying a SISG device on a fixed-wing UAV with suitable endurance, less cost, and less carbon for commercial gravity data surveys	The long-endurance Prion Mk3 fixed-wing UAV	iMAR's iCORUS strapdown inertial scalar gravimeter (SISG)	[134]
Error compensation based on the undulating flight in UAV gravimetry	A type of UAV	Strapdown gravimeter	[155]
Arctic research: Explorations of geophysics in the Arctic region, encompassing mineral, oil, and gas investigations.	The Russian unmanned helicopter-type BAS-200	A modern 31 kg UAV-borne gravimeter	[156,157]

Preprints.org (www.preprints.org) | NOT PEER-REVIEWED | Posted: 1 November 2024 doi:10.20944/preprints202411.0058.v1

Aim of the study/Application	Platform	Gravity Sensor	Reference
DroneSOM: Using commercially available drones for the acquisition of gravity and EM data, followed by data interpretation using integrated modeling software.	Long-range fixed-wing drone	UAV-borne gravity and EM sensors	[158–160]

3.1.3. Unmanned Aerial Gamma-ray Spectrometry and Radiometry

GRS geophysical technologies are challenging to integrate with drones due to their bulkiness and traditional design [161,162]. New UAV-compatible spectrometer systems, designed within drone weight constraints, and improved data processing methods, e.g., [163,164], show promise for enhanced survey efficiency and accessibility. This shift requires innovative equipment design and data analysis methods to maximize potential.

UAV-borne GRS feasibility relies on precise gamma-ray radiation measurement in low-altitude environments with limited air attenuation [165,166]. UAVs use gamma-ray spectrometers to map soil properties, texture, and contamination [167], advancing from proof-of-concept to common practice [168,169]. Radiation mapper UAVs carry payloads suitable for efficiently mapping radionuclide activities [170]. UAV GRS combines ground-based and traditional airborne methods, using UAVs for gamma radiation investigations at lower altitudes, minimizing risks and costs, especially in smaller survey areas [169,171,172]. Radiometric surveys by UAVs are more common than spectrometric surveys due to lightweight UAV constraints, limiting traditional GRS methods' effectiveness [171]. Ground-based GRS requires stops, while airborne GRS uses large-volume scintillation detectors for high-quality surveys [173]. Semiconductor detectors are expensive and less adopted compared to classical scintillation detectors, preferred for spectrometric measurements during movement [174–176]. Unmanned systems utilize heavy detection units with multiple crystals [171,174,175], impacting UAV flight time and range. Increasing UAV size is not cost-effective. Compact scintillation detectors offer economical and reliable data acquisition for geological mapping, ensuring high-quality outcomes in gamma-ray survey [171,175,177].

Let's examine how a UAV GRS system operates. In a UAV GRS system (Figure 9), the calibrated gamma-ray spectrometer is mounted beneath the UAV to measure radionuclide concentrations [167]. An onboard rover logs GNSS data for georeferencing, with corrections from a ground-based receiver improving accuracy. The spectrometer captures radiation spectra at each position, synchronized with location data and processed onboard [168,178]. Spectrometer data is transmitted to the GCS via RF systems like TETRA network, UMTS, and others [178–181]. Post-flight processing includes spectrum analysis for radiation heatmap generation [180]. The GCS software integrates radiation levels, coordinates, and altitude for visualization [181]. Measured radionuclide concentrations obtained from the spectrometer are used in application models, correlating them with soil properties or contaminants. Proper sensor calibration is crucial for accurate results, often achieved through laboratory analyses known as ground truthing [167,180]. During field operations, soil samples are collected. These samples undergo air-drying, milling, and sieving for clay and sand content analysis [169,182]. Lab testing includes radionuclide content, grain-size distribution, and clay fraction analysis, essential for application model development. Models can be developed based on as few as 14-20 soil samples, generating soil maps for various applications [167]. Expert analysis can further enrich the final map.

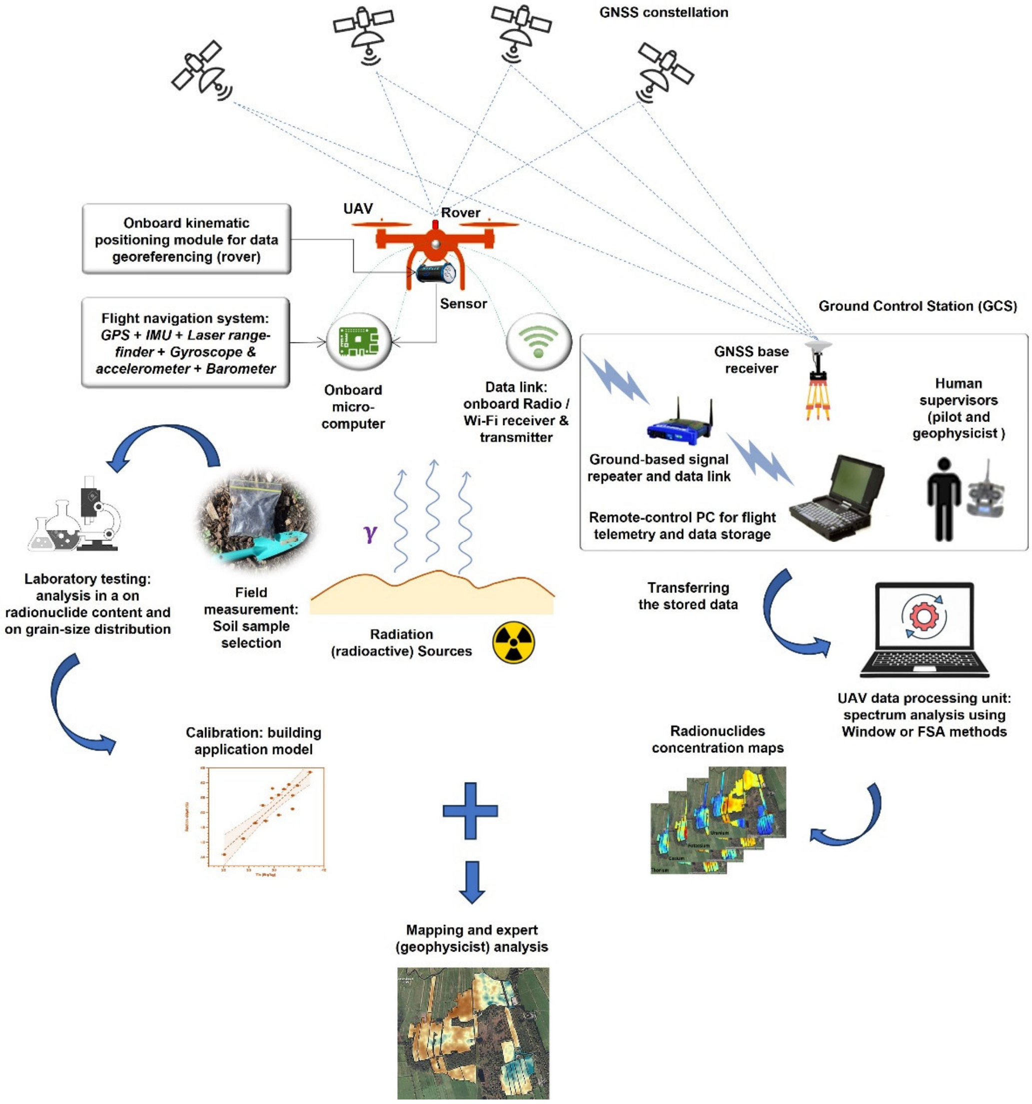

Figure 9. The manner a UAV GRS system operates (depicted based on the outputs of [161]).

In this section, spectral data processing is explored, specifically the methods for calculating radionuclide concentrations. Fundamental processing steps involve consolidating data from different detectors and filtering out points during UAV stationarity or survey line transitions [183]. Spectrum analysis techniques, such as the Windows method and Full Spectrum Analysis (FSA) procedure, are used to derive radionuclide concentrations from recorded spectra [161,170,184]. The Windows method extracts ^{40}K, ^{238}U, and ^{232}Th concentrations from specific energy windows [161,169]. In contrast, the FSA method, introduced in [185,186], utilizes nearly all spectral data, enhancing precision [161,184]. FSA fits “standard spectra” to acquired spectra, reflecting the detector’s response to pure radionuclide sources (^{40}K, ^{238}U, or ^{232}Th) [169,184]. Monte Carlo simulations and modeling generate standard spectra, a standardized practice detailed in references such as [163,169,187]. FSA reduces uncertainties by half compared to the Windows method, improving data quality [184]. It enables the use of smaller detectors while maintaining quality and provides richer count and spectrum structure [161].

In UAV-borne GRS, elevation impacts signal reception and footprint size. Higher altitudes reduce detected signal quantity due to increased air attenuation [163]. Elevating the spectrometer broadens the footprint, known as the “table lamp effect,” expanding the effective measured area [169,182]. Gamma-ray spectra conversion to radionuclide concentrations requires altitude correction for signal attenuation and detector field-of-view variations. Traditional corrections for airborne ranges may not suit UAV altitudes. Previous studies proposed corrections, but wide adoption was

Preprints.org (www.preprints.org) | NOT PEER-REVIEWED | Posted: 1 November 2024 doi:10.20944/preprints202411.0058.v1

lacking. Some surveys (e.g., [175,188–190]) used International Atomic Energy Agency (IAEA) corrections even at lower altitudes. In [169] the corrections was refined specifically for UAV GRS operational ranges (0-40 m) using experimental and computational methods, as detailed in the cited study. For more detailed insights of the commonly used footprint and height corrections applied in the domain of UAV-borne spectrometry and radiometery and also some innovative methods in this domain type refer to [169,180,191,192].

To provide an overview of UAV-compatible radiation sensors, it is important to note that several ready-to-use gamma-ray spectrometers have been tested and confirmed to be attachable to drones. These spectrometers are listed in Table 7. In Table 8, a thorough list of state-of-the-art UAV-borne GRS systems is provided, offering detailed technical specifications sourced from published papers.

Table 7. Review of the most widely available UAV-compatible gamma-ray spectrometers.

Radiation Sensors	Specifications	Figures	References
Medusa MS Spectrometer Series	Medusa Radiometrics provides UAV-ready gamma spectrometers, like the MS-1000 for real-time analysis, MS-2000-CsI-MTS for vehicle mounting, MS-4000 for airborne mapping, and MS-700 series for on-foot or drone-based applications. The MS-350 ultralight detector serves for small-scale UAV surveys and handheld use.		[163,169,182]
Georadis D230A Spectrometer	This spectrometer, suitable for drone-based applications, serves multiple fields including security, environmental monitoring, health protection, and exploration.		[175,183]
CeBr3 (and Twin NaI-CeBr3) Scintillation Detector	Medusa offers the CeBr3 scintillation detector for UAV applications, featuring a 3x6-inch crystal and 2,048 spectral channels. They also provide a twin NaI-CeBr3 scintillation detector, with a NaI detector boasting a 3x3-inch crystal and a CeBr3 detector featuring a 2x2-inch crystal.	-	[180]
CsI(Tl) detector	The Hamamatsu C12137-01 CsI(Tl) scintillator and CsI 6.5/100 cm³ device are designed for drone-mounted radiometric and spectrometric surveys.	Since the sensor is connected to other subsystems, readers are referred to the references for high-quality images.	[171,193,194]
Cadmium Zinc Telluride (CdZnTe or CZT) Semiconductor Detector and GR1/-A Kromek Spectrometer	The CZT semiconductor radiation detector integrates seamlessly with UAVs, offering lightweight and low-power operation. The GR1-A CZT module by Kromek, designed for UAVs like multicopters, features a compact 1 cm³ CZT crystal, providing discrete gamma spectra data. It operates with low power consumption (~250 mW) and covers an energy range of 30-3,000 KeV, ensuring versatile performance.		[168,172,194–196]

Cs2LiYCl6:Ce3+ (CLYC) Elpasolite scintillation sensor	A cylindrical CLYC sensor, measuring 2.54 cm × 2.54 cm, facilitated gamma-neutron sensing on a UAV platform. Emitting scintillation light in the 275-450 nm range, peaking at 370 nm, it boasted a 95% 6Li isotope enrichment and operated sans cooling. The setup comprised a customized housing, super bialkali photomultiplier tube, compact digitizer, and high-voltage generator.	Since the sensor is connected to other components, readers are referred to the references for a high-quality image.	[172,197,198]
Geiger-Müller Tube Particle Counter	Geiger-Müller tube detectors are commonly used for drone-mounted radiation detection due to their simplicity and compatibility with digital systems. Although they lack energy measurement capabilities and may miss radiation events at higher levels, they offer a solution for basic radiation detection tasks.	Since the sensor is mounted on a UAV, refer to the reference for a high-quality image.	[199]

Table 8. Review of the state-of-the-art UAV-borne GRS systems.

Sys.	Specifications	Objectives	Reference
1	*Platform:* APID One unmanned helicopter; Engine type: petrol-powered; Rotor diameter: 3.3 m, Weight: 130 kg; Max take-off weight: 210 kg; Payload: 25 kg; Endurance: 4 h. *Payload and sensors:* A suite of three gamma spectrometers, crafted by Medusa Radiometrics, comprises the MS-2000 Agri detector, MS-1000 UAV-borne detector, and MS-350 ultralight UAV detector, securely housed in a dedicated container. These detectors feature scintillation crystals of varying sizes—2000 ml CsI(Na), 1000 ml CsI(Tl), and 350 ml CsI(Tl), respectively. The survey system seamlessly integrates GPS, LiDAR, and a barometer within its navigation modules to ensure precise 3D positioning of the measurements.	System development: Enhancing the efficiency of UAV-borne gamma spectrometers for geophysical applications.	[169]
2	*Platform:* RMAX G1 unmanned helicopter; Weight: 94 kg; Payload: 10 kg; Max speed: 72 km/h *Payload and sensors:* The setup includes three 38.1×38.1 mm LaBr3:Ce scintillation detectors, forming the Aerial Radiation Measurement System (ARMS), weighing about 6.5 kg. It features a DGPS module and a Multi-Channel Analyzer (MCA) to process pulse signals within the 0 to 3,000 keV range across 1,024 channels.	Nuclear emergencies monitoring (the FDNPP case study).	[200]
3	*Platform:* SibGIS hexacopter; Flight speed during the survey: 5 m/s *Payload and sensors*: three types of payloads were used including a gamma spectrometer with a CsI(Tl) detector and with a superior crystal and PMT providing an energy resolution of 6% for ^{137}Cs mapping. The spectrometer has 8,096 ADC channels. The recording frequency of the spectra is 0.3 Hz.	Developing a triad of UAV-borne GRS-TDEM-Magnetic prospecting systems for geological mapping (blind ore deposits prospecting).	[201]

Preprints.org (www.preprints.org) | NOT PEER-REVIEWED | Posted: 1 November 2024 doi:10.20944/preprints202411.0058.v1

4	*Platform:* SibGIS UAS. *Payload and sensors:* Including three payloads: (**1**) A radiometer equipped with a CsI(Tl) crystal measuring 6.5 cm^3 and a silicon photomultiplier (SiPM), (**2**) A spectrometer featuring a CsI(Na) crystal measuring 30×150 mm and a Hamamatsu 6,095 photomultiplier, (**3**) A spectrometer equipped with a CsI(Tl) crystal measuring 40×80 mm and a SiPM, featuring a detector volume of approximately 100 cm^3.	Comparative analysis of gamma spectrometry and radiometry using compact detectors at various altitudes and ground levels.	[171]
5	*Platform:* DJI-S1000 octocopter *Payload and sensors:* CZT GR1-A Kromek and Cs2LiYCl6:Ce3+ radiation sensor for gamma and neutron detection, gas sensors, thermal imaging camera, LiDAR system, RTK GPS module, SONAR sensor, manipulator, sampling equipment, and radio transceiver.	Creating an integrated sensor for UASs dedicated to remote monitoring of gamma and neutron radiation.	[172,198]
6	*Platform:* A hexacopter (the Kingfisher model from Robodrone Industries). *Payload and Sensors:* Equipped with a 1,024-channel Georadis D230A gamma spectrometer, this setup uses two Bismuth Germanium Oxygen scintillation detectors with a volume of 103 cm^3.	Evaluation of the D230A for the detection and localization of uranium anomaly.	[175]
7	*Platform:* DJI Spreading Wings S1000+. *Payload and Sensors:* Compact Compton camera with a wide field of view fisheye lens. The camera includes scatterer and absorber layers, both featuring Ce:Gd3(Al,Ga)5O12 (Ce:GAGG) scintillator arrays optically coupled to a multi-pixel photon counter array.	Identification of nuclear disaster-related contamination in residential areas, exemplified by the Fukushima Daiichi NPP case.	[202]
8	*System's name:* Radai's UAV-based radiometric measurement system. *Platform:* A custom-designed quad-copter drone (Terrain Scout 3.2) *Payload and sensors:* Georadis D230A digital spectrometer equipped with two sets of 1,024 channels each for gamma radiation intensity measurement. Detectors include BGO and NAI/TI.	Using UAVs for radiometric surveys over the tailings of the deserted Rautuvaara iron mine to assess the feasibility of radiometric data collection.	[183]
9	*Platform:* A customized hexa-rotor aerial vehicle (Hexa XL, Mikrokopter) *Payload and sensors:* GR1 Kromek spectrometer, AR2500 LiDAR, and GPS module.	Creating a UAV-based system for rapid high-resolution evaluation of radionuclide contamination in radioactive incidents.	[168]
10	*Platforms:* Electric-powered multirotors such as Hexacopter V680, Quadcopter V650, Octocopter V1000, and Heavy Lift Quadcopter V690. *Payload and sensors:* The system incorporates detectors for beta radiation (electrons), gamma radiation (photons), and X-rays. Additionally, it features an air/gas sensor for collecting air quality data. Supplementary sensors include HD Video/DSLR/thermal cameras.	Monitoring NPP events/disasters using drones for radiation source detection and injured personnel location	[203]

Preprints.org (www.preprints.org) | NOT PEER-REVIEWED | Posted: 1 November 2024 doi:10.20944/preprints202411.0058.v1

	System description: A wireless radiation monitoring system, named Aretas Aerial-Live Actionable Data, has been developed with the capability to remotely detect beta (electrons), gamma (photons), and X-ray radiations.		
11	*System's name:* Radiation Monitoring System (RMS) *Platform:* DJI MATRICE–600 *Payload and sensors:* The system comprises various modular components, such as the RMS-000 communication and control module, the RMS-WASP communication software, and three distinct sensor modules: RMS-001, RMS-002, and RMS-003. RMS-001 is dedicated to online measurements of the effective dose rate of gamma and beta radiation, RMS-002 serves as the air sampler module, and RMS-003 functions as the GPS tracker.	Monitoring radiations in the proximity of an NPP or any area where ionizing radiation sources may exist.	[204]
12	*Platform:* A hexapod-type drone *Payload and sensors:* CdZnTe semiconductor detector and a video camera *System description:* The gamma monitoring system integrates a drone module and supplementary components attached to the drone. These modules incorporate lightweight radiation detection and position monitoring elements crafted to gather data on radiation levels along with the respective coordinates of the locations.	Environmental radionuclide surveillance	[181]
13	*Platform:* DJI M600 Pro UAV *Payload and sensors:* The instruments comprise the Medusa MS-1000 sensor, housing a 1-liter NaI scintillation crystal, and equipped with a GPS module.	Soil nuclide concentrations mapping	[182]
14	*System's name:* RotorRAD *Payload and sensors:* Specifications and technical attributes include a system mass of less than 15 kg, a dose rate range spanning 0.1 μSv/h to 100 mSv/h, gamma rays' energy coverage from 20 keV to 3 MeV, energy resolution below 7% at 662 keV, a flight endurance of approximately 30 minutes, a maximum transmission distance of 5 km, and an operational temperature range from -20 to 40 °C.	Swiftly locating lost radioactive sources	[205]
15	The team of developers installed gamma radiation and gas sensors on a custom-built robotic fixed-wing unmanned aircraft, named Chelidon, and on multirotors, known as Inspire drones.	Detection of gamma radiation and airborne pollutants in three dimensions.	[206]
16	*System's name:* AARM—stands for "autonomous airborne radiation mapping" *Platform:* WingtraOne Gen One COTS fixed-wing VTOL drone. *Payload and sensors:* The instrumentation comprises a Hamamatsu C12137-01 CsI(Tl) scintillator, a Kromek GR-1 CZT semiconductor detector with volumes of 1 cm^3 and 36.1 cm^3, respectively, alongside an SF11/C LiDAR, and a GNSS receiver.	Incorporating gamma spectrometry capability into the drone for the purpose of mapping legacy uranium mine sites.	[194]

17	*Platform:* The Penguin C fixed-wing UAV. *System description:* Communication between UAV and GCS is established through long-range data transferring using a tracking antenna, providing an impressive range of 100 km and a data transfer rate of 12 Mbps. The UAV operates within an altitude range of 120-5,000 m, maintaining a cruise speed between 19-22 m/s, and reaching a maximum speed of 32 m/s.	Radiological monitoring—to identify and quantify releases or contamination in scenarios involving gamma-emitting nuclides.	[166]
18	*System description:* The Patria mini-UAV stands as a versatile modular multi-mission airborne RS system, proficient in executing a spectrum of tasks ranging from reconnaissance to the surveillance of radiological, biological, chemical, and nuclear elements. *Unmanned systems configuration:* The configuration comprises one to three UAVs, each equipped with a range of payload options. Additionally, the system includes a communication suite, a GCS featuring a laptop PC, a telescopic antenna mast, launching equipment, and a dedicated sampling unit. *Payload and sensors:* Using a handheld radiation detection device featuring a cylindrical CsI probe with a volume of 5 cm^3, diameter of 13 mm, and length of 38 mm, complemented by a photodiode.	UAV-based remote radiation surveillance	[207]

Table 9 presents an overview of the applications of UAV-borne GRS derived from existing research in the field.

Table 9. Review of UAV-borne GRS applications.

Applications	Descriptions	References
Precise soil mapping (for precision farming and related topics)	Agricultural field properties, like clay content and grain size, were mapped using drone-borne GRS with MS-1000 spectrometers mounted on a DJI M600 PRO drone. Results closely matched ground measurements, demonstrating UAV GRS' effectiveness in predicting soil properties.	[161–163,169]
Soil texture and environmental contamination mapping	A DJI M600 multi-rotor drone with an MS-1000 mapping system assessed sediment contamination along Spittelwasser Creek floodplains. Results (Dioxin concentrations maps) informed basin-scale remediation decisions.	[161,167]
Contamination mapping and monitoring at critical sites—mapping mine tailings	A drone-mounted MS-1000 system mapped an inaccessible mine tailing area, replacing expensive helicopter surveys. Flying at 15 meters, it identified a significant 238U hotspot above the tailings, challenging to detect with ground-based or higher-elevation helicopter surveys.	[162]
Contamination mapping and monitoring at critical sites— monitoring radioactive substances in industrial plants	UAV-borne GRS conducted at the Novellara landfill in Italy used a CdZnTe gamma detector to detect nuclear waste materials. Altitude trials confirmed no nuclear waste detection, with garbage shielding reducing background gamma radiation. The prototype's effectiveness in localizing dispersed nuclear materials was validated through laboratory and operational tests involving an intense 192Ir nuclear source and the landfill scenario.	[196]
Contamination mapping and monitoring at critical	A method for rapidly localizing lost radioactive sources was proposed using RotorRAD, a UAV-based radiation mapping/monitoring system. Upon	[205]

sites— locating lost radioactive sources	detecting a radiation anomaly, the UAV surveys a selected square area for precise localization, calculating the actual source location in real-time after completing the final hover.	
Characterization and surveillance (exploration and monitoring) of Uranium Legacy Sites (ULSs)	In the DUB-GEM project, a UAV-borne GRS system with CeBr3 and NaI gamma spectrometers was integrated into a multi-rotor drone for prolonged surveillance of ULSs. Test flights over ULSs in Kyrgyzstan and Kazakhstan demonstrated satisfactory lateral resolution for risk assessments. UAV-borne GRS holds promise for nuclear emergency response and historical uranium mine exploration and monitoring.	[180,194,208]
Accurate mapping of radiation sources (gamma rays) and polluting gases	Practical systems were developed, using gamma detectors for localizing low radiation doses and generating gamma radiation maps. Gas sensors were utilized for visualizing pollutant distribution, finding primary applications in field scenarios for detecting low-activity gamma emitters, and analyzing emissions from industrial facilities.	[206]
Radiometric measurements for mining applications	The Rautuvaara mine near Hannukainen village, Finland, was subjected to a UAV-based radiation survey. The survey employed a quadcopter system, with measurements taken at heights of 2, 5, and 10 meters AGL, employing a 50 m line spacing covering approximately 14.4 kilometers in total.	[183]

3.1.4. Unmanned Aerial Imaging Geophysics

A UAV photogrammetry system comprises both aerial and ground sections, with the aerial section featuring the UAV and various imaging sensors such as visible-light (RGB), multispectral (MS), hyperspectral (HS), or thermal-infrared (TIR) cameras [209,210]. The system operates through fieldwork, including ground operations and aerial surveys, and office tasks involving survey planning and data processing. Key steps involve acquiring overlapped images, identifying key points, and performing Structure-from-Motion (SfM) and Multi-View Stereo (MVS) [211] to generate dense point clouds, orthomosaics, and different other geospatial products. While this overview doesn't delve deeply into UAV photogrammetry, interested readers can refer to relevant references (e.g., [212]) for more details. UAV photogrammetry extends beyond civil applications [213], offering valuable geometrical, structural, spatial, and spectral data about the natural Earth. Consequently, it's a versatile UAV RS method applicable to various geoscientific endeavors.

This section provides an overview of UAV-compatible optical and TIR imaging sensors. In the UAV visible photogrammetry category, two types of visible cameras are commonly used on UAV platforms for imaging and photogrammetry [214]. These include UAV-integrated cameras, exemplified by the 20-MP 4/3-inch image sensor (e.g., used in DJI Mavic 3 drone) and the 20-MP 1-inch image sensor (e.g., used in AUTEL's EVO II Pro V3 drone), and Digital Single Lens Reflex (DSLR) cameras like the Sony A7RIII. In UAV MS photogrammetry and RS, state-of-the-art sensors include the Parrot Sequoia+, MicaSense Altum-PT, MicaSense RedEdge-MX/P, Sentera 6X, and DJI P4 Multi [214,215]. State-of-the-art TIR sensors include the WIRIS Pro/Pro Sc, Zenmuse XT 2 (dual-light TIR imager), Uncooled FPA 6404, FLIR SC305, and TELEDYNE FLIR VUE Pro. In the realm of UAV HS photogrammetry, cutting-edge sensors include OCI™-UAV-1000/2000, OCI™-F series, and GoldenEye™ (by BaySpec); CHAI S/V-640, S 185 FIREFLEYE SE, S 485 FIREFLEYE XL, and Q 285 FIREFLEYE QE (by Cubert); Nano/Micro-HyperSpec, VNIR-1024, Mjolnir V-1240, and SWIR-384 (by Headwall Photonics HySpex); Rikola, vis-NIR microHSI, Alpha-vis microHSI, SWIR 640 microHSI, and Alpha-SWIR microHSI by MosaicMill NovaSol; MV1-D2048x1088-HS05-96-G2 (by PhotonFocus); Hyperea 660 C1, Pika L, Pika XC2, Pika NIR, and Pika NUV (by Quest Innovations Resonon); VIS-VNIR Snapshot by SENOP; SPECIM FX10/17 (by SPECIM); SOC710-GX (by Surface Optics); and MQ022HG-IM-LS100-NIR/ IM-LS150-VISNIR (by XIMEA) [209]. For the sake of brevity,

Preprints.org (www.preprints.org) | NOT PEER-REVIEWED | Posted: 1 November 2024 doi:10.20944/preprints202411.0058.v1

no further details about the sensors or their specifications are provided here. Readers are referred to the cited references for more information.

In UAV photogrammetry, spatial resolution—denoted by ground sampling distance (GSD)—along with spectral resolution (referring primarily to the number of bands the sensor can capture) and radiometric resolution, are key factors [216,217]. Common corrections in UAV photogrammetry include radiometric and geometric calibration [218,219]. Radiometric calibration aims to derive absolute reflectance measurements from the digital number (DN) [218]. Geometric calibration encompasses band-to-band registration (primarily for multi-lens sensors) and true orthorectification, which allows objects in the orthomosaic to be viewed from a top-down perspective [219]. Additionally, point cloud filtering is another type of correction applied not to images but to point clouds, eliminating non-ground points to generate a bare-land point cloud and digital terrain model (DTM) from the initial point cloud [220].

The geoscientific applications of UAV photogrammetry can be listed as follows:

- *Digital Terrain Modeling for Geomorphological Applications:* The initial application of UAV photogrammetry in geoscience focuses on ultra-high-resolution digital terrain modeling for geomorphological purposes. A crucial step in this process involves filtering the original point cloud to isolate the natural terrain points [220]. Subsequently, topographical maps are generated by combining the orthomosaic with contour lines. These maps facilitate further geomorphological analysis and applications.
- *Landslide Mapping and Monitoring:* Table 10 presents a comprehensive review of efforts in landslide mapping and monitoring using UAV photogrammetry.
- *Land Subsidence and Ground Failure Mapping:* Table 11 provides a thorough list of research conducted in the realm of land subsidence and ground fissure mapping.
- *Geothermal Exploration:* The application of UAV photogrammetry in geothermal exploration is explored here, with a collection of them provided in Table 12.
- *Soil Moisture Mapping:* Research conducted in the realm of soil moisture mapping using UAV photogrammetry has been reviewed in Table 13.

Table 10. Landslide studies using UAV photogrammetry.

Reference	Objectives	Equipment and Methods	Descriptions (Additional Information)
[221]	Employing UAV photogrammetry for high-resolution mapping of landslides.	*Platform:* Quadcopter UAV *Sensor:* Praktica Luxmedia 8213 camera *Method:* Analysis used OrthoVista software, while DTM generation employed VMS and the GOTCHA algorithm.	Manual data acquisition and processing took considerable time. However, errors introduced during plane rectification degraded the georeferencing accuracy to about 0.5 m over most of the landslide.
[222]	The workflow entails processing UAV images into very high-resolution DEMs and orthomosaics, facilitating the quantification of landslide dynamics via multi-temporal image correlation.	*Platform:* Octocopter UAV *Sensor:* Canon 550D DSLR camera *Method:* Agisoft PhotoScan (for image processing and analysis) and GeoSetter (for geotagging).	SfM accuracy, confirmed with 39 DGPS GCPs, achieved a horizontal RMSE of 7.4 cm and a vertical RMSE of 6.2 cm. It tracked ground material movements, vegetation patches, and landslide toes, but faced difficulties in mapping the main scarp's retreat.
[223]	UAV imaging system was employed to capture high-resolution RGB images for monitoring a large landslide.	*Platform:* MikroKopter OktoXL *Sensor:* Canon EOS 650D DSLR Camera *Method:* Processing in Metashape	A comparison of both models, i.e., GCP-referenced vs. UAV-referenced, revealed a deviation of 11.3 m ± 1.6 m.
[224]	Applying the image correlation methods for surface motion detection to a UAV multi-temporal imagery dataset.	*Platform:* Octocopter micro-UAV *Sensor:* Canon 550D DSLR camera *Method:* Analysis used Mikrokopter autopilot, a Photoshop One camera gimbal; and Photoscan.	RMSE averages 4-5 cm horizontally and 3-4 cm vertically. Coregistration errors between successive DSMs minimize alignment error to ±0.07 m on average.
[225]	Automated approaches to detect and extract the	*Platform:* DJI Phantom 2 UAVs *Sensor:* LFOV GoPro Hero 3 digital camera	RMSE for the Eigenvalue ratio, topographic surface slope, and surface roughness index methods

Preprints.org (www.preprints.org) | NOT PEER-REVIEWED | Posted: 1 November 2024 doi:10.20944/preprints202411.0058.v1

	geomorphological features of landslides scarps.	*Methods:* Simultaneous Multi-frame Analytical Calibration (SMAC) to generate a dense point cloud; both SfM and SGM methods are used.	were 11.98 cm, 9.05 cm, and 10.45 cm, respectively.
[226]	Multi-temporal analysis of an earthflow impacting an olive grove.	*Platforms:* Falcon 8 Asctec and FV-8 Atyges *Sensors:* Sony Nex 5N *Method:* Generation of dense point clouds using Agisoft PhotoScan.	Automated point identification and matching between multi-temporal images face challenges due to factors like sun illumination, vegetation, and landslide movement. Achieved accuracy is 10 cm in XY and 15 cm in Z.
[227]	Quantification of vertical measurement sensitivity and accuracy (for a real-world landslide over two years)	*Platform:* Mini fixed-wing UAV (Quest UAV 300) *Sensor:* Panasonic Lumix DMC LX5 *Method:* Analysis used PhotoScan, TerraSolid TerraScan, and Cloud Compare.	Seasonal vegetation influences created elevation differences. A value of ± 9 cm vertical sensitivity for the SfM-derived change measurement was derived.
[228]	Mapping landslide potential area	*Platform:* DJI Mavic Pro™ *Sensor:* A 4K resolution digital camera. *Method:* Chan-Vese segmentation approaches.	The ability of UAV photogrammetry to map landslide potential areas is highlighted.
[229]	Studying kinematic and geometric features of the Mabian landslide (in China) combined with video captured by residents.	*Platform:* DJ Pro4 *Sensor:* An unknown digital camera *Method:* The DEM and orthographic data of the landslide were acquired by the SfM technique.	A 0.15m-DEM was used to recover and correct the pre-landslide contours.
[230]	Survey a village (in Italy) that was strongly affected by active landslides.	*Platform:* "Saturn" multicopter UAV. *Sensor:* Sony RGB camera with 8-MP resolution *Methods:* Multiple photogrammetric surveys provided multitemporal 3D models of the slope. Orthomosaics were processed in Photoscan.	Two mass movements were detected and characterized with a ground resolution of 0.05 m/pix.
[231]	Using spectral and point cloud data to digitize structural features like faults, joints, and bedding planes for kinematic analysis of the sea cliffs at Telscombe, UK.	*Platform:* DJI S1000 octocopter *Sensor:* Nikon D810 FX DSLR 36-MP camera *Method:* Image analysis used ADAM 3DM Technology Mine Mapping Suite.	The accuracy and density of the point cloud are comparable to those produced by TLS.
[232]	UAV imaging was employed in two landslide-prone/rockfall areas in Greece to assess an Object-Based Image Analysis (OBIA) approach for landslide detection.	*Platform:* DJI Phantom 4 Pro V2.0 *Sensor:* A stabilized built-in camera *Methods:* Pix4D SfM-MVS was used to generate 3D point cloud, DSM, and orthophoto supplying data for the OBIA phase in eCognition software.	The proposed method's spatial level of detection (LoD) was 0.5 m.
[233]	UAV imaging was used to characterize the activity of the Maierato landslide in Italy and evaluate residual risk.	*Platform:* DJI Phantom 4 Pro *Sensors:* 20-MP visible and RedEdge MS sensors. *Method:* Metashape SfM algorithm for image processing and 3D model reconstruction. Using an open-source GIS environment, several DEM of differences (DoD) were obtained.	Ground resolution of 0.05 meters and point cloud density up to 419 points/m² were achieved, enabling quantification of morphological changes induced by the landslide using the MS sensor.
[234]	UAV-based multi-temporal imaging for landslide detection and monitoring in an extensive area	*Platforms:* MD4-1000 quadrocopter and Feima F1000 fixed-wing UAV *Sensors:* Sony ILCE 7R and ILCE-5100 cameras *Method:* Mesh model differentiation.	UAV photogrammetry was conducted five times over two years for mapping historical landslides, measuring landslide volume, and monitoring horizontal and vertical displacement.
[235]	Extraction of landslide information based on UAV survey	*Platform:* DJI Phantom Pro 4 *Sensor:* A 1-inch 20-MP visible camera *Method:* Photogrammetric processing and extraction of deformation data based on DEM and orthomosaic image	UAV photogrammetry rapidly detects landslide changes, aiding monitoring and analysis.

 doi:10.20944/preprints202411.0058.v1

[236]	Analyses for landslide monitoring in a mountainous area	*Platform:* DJI Phantom 4 Pro *Sensor:* A 20-MP visible camera *Method:* Change detection approach between the generated point clouds.	A time period of two years was considered for this change detection project.

Table 11. Land subsidence and fissure mapping studies using UAV photogrammetry.

Reference	**Objectives**	**Equipment and Methods**	**Descriptions (Additional Information)**
[237]	Investigating the limitation and potential of UAV photogrammetry for subsidence mapping and monitoring in municipal landfills	*Platform:* UAV helicopter system *Sensor:* Visible-light camera *Method:* Photogrammetric processing	It was shown that UAV photogrammetry (using an unmanned helicopter) is more flexible and productive than some other counterpart techniques for similar precision.
[238]	Application of UAV-based digital terrestrial photogrammetry for landslide mapping.	*Platform:* Fixed-wing GATEWING X100 *Sensor:* A 10-MP visible camera *Method:* MetaShape-based processing	UAVs documented landslides and remote mines at the Czech Nástup Tušimice mine, capturing aerial photos and generating orthophotos and 3D models
[239]	Surveying hazardous mining-induced sinkhole subsidence by UAV photogrammetry	*Platform:* Phantom 2 Vision+ drone *Sensor:* A 14-MP visible camera *Method:* Sinkhole subsidence was identified using orthoimages and DTMs, with area and volume calculated using vertical profiles.	GCP validation showed a 14 cm error in the DTM, acceptable for subsidence mapping. This method offers accurate, rapid, low-cost, and safe surveying, complementing conventional methods at mining subsidence sites.
[240]	Subsidence mapping and land-surface deformation modeling using UAV photogrammetry	*Platform:* Quadrotor UAV *Sensor:* A 28-mm fixed-lens camera *Method:* Depth info. extraction from overlapping photos using SfM.	SfM-built topographic models align with high-resolution LiDAR topography, boasting vertical accuracy of about 12 cm.
[241]	Investigation of the capability of UAV photogrammetry for large mine subsidence mapping	*Platform:* DJI Phantom 4 *Sensor:* DJI FC330 camera *Methods:* utilization of total stations, GNSS, and UAV photogrammetry	Both GNSS RTK and UAV photogrammetry are effective for mine subsidence monitoring. UAVs offer dense and high-resolution DEMs while reducing human exposure to hazardous areas.
[242]	Measuring land subsidence throughout DEM and orthomosaics using GPS and UAV	*Platform:* DJI Phantom 4 *Sensor:* 20-MP camera *Method:* MetaShape-based processing	The DTM revealed a significant variation between extremes, pinpointing the fault location that delineates the subsidence zone.
[243]	Monitoring the deformation and spatiotemporal evolution	*Platform:* Dajiang M300 quadcopter	The novelty lies in integrating UAV and DInSAR for enhanced accuracy in mining subsidence analysis.

	of mining areas using D-InSAR and UAV technology	*Sensor:* The Saier 102s five-lens camera *Methods:* SAR data processing and UAV photogrammetry	
[244]	Subsidence mapping induced by underground coal mining by combining UAV photogrammetry and DInSAR technique	*Platform:* D2000 FEIMA Intelligent Aerial Survey System *Sensor:* D-CAM2000 camera *Methods:* Fusion of UAV and DInSAR data	Combining DInSAR and UAV technology yielded more precise settlement monitoring compared to using either technology alone.
[245]	Simulating the use of UAV photogrammetry for urban land subsidence monitoring.	*Platform and Sensor:* Not specified *Method:* Generation of a model from sampled data from DTMs of two times.	Photogrammetry was done at different heights and epochs, with a one-month gap between collections, aligning with changes due to dredging.
[246]	Investigating slope displacements over time (time-series analysis) with UAV photogrammetry and its correlation with rainfall intensity.	*Platform:* DJI's Phantom 4 pro *Sensor:* Visible camera *Method:* Image processing used Pix4D software, enabling horizontal and vertical deformation mapping via orthoimages and DSMs.	Various UAV photogrammetry campaigns between 2019 and 2020 monitored slopes, generating orthoimages and DSMs. Ground displacement was estimated via slope extraction, displacement area evaluation, and analysis of vertical and horizontal displacement.
[247]	Mine subsidence mapping integrating DS-InSAR with UAV photogrammetry products	*Platform:* Trimble UX5 UAV *Sensor:* SONY A5100 SLR camera *Method:* Fusion of multi-source geospatial data	DS-InSAR technology, combined with UAV photogrammetry products, was utilized to monitor subsidence in two mining areas with diverse landforms and mining characteristics.
[248]	Mapping mining-induced ground fissures and their evolution utilizing UAV photogrammetry	*Platform:* DJI M100 quadcopter *Sensor:* DJI X3 gimbal visible camera *Method:* Combining RS and field survey data for extraction and spatial-temporal evolution mapping of ground fissures.	This method combines regional gradient changes of ground fissures in images with statistical feature differences from other ground objects to highlight ground fissures.

Table 12. Geothermal mapping studies using UAV photogrammetry.

Reference	Objectives	Equipment and Methods	Descriptions (Additional Information)
[249]	Thermal imaging of subsurface coal fires using a UAV in Xinjiang, PRC.	*Platform:* An octocopter drone *Sensor:* Thermography and visible camera *Method:* Analysis of georeferenced mosaicked thermal and visual images.	The study demonstrated that UAV-borne data effectively match ground-level temperature measurements and offer detailed coverage over extensive areas.

Preprints.org (www.preprints.org) | NOT PEER-REVIEWED | Posted: 1 November 2024 doi:10.20944/preprints202411.0058.v1

[250,251]	Highlighting drones' potential as a key tool in geothermal exploration.	*Platform:* DJI Phantom 2 Vision+ *Sensor:* ICI 640x480 uncooled thermal camera	Outputs include thermal and visible orthomosaics, 3D thermal model, and DEM.
[252]	Demonstrate the use of quadcopter to map the biological and physical characteristics of geothermal areas safely and accurately	*Platform:* Blade 350 QX2 Quadcopter *Sensors:* Spectrum DX5e DSMX 5-channel transmitter equipped with a Sony HDR-AS100V, FLIR Tau 320 camera, and sensors for capturing TIR videos.	Outputs include visible and thermal orthophotos.
[253]	Assessment of groundwater discharge into the coastal zone using UAV thermal infrared mapping	*Platforms:* DJI S1000 octocopter and a manned aircraft *Sensors:* FLIR T450sc/A615	UAVs excel in studying localized submarine groundwater discharge dynamics, while manned aircraft are better suited for regional characterization of discharge locations.
[254]	UAV-based thermal imaging for monitoring volcanic geothermal areas	*Platform:* AI-RIDER YJ-1000-QC *Sensors:* XM6 TIR camera, GPS, compass, air pressure sensor, and IMU.	A solution for addressing challenging terrains, diverse topography, and extreme environmental conditions was offered.
[255]	Assessing the suitability of UAVs for monitoring geothermal plant environments.	*Platform:* Geoscan 201 UAV *Sensors:* Thermoframe-MX-TTX thermal imager and Sony DSX-RX1 optical camera	Outputs include visible and thermal orthophotos
[256]	UAV-based surface temperature mapping	No information has been provided from platform, sensor, and methods.	UAV surface temperatures are compared with ground temperature measurements and Landsat-8 thermal imagery.
[257]	Demonstrating the efficiency and affordability of an integrated UAV system with optical and thermal cameras	*Platform:* DJI Matrice 210 *Sensor:* Optical and thermal cameras.	Outputs include thermal orthomosaic, DSM, and surface temperature map
[258]	Assessing the potential of drone-borne TIR imagery in measuring river temperature variation/heterogeneity.	*Platform:* DJI Inspire 1 Quadcopter *Sensor:* DJI Zenmuse XT Radiometric thermal camera	UAV imaging improved river advective input quantification at intermediate spatial scales.
[259]	Finding the relationship between deep and surface expressions using UAVs	*Platform:* DJI Matrice 100 *Sensor:* FLIR Tau 2 thermal camera and DJI Zenmuse X5R optical camera	Outputs include DEM, thermal 3D model, and infrared mosaic (a case study in Geysir geothermal field)

[260]	Examine surface temperature and thermal signature distribution in the geothermal regions of Tuscany.	*Platform:* FlyBit octocopter *Sensor:* FLIR VUE PRO R thermal camera	Outputs include RGB orthomosaic and surface temperature maps (thermal orthomosaic)
[261]	Controls of cold-water areas over a groundwater-dominated Riverscape using UAV TIR and optical imagery	*Platforms:* Inspire 1 Pro and Phantom 4 Pro *Sensors:* Zenmuse X5/XT (thermal and vis.) *Method:* Image processing in Pix4D	Outputs include RGB and thermal orthomosaics
[262]	Study the efficacy of UAV MS and thermal sensors in soil water content (SWC) estimation.	*Platform:* DJI Matrice M210 *Sensor:* Zenmuse XT2 camera *Method:* ML approach	UAV-based SOC mapping aids precision irrigation despite prediction errors.
[263]	Geothermal mapping and RS of thermal anomalies at Grændalur area, Hveragerði, SW Iceland	*Platform:* DJI Matrice 200 *Sensor:* Zenmus XT thermal camera *Method:* Combining satellite (Landsat and ASTER) and UAV thermal anomaly images.	A geothermal mapping survey identified various surface manifestations like hot springs, mud pools, and fumaroles. Additionally, it detected new geothermal activity likely triggered by an earthquake.
[264]	Analyze and construct a DEM map of the geothermal manifestations using drone-borne thermal imaging.	*Platform:* DJI Phantom 4 *Sensor:* FLIR One Gen 2 thermal camera and Milwaukee Mi306 *Method:* Elevation and slope analysis	UAV imaging emerges as a valuable tool for ensuring safety during exploration in geothermal manifestation areas.

Table 13. Soil moisture mapping studies using UAV photogrammetry.

Reference	**Objectives**	**Equipment and Methods**	**Descriptions (Additional Information)**
[265]	Assessment of surface soil moisture using high-resolution MS images and artificial neural networks (ANNs)	*Platform:* AggieAir (self-built) *Sensors:* A MS camera including visible, NIR, and thermal sensors. *Method:* An ANN model.	UAV images and vegetation indices helped estimate moisture via an ANN model for irrigation management. Model accuracy varies with location and time.
[266]	Combining UAV HS imagery and ML algorithms for soil moisture content (SMC) mapping	*Platform:* DJI Matrice 600 Pro *Sensor:* Headwall Nano Hyperspec *Methods:* The random forest (RF) and extreme learning algorithms.	A ML algorithm was applied to spectral indices derived from UAV HS images to estimate SMC.
[267]	Proposing a method to estimate grassland SWC using UAV visible images.	*Platform:* DJI Phantom3 Pro *Sensor:* RGB camera with 4K lens, which can take 12-MP images.	The study validated estimating soil moisture at 0-10 cm depth. A linear regression model achieved an R^2 of 86% for moisture estimation.

Preprints.org (www.preprints.org) | NOT PEER-REVIEWED | Posted: 1 November 2024 doi:10.20944/preprints202411.0058.v1

[268]	Estimating SWC of agricultural land based on UAV HS images.	*Platform:* DJI Matrice 600 Pro *Sensor:* Headwall Nano-Hyperspec *Methods:* Processing in Hyperspec III SpectralView, and MATLAB.	By using an XGBoost classifier, the correlation coefficient R^2=83.5% was obtained.
[262]	Estimating SWC based on UAV MS and thermal images	*Platform:* DJI Matrice M210 *Sensor:* Zenmuse XT2 camera *Method:* Machine learning (ML) approach	Estimating SWC using MS image yielded better results than using thermal image, with an R2 of 96%.
[269]	Prospecting thermal water using UAVs, cost-effective sensors, and Geographic Information Systems (GIS)	*Platform:* DJI Matrice 600 *Sensors:* WIRIS Pro dual TIR and non-metric visible cameras *Methods:* SfM-MVS processing	UAVs with dual sensors and GIS tools offer a fast, affordable, and simple alternative to conventional methods, producing high-quality results adaptable to challenging terrain.
[270]	Application of UAV photogrammetry and normalized water index to estimate rock mass rating	*Sensors:* VNIR (RGB+NIR bands) *Methods*: data preprocessing (image stitching and layer stacking) and processing (extracting information from water indices)	Spectral indices were used to generate the existence of water bodies on the slope, and to rate water conditions.
[271]	Estimation of SMC in corn fields	*Sensors:* Visible, MS, and TIR cameras *Methods:* ML algorithms such as partial least squares regression, K nearest neighbor, and random forest regression	Fusion of UAV multimodal data improved the estimation accuracy regardless of the ML, especially the joint use of thermal and MS data.

- *Mineralogy, Mining, and Soil Mapping:* Table 14 provides a comprehensive overview of UAV-based imaging and photogrammetry applications in mineralogy, mining, and soil mapping. It is noteworthy that research focusing on mining was gathered and reviewed building on [272].
- *Volcanoic Research:* Table 15 offeres a collection of researches in the realm of volcanoic mapping using UAV photogrammetry.

Table 14. Mineralogy, mining, and soil mapping studies using UAV photogrammetry.

Reference	Objectives	Equipment and Methods	Descriptions (Additional Information)
[273]	Semi-automatic mapping of geological structures using UAV photogrammetry	*Platform:* Octocopter Micro-UAV *Sensor:* Canon 550D DSLR Camera *Method:* An image analysis-based approach	The proposed method automates fault detection and orientation calculation, improving fault mapping efficiency.
[274]	Meeting the demand for radiometric and geometric corrections of UAV HS images in mineral exploration	*Platforms:* Sensefly ebee fixed-wing and Aibotix Aibot X6v2 hexacopter. *Sensors:* Canon Powershot S110, Rikola HS Imager, and Nikon Coolpix A *Method:* Standard SfM (Photoscan).	UAV HS data's utility in geological studies is underscored, along with the introduction of a specialized toolkit for

			preprocessing drone-acquired HS data for geological applications.
[275]	Leveraging UAVs for the study of carbonate geology	*Platform:* DJI Phantom 3 Pro *Sensor:* A 12-MP digital camera *Method:* An SfM processing workflow and further processing in ArcGIS.	The research showcases the capability of UAVs in conducting geological studies focused on carbonate formations.
[276]	Combining terrestrial and UAV-based HS and photogrammetric sensing methods for mining monitoring and exploration mapping.	*Platform:* Aibotix Aibot X6v2 hexacopter *Sensor:* Senop Rikola VNIR HS Imager (with 50 bands and spectral coverage of 500–900 nm) *Method:* Integration of SfM photogrammetric point clouds and VNIR–SWIR–LWIR HS data.	Integrating ground- and UAV-based photogrammetry with hyperspectral imaging optimizes ground surveys for structural, geochemical, and petrological analyses.
[277]	Exploring multi-sensor drone-borne geophysics for geological mapping and mineral exploration	*Platform:* A multicopter from HZDR-HIF *Sensor:* HS frame camera which captures images in the VNIR part of the EM spectrum.	The combination of magnetometry and HS photogrammetry has undergone testing for geological surveys.
[278]	Investigating the fusion of drone-borne HS and magnetic data for deposit/ mineral mapping.	*Platforms:* Aibotix Aibot X6v.2 multicopter and SenseFly Ebee Plus fixed-wing UAV *Sensors:* Visible, MS, and Rikola HSI *Method:* SfM-MVS processing in PhotoScan	Combining lightweight UAS tech. with visible, MS, and HS cameras, alongside fluxgate magnetometers, forms a foundation for thorough data analysis in non-invasive mineral exploration.
[279]	Utilizing UAVs for HS environmental monitoring of water bodies impacted by acid mine drainage.	*Platform:* Tholeg THO-R-PX8 multi-copter *Sensor:* Rikola HS sensor *Method:* HS data were preprocessed using the Python MEPHySTo toolbox. Further processing was done based on supervised classification.	The paper highlights the potential of UAV HIS data as a tool for environmental monitoring of surface water impacted by acid mine drainage, applicable across various hydrogeological applications.
[280]	Mapping materials with the potential to generate acidity on abandoned mines utilizing remotely piloted aerial systems	*Platform:* Tarot 650 RPAS *Sensors:* RedEdge and Nano VNIR Hyperspec *Methods:* Using SfM image processing in Pix4D and ML classification methods (for surface materials identification).	Monitoring acid-generating material and acid mine drainage using MS/HS sensors offers an alternative to field surveys, aiding in prioritizing regions for detailed investigation and remediation.
[281]	Investigating mining exploration through the use of UAVs, cost-effective	*Platform:* DJI Matrice 210 V *Sensors:* Zenmuse XT2 dual radiometric sensor	Using UAV-borne infrared sensors for mining prospecting has shown substantial promise,

	thermal cameras, and GIS tools	*Method:* Processing of RGB and thermal images using SfM-MVS in two parallel branches.	expediting research economically and effectively, particularly in challenging and remote terrains.
[282]	The automated identification of magnetite in placer deposits through the utilization of a MS camera mounted on a UAV.	*Sensors:* RGB and DJI P4 MS cameras *Methods:* Spectral angle mapping (SAM) and AI (traditional and deep learning) methods implemented in MATLAB	Using 6-band MS imagery data, a 1D CNN deep learning model achieved accuracy of 99.7% and per-class precision of 99.4%, emerging as the most effective AI model.
[283]	Combining UAV magnetic data and MS images for 3D modeling in a mineral exploration project.	*Platform:* DJI Mavic Pro *Sensors:* A 12.3-MP visible camera and a vessel-based DSLR photographer *Methods:* Geosoft Oasis Montaj and photogrammetric processing software.	Combining UAV optical and magnetic data with ground and drill-hole measurements refines the identification of Ni-Cu-Co-PGE mineralization targets.
[284]	Assessing mercury and arsenic pollution in the soil-plant system using a method combining UAV data, geochemical survey, and ML.	*Platform and sensor:* A P4 MS UAV-RS from SZ DJI *Methods:* Multiple Linear Regression, RF, Generalized Boosted Models, and Multivariate Adaptive Regression Splines.	The study demonstrated the modeling of As and Hg concentrations in soil-plant systems using low-density geochemical surveys and UAV high-resolution images.
[285]	Application of UAV-geological mapping, satellite RS, and ML methods in podiform Chromite deposits exploration	*Platform:* DJI Phantom *Sensor:* Visible camera *Methods:* Processing of satellite data using ENVI, ArcGIS, and Geomatica, and supervised classification of the outputs of field surveying, UAV mapping, and satellite images.	The ultimate result of the proposed approach is a geological map at a 1:5000 scale, facilitating the identification of novel podiform chromite outcrops.
[286]	Presenting the possibility of creating 3D point clouds from UAV video images (rock slope analysis)	*Platform:* Aeryon Scout VTOL UAV *Sensor:* A camera for capturing video images at a resolution of 640 x 480 pix and 12 fps.	Besides its significance in mining, there are potential geological applications, such as assessing slope stability.
[287]	Accuracy analysis of 3D geometry generated from low-attitude UAV images for topographic surveying in open-pit mines	*Platform:* BNU-D8-1 hexacopter *Sensor:* Canon 5D mark II Method: SfM and patch-based MVS algorithms	UAV-driven point cloud and DSM of the study area were compared with TLS data. Deviations in 3D distance map within ±0.4m, relative volume error 1.55%.
[288]	Verification of on-site applicability of aerial triangulation using UAV images	*Platform:* DJI S1000 *Sensor:* Cannon Mark VI *Method:* A Photoscan-based processing	Study creates orthophotos and DEMs for monitoring ore production and landslides using rapid and low-cost photography.
[289]	Topographic mapping of open-pit mine using a rotary-wing drone	*Platform:* DJI Phantom 2 Vision+ *Sensor:* A digital RGB camera	DGPS-measured GCPs compared to those from UAV

			photogrammetry had an RMSE of about 10 cm for all coordinates.
[290]	Investigation of open-pit mines' characteristics employing topographic maps and landscape metrics	*Platform:* Skywalker X5 fixed-wing *Sensor:* Sony QX100 20.9 MP camera *Method:* SfM methodology in Agisoft Metashape and point cloud manipulation in CloudCompare.	The method used landscape metric, high-resolution topography from UAV, and SfM to characterize open-pit mine geomorphic features.
[291]	Proposal of UAV's usefulness in investigating outcrops of geological rocks	*Platform:* Phantom 2 Vision+ *Sensor:* A 14-MP FC200 camera *Method:* SfM (PhotoScan).	UAV photogrammetry documented inaccessible geological outcrops, enhancing efficiency and accuracy.
[292]	Volume evaluation, monitoring the safety of slopes, and mapping the underground mine	*Platform:* A fixed-wing UAV *Sensor:* A digital camera	UAVs mapped the Ulan and Tahmoor mines in Australia, measuring stockpiles, monitoring slope safety, and mapping mine subsidence.
[293]	Proposal methodology for reconstructing the topography using oblique and nadir imageries	*Platform:* ESAFLY A2500 hexacopter *Sensor:* Canon EOS 550D camera *Methods:* Image processing with Photoscan and Pix4D mapper.	UAV photogrammetry aids in the regular monitoring of mining activities and quarry management by operators, utilizing nadir and oblique imagery.
[294]	Prototype development of UAV for underground mining surveying	*Platform:* Rotary-wing UAV *Sensor:* A drone-deployed digital camera	UAV's role in underground mining, including a prototype with auto-rotation for scanning, was outlined.
[295]	UAV design for imaging in areas inaccessible to underground mines due to mining and blasting	*Platform:* A quadcopter *Sensor:* A digital RGB HD camera	GPS-free UAV illuminated underground mine features, revealing rock walls, structures, blast evidence, and support elements during sublevel stope tests.
[296]	3D modeling of an underground mine using the forward-looking infrared (FLIR) imagery.	*Platform:* A UAS that included thermal imagery, obstacle detection, lighting, and software. *Sensors:* Visible and thermal cameras	UAV thermal imagery created 3D models in underground mines revealing geological data for geotechnical analysis.
[297]	Development of automation technology for lithological classification using ML and small drones	*Platform:* DJI Phantom 4 Pro *Sensor:* Visible-light camera *Methods:* Four ML techniques including SVM, kNN, RF, and gradient tree boost (GTB).	A UAV camera was used to classify rock types at the Cajati opencast phosphate mine in Brazil, with ML improving precision over manual methods.
[298]	Mapping opencast highwall using UAV RS technology	*Platform:* A rotary-wing UAV *Sensor:* A digital RGB camera *Methods:* Metashape SfM algorithm	UAV tech. mapped opencast highwalls, processing raw data to

			generate a model that correlated with the resource model.
[299]	Review of the application of field and RS approaches for rock slope characteristics	*Platform:* Different rotary-wing UAVs *Sensor:* Digital visible cameras *Method:* SfM-based image processing	UAV RS for rock slope investigations has been explored, emphasizing its applications, advantages, and limitations relative to traditional field methods.
[300]	Proposal of a UAV-based surveillance system suitable for underground mining operations	*Method:* A UAV monitoring system for enhancing safety, providing real-time results, and reducing human exposure in hazardous underground conditions.	UAV image capture is enhanced for rock mass analysis in confined, low-light spaces, improving geotechnical analysis in challenging environments.
[301]	Proposal of a method to detect and quantify geological discontinuities using thermal and MS images	*Platform:* Not specified *Sensors:* Thermal and MS cameras and LiDAR system	UAV thermal and MS imaging mapped geological discontinuities in hard rock masses. Thermal, MS, RGB, and LiDAR data were used to generate georeferenced meshes and 3D point clouds for mapping.
[302]	Using UAV photogrammetry for geological mapping (exploring Vein-type Copper mineralization)	*Platform:* DJI Phantom 4 Pro V2.0 *Sensor:* A built-in 20-MP CMOS camera *Method:* PhotoScan photogrammetric processing	UAV photogrammetry proved efficient for quickly and affordably preparing base geology maps in rugged, remote areas for vein-type mineralization exploration.

Table 15. Volcanic studies using UAV photogrammetry.

Reference	**Objectives**	**Equipment and Methods**	**Descriptions (Additional Information)**
[303]	Using thermal UAV photogrammetry for 3D modeling and studying an active volcano in Stromboli, Italy	*Sensors:* Visible and TIR cameras *Method:* RGB and thermal data underwent processing separately. Integration of data resulted in the first 3D thermal photogrammetric model of the active volcano.	Their method, as an easy-to-use workflow, is applicable to any volcano, offering a low-cost monitoring system suitable for remote areas with limited budgets and poor access.
[304]	UAV-based multi-temporal RS surveys of volcano unstable flanks	*Platform:* Not specified *Sensor:* Canon IXUS *Method:* SfM photogrammetric processing technique	The approach enables detailed volume assessments at a local scale, facilitating rapid UAV-based georeferenced surveys, valuable in emergencies.

Preprints.org (www.preprints.org) | NOT PEER-REVIEWED | Posted: 1 November 2024 doi:10.20944/preprints202411.0058.v1

[305]	Using cost-effective UAVs for studying dynamic tropical volcanic landforms	*Platform:* A low-cost UAV *Sensor:* An optical imaging sensor with a GSD of 8 cm/pix	UAV photogrammetry enabled precise analysis of volume, surface roughness, morphometric features, and surface classifications.

3.2. UAV-Borne Geophysical Survey: Active Methods

3.2.1. Unmanned Aerial EM Survey

The EM method, utilizing induced currents to detect conductive underground structures, aids in subsurface geology understanding. It's divided into time-domain EM (TDEM) and frequency-domain EM (FDEM) survey methods. Aerial EM (AEM) schematics depict induced and measured magnetic fields (see Figure 10). Measurements involve primary EM fields from the transmitter and secondary EM fields correlated with geological features [306–309]. AEM methods are categorized by excitation modes (AFEM and ATEM), platform types (fixed-wing TEM, fixed-wing FEM, helicopter-borne TDEM or simply HTEM, and helicopter-borne FDEM or simply HFEM), and EM field transmission types (active, passive, and semi-passive/airborne systems) [306,310–314]. Different ATEM and AFEM systems have been developed based on various types of manned aerial platforms [311,313,315–327]. Despite this variety, UAV-borne EM survey systems are a relatively new topic compared to traditional methods.

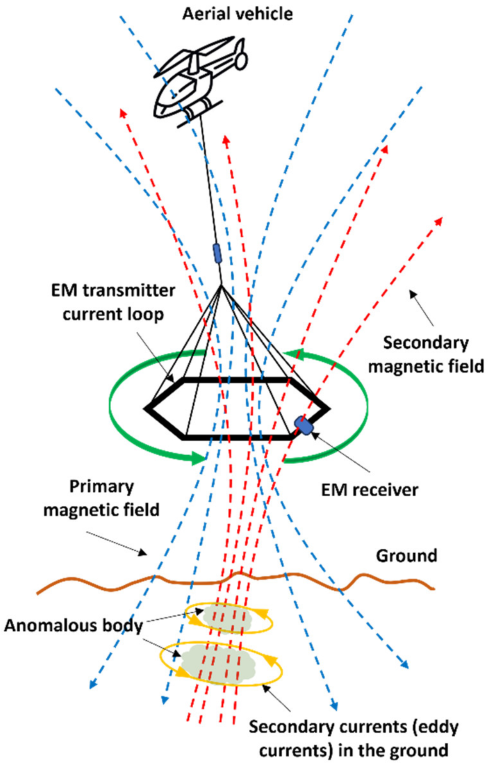

Figure 10. AEM survey—induced vs. measured magnetic fields (depicted based on [311,313]).

AEM has found various geoscientific applications including finding Quick Clay [328–330], identifying hazardous substances [331], mapping the fresh-saltwater interface [332], freshwater potential investigation [333], deep groundwater mapping in Antarctica [334–336], hydrologic mapping and environmental assessments [337], detection and mapping impermeable aquifer boundaries [310], groundwater and soil investigations [338], exploring the relationship between groundwater and surface water [339], 3D geological modeling of complex buried valleys [340], observations of a collapse-prone volcano [341], mineral exploration [327], gold exploration [342], mapping sub-Phanerozoic basement features [343], UXO detection [63], magnetite ore tonnage estimation [344], and application in the fields of uranium exploration [345,346].

Developing EM-sounding systems for lightweight UAVs faces challenges due to weight and bulkiness issues with conventional techniques, such as helicopter-based systems. Aerial exploration presents difficulties like precise loop positioning and adapting methods to UAVs, requiring bulky generator setups [347]. Integrating EM sensors with UAVs introduces stability, interference, and control challenges, addressed with solutions like sensor suspension, tail fins, noise avoidance, and real-time monitoring [348,349]. These innovations aim to enhance data quality and address engineering challenges in UAV-based EM surveys. The scheme of Figure 10 is also valid for the UAV EM method.

There are two configurations in UAV-borne EM surveys: single-drone and dual-drone configurations. To illustrate these configurations, we focus on the Louhi geophysical EM survey system. Developed by Radai Ltd. under the NEXT project, this system facilitates practical drone-based operations for FDEM methods [309]. It features a single drone equipped with a transmitter, offering flexibility in surveying approaches (see Figure 11). Additionally, a two-drone configuration is utilized to maintain consistent separation distance between the receiver and transmitter drones, allowing for deeper exploration and rapid deployment in challenging terrains [350]. The fixed loop transmitter system enhances source moment and signal-to-noise ratio (SNR), crucial for subsurface exploration. Accurate position and orientation measurements enable conversion to global 3D coordinates, although variations in loop spacing and orientation can introduce noise. Synchronization between the receiver and transmitter units is achieved using GNSS time, allowing for precise data recording and analysis. Payload constraints and synchronization between dual-drone autopilots pose challenges, necessitating ongoing research and development efforts [309].

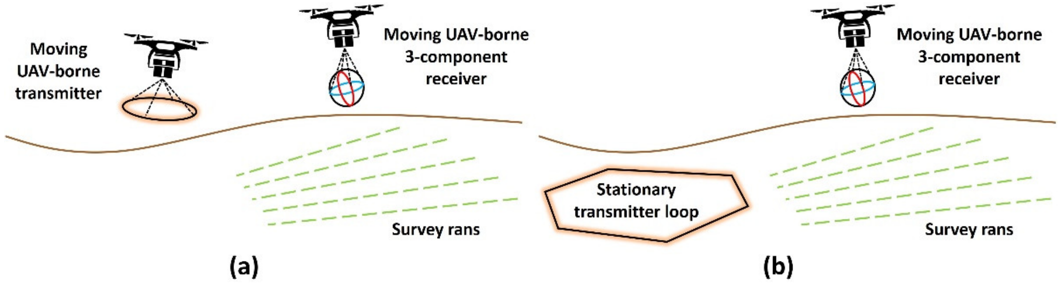

Figure 11. Single-drone and dual-drone configurations in UAV-borne EM: The EM primary field is produced using either (**a**) a compact mobile current loop transported by a UAV or (**b**) a large loop placed on the ground. In both scenarios, the EM response is detected with a receiver transported by another UAV (depicted based on [309]).

In the realm of UAV-based EM RS, the concept of the "Semi-UAV-borne EM (SUEM) System" is emerging as a promising innovation. The Semi-Airborne EM (SAEM) setup presents a promising avenue for UAV-based EM surveys [351]. In this configuration, the transmitter remains stationary on the ground while the receiver is deployed on a UAV (similar to Figure 11b), offering unique advantages over conventional AEM [352,353]. However, the payload limitations of current UAVs restrict the maximum speed of the SAEM system. Addressing challenges related to turbulence-induced shaking and motion-related noise in the dataset necessitates innovative solutions [311]. Advancements in drone technology have enabled the adaptation of SAEM systems to UAVs, reducing application and maintenance costs and facilitating multi-component surveys. Notably, MGT's SAEM system, developed in collaboration with the geophysical industry and research organizations in Germany, exemplifies the successful integration of an EM system onto an unmanned multicopter, enabling data collection with enhanced depth penetration and accuracy. These developments mark significant progress in the evolution of SUEM systems, holding considerable potential for future UAV EM RS applications [311,352–354].

Very-low Frequency (VLF) EM methods are frequently mentioned in the literature, especially in the context of UAV EM applications. UAV integration with the VLF method evolved since Kipfinger's

Preprints.org (www.preprints.org) | NOT PEER-REVIEWED | Posted: 1 November 2024 doi:10.20944/preprints202411.0058.v1

lightweight system in 1996-97 [353,355]. Recent developments led to VLF systems on rotary-wing UAVs with a 12 kg payload capacity [356]. VLF induces primary horizontal magnetic fields and captures secondary fields in conductive subsurface formations with a receiver equipped with two coils [357–359]. Equation (3) calculates the vertical magnetic field component using transfer functions or "tippers" [360,361].

$$H_z(\omega) = A(\omega).H_x(\omega) + B(\omega).H_y(\omega) \quad (3)$$

Modern VLF instruments capture time series data for all three magnetic field components, enabling analysis in both time and frequency domains. Automated spectral analysis, like the method proposed in [362], identifies VLF transmitters. These advances highlight the potential of UAV-based VLF EM systems for large-scale geophysical surveys [356,363].

Let's explore the data collection modes in UAV-borne EM surveys. UAV-borne EM surveys use fixed-point and continuous data collection modes [364]. In fixed-point mode, the UAV hovers at each measurement point, ensuring high-quality data but limiting data points due to energy-intensive hovering. Continuous mode collects data seamlessly during low-level flight, offering substantial data volumes similar to grasshopper mode [125]. Post-processing ensures data quality comparable to fixed-point mode [365].

This section discusses three key aspects of UAV-based EM surveys: compatible EM sensors for UAVs, UAV platforms used in EM surveys, and the development of UAV-based EM systems.

- *EM Sensors:* Various EM instruments have been utilized in UAV-borne surveys, including GEM-3D, MPV, MPV-II, Pedemis, High-Frequency EMI, Dualem-1S, EM38, Profiler 400-EMP, CMD MiniExplorer, US Army's drone-mounted EM induction sensor, CAS & Jilin University single-component sensor and others [311,349,366,367]. Among these, the GEM-2UAV is prominent, weighing 3 kg and operating at ten frequencies (25 Hz to 96 kHz). It requires a GNSS antenna, WinGEM software, and consumes 20 W during surveys, offering configurable operational modes and data logging initiated through a control unit [348,349,368].
- *UAV Platforms:* UAV platforms for carrying EM instruments are categorized into four types: multi-rotor [347,349,352], fixed-wing [73,369], helicopters [356], and airships/balloons [370]. The choice of platform depends on factors like survey objectives and the size of the EM instrument.
- *UAV-borne EM Survey Systems:* Building on the information provided in the preceding two bullets, Table 16 offers a thorough overview of the UAV-borne EM systems that have been developed.

Table 16. Review of state-of-the-art UAV-borne EM survey systems.

Sys.	Platform Type	UAV Name/Model	EM Instruments	References
1	Multi-rotor	MTOW octocopter	Miniaturized induction coil triple	[352,353]
2	Multi-rotor	X825 octocopter	Metronix SHFT-02e induction coil triple	[351]
3	Multi-rotor	SibGIS hexacopter	A measuring system with an inductive sensor	[201,347, 371,372]
4	Multi-rotor	SibGIS hexacopter	A grounded transmitter line spanning 2.2 km serves as the origin of the current pulses, coupled with an airborne PDI-50 receiver loop on the UAV.	[373]
5	Helicopter	Aeroscout Scout B1-100	The Super High-Frequency Induction Coil Triple sensor, in conjunction with the ADU07 data logging module, both developed by MGT.	[356]
6	Multi-rotor	DJI Matrice 600 Pro	GEM-2UAV CSEM sensor	[349]
7	Fixed-wing	VTOL Mother-Goose	Louhi portable EM transmitter and three-component receiver	[309]

Preprints.org (www.preprints.org) | NOT PEER-REVIEWED | Posted: 1 November 2024 doi:10.20944/preprints202411.0058.v1

8	Unmanned VTOL airship	Quaddirigible (filled with helium)	A VLF-type EM survey system	[370]
9	Multi-rotor	ZION CH940 and LAB6106 multicopters	GEM-2	[348]
10	Multi-rotor	Hexacopter	A coil wound with enameled copper wire, comprising 25 turns and a diameter of 25 cm, designed for the generation of a magnetic field.	[374]
11	Hexacopter and fixed-wing	SGU's fixed-wing VLF	Three orthogonally mounted induction coil sensors and a data acquisition system with up to 1 MHz continuous data sampling of the EM components.	[369]
12	Multi-rotor	Hexacopter	The drone-borne TEM system utilized a central loop device.	[365]
13	Not specified	Not specified	D-GREATEM system	[375]
14	Fixed-wing	Silver Fox UAV	A sensing coil towed behind the UAV	[73]
15	Multi-rotor	Hexacopter	A measurement setup using an inductive sensor (receiving loop) is tethered by a UAV, while a galvanically grounded power transmitter is positioned on the ground and linked to a pulse generator.	[376]
16	Unmanned helicopter	Tianxiang V-750	A SAEM system, designed by the CAS, encompasses a single-component sensor, transmitter, and receiver, all equipped with vibration isolation.	[311]
17	Multi-rotor	Hexacopter	A SAEM system, engineered by Jilin University, consists of a robust ground-based transmitter generating high-power signals and a single-component sensor.	[311]
18	Multi-rotor	DJI Matrice 600	The Geophex multi-coil, CMD MiniExplorer EM instruments, and GEM-2	[366]
19	Multi-rotor	DJI Wind4 quadcopter	Geophex GEM-2UAV	[377]
20	Fixed-wing	A long-range drone	UAV-borne gravity and EM sensors	[158,160]
21	Octocopter	System name: MGT-GEO Radio EM	The sensor system weighs 6.5 grams, operates in a frequency range of 1-524 kHz, encompasses channels for Hx, Hy, and Hz, boasts a sample rate of up to 524 kHz, achieves synchronization through GPS, and utilizes compact flash disk storage media.	[366]
22	Rotary-wing	DroneSAM	A low-frequency hybrid geophysical system integrating a ground active source transmitter system with a drone for slow-flying, low-level data acquisition of TEM and magnetometric resistivity data.	[378]
23	Rotary-wing	Multi-rotor (DronEM)	Drone for EM fields Measurements (DronEM) is outfitted with a Selective Electric Triaxial Probe and is capable of scanning the EM spectrum ranging from 10 MHz to 3 GHz at altitudes up to 200 m.	[379]

24	Rotary-wing	Not specified	UAV VLF EM System: two VLF UAV sensor coils with cables accompanied by other instruments.	[380]
25	Rotary-wing	Octo/helicopter	3-component EM sensor (induction coil DEEP) and fluxgate magnetometer.	[381]
26	Rotary-wing	Hexacopter	Time-domain EM system suspended beneath the UAV	[10]

In this part an overview is provided on the data integration, processing and inversion principles, and methods applied. The UAV-based EM data processing, following methodologies by [366,382], involves several key steps (Figure 12). Initially, raw datasets from various sources, including drone, EM instrument data, and additional sources (e.g., LiDAR, if available) are integrated, synchronized, and preprocessed for interpretation [383]. Noise filtering enhances data quality by removing high-frequency noise using a low-pass filter. Data segmentation categorizes raw EM sensor data into non-informative, grid/profile, and vertical sounding segments, facilitating anomaly analysis [366]. Inversion iteratively updates resistivity models by comparing field data with synthetic data, employing methods like Layered Constrained Inversion and Spatially Constrained Inversion [384–386]. Validation involves addressing noise sources and correlating EM data with geological maps and boreholes to discern soil characteristics and validate results. Additional geophysical data and hand drilling may be utilized for validation when alternative datasets are unavailable. A comprehensive review of UAV-borne EM survey geoscientific applications is summarized in Table 17.

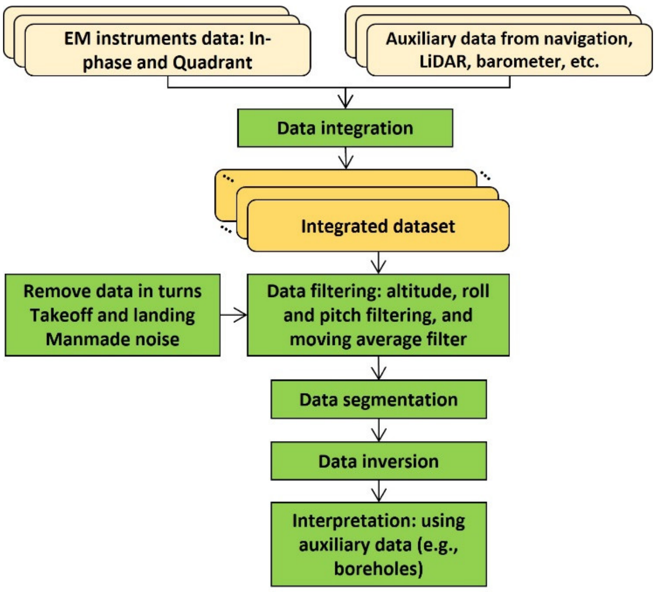

Figure 12. The processing chain of UAV-borne EM data (depicted based on [366]).

Table 17. Review of UAV-borne EM applications.

Applications	Descriptions	References
Mapping structural discordance and tectonics	UAV-TEM mapped Eastern Siberia's uranium region, overcoming terrain challenges. Surveying at 7.5 m/s and 40 m altitude, it covered 20 km in four hours, excluding transmitter setup. Control measurements followed opposite and orthogonal routes.	[347]
A drone-borne TEM survey over Lake Baikal	UAV-based TEM systems identified uranium ore-bearing strata in Bolshoe Goloustnoye, Lake Baikal. High-resistivity layers over the lake and deposit area indicated sediment deposits. Productive uranium ore deposits were reliably detected at depths of 120-170 m.	[373]

and Uranium deposits		
Detection of buried power cables and pipelines in Neuchatel, Switzerland	UAV-based VLF surveys identified a buried pipeline and power cable spaced 90 m apart. Using frequencies of 18.3 kHz and 23.4 kHz, anomalies were successfully detected, showing good agreement with results from the RMT approach.	[356,387]
A survey over a Transition Zone from Freshwater to Saltwater in Cuxhaven, Germany	UAS-VLF effectively mapped the freshwater-saltwater transition zone, showing conductivity shifts via transfer functions. Alignment with RMT data confirmed its efficacy.	[356]
Mapping soil resistivity and investigating buried vehicles	A drone system for EM mapping utilizes GPS, Wi-Fi, and ultrasonic sensors to control height, detect buried objects (e.g., vehicles), and map soil resistivity. It focuses on shallow subsurface resistivity surveys across large areas.	[348]
Landmine detection	A hexacopter-mounted EM sensor introduces a method for landmine detection, enhancing safety and efficiency in clearance operations by effectively locating landmines in mined areas.	[374]
UXO detection	A drone-borne TEM system was developed for UXO and ground fissure detection. It used compact coils for ATEM data collection, offering efficiency and safety in challenging terrains. The system proved effective in detecting near-surface UXO.	[365]
Investigation of slope subsurface resistivity structure	The D-GREATEM drone system mapped a steep slope, revealing shallow, intermediate, and deep resistivity layers. This validated the effectiveness of drone-borne EM surveys in mapping slope resistivity structures.	[375]
Detection of underground tunnels and buried wires	In a lecture note on UAV applications in resource exploration, a drone-mounted EM system was studied for detecting underground tunnels and buried wires. The setup included a sensing coil towed by a hexacopter.	[73]
Fresh-saline water mapping	A Netherlands site near Gouda was surveyed for brackish groundwater using a UAV equipped with a CMD MiniExplorer on a DJI Matrice 600. Within four hours, it generated a 3D resistivity model, shedding light on fresh-saline water interactions.	[366]
Sand-clay lithology mapping	A UAV-EM system was used to map diverse lithology along the southern levee of the Lek riverside in Vianen, Netherlands, outpacing ground-based FDEM mapping by 2-4 times and successfully identifying distinct lithological units.	[366]

 doi:10.20944/preprints202411.0058.v1

Cable, pipeline, and fence crossings	A UAV-EM system, using GEM-2 with DJI Matrice 600, validated in Vianen, Netherlands, revealed line objects with clarity through multiple profiles and a single grid survey.	[366]
Deep resistivity distribution mapping	The "grounded electrical-source airborne transient EM system (GREATEM)" was introduced for resistivity distribution assessments at deep levels. It uses a grounded wire as a transmitter on the ground and a receiver coil suspended from a drone.	[348,388]
Tunnel investigation	A novel semi-airborne method for tunnel exploration was introduced, utilizing a UAV-based SATEM system with a grounded-wire source and an induction coil carried by a UAV. Its efficacy was validated at the Damo Tunnel in Guangxi, China.	[389]
Subsurface target detection	A hexacopter-based TDEM survey, combined with YOLOv8, was utilized to identify anomalous regions for subsurface target detection.	[10]

3.2.2. Unmanned Aerial GPR

Over the past decade, UAV-based radar imaging has seen significant advancement, with various radar technologies, unmanned platforms, and payload configurations showcased [390–395]. Early research by [396,397] laid the foundation, leading to tests with high-frequency radars at P, X, and C bands [398–400], despite limited penetration capabilities. In [401] multi-frequency GPR for rotary-wing UAVs was explored, sparking a surge in contactless GPR research with UAV platforms. The convergence of UAVs and radar technology offers all-weather data recording and buried object detection, driving interest across scientific and industrial sectors [402–405]. Applications range from landmine detection to environmental monitoring, highlighting UAV-based GPR's promising future in geophysical surveys and underground exploration [406–408]. UAV-based GPR systems are categorized as prototypes explicitly designed for UAVs or conventional GPR devices adapted for UAVs, with systems further classified based on whether antennas contact the ground, leading to ground-coupled and air-launched GPR systems [409–411].

Two approaches exist for assembling payloads in the UAV-GPR systems: independent and integrated designs (see Figure 13). In the independent approach, the UAV and payload are separate subsystems, while in the integrated method, they are developed collaboratively. The independent setup allows for compatibility with various UAV platforms but requires a separate interface for integration. Conversely, the integrated architecture simplifies subsystem synchronization and enables high-accuracy geo-referencing for navigation without redundant sensors. This approach is preferred for UAV systems with advanced sensors or specialized flight modes [24]. Visual examples include [412], for independent architecture, and [392], for integrated architecture.

In this part, the observation modes in UAV-borne GPR are reviewed. The scanning strategies employed in UAV-borne GPR are of significant importance. These systems are categorized into three main types based on observation modes and antenna orientation relative to the Earth's surface (see Figure 14) [392,413].

Preprints.org (www.preprints.org) | NOT PEER-REVIEWED | Posted: 1 November 2024 doi:10.20944/preprints202411.0058.v1

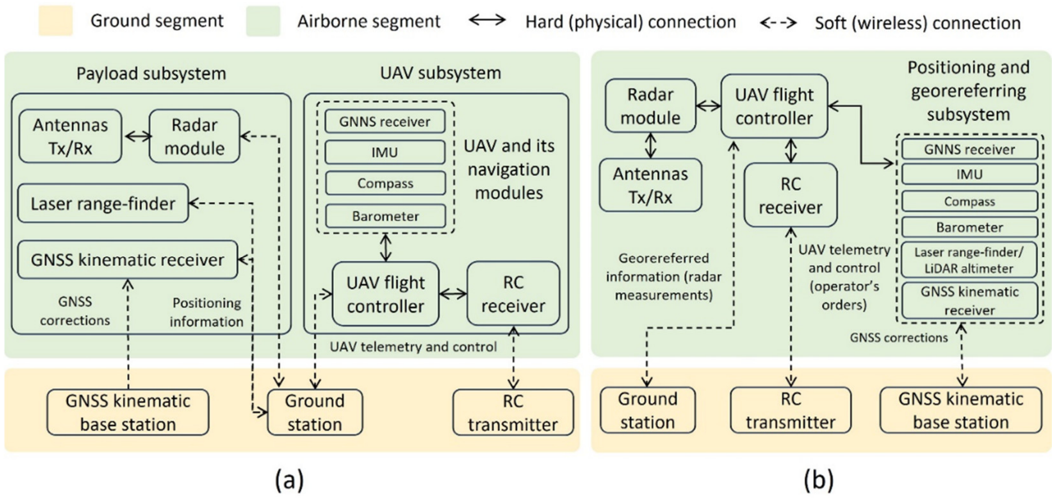

Figure 13. Payload assembly architectures in UAV-GPR systems: (**a**) Independent-payload and (**b**) Integrated-payload architectures. The principles were borrowed from [24,414], with the flowcharts being reconfigured.

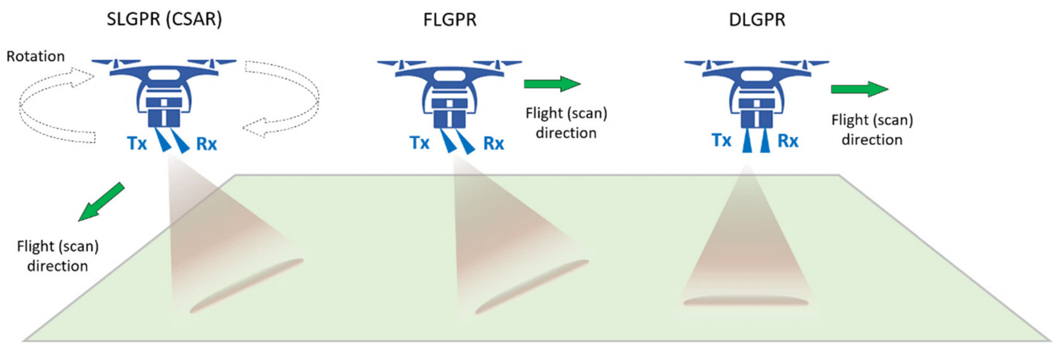

Figure 14. Observation modes in UAV-borne GPR survey (reconfigured based on [24]).

Down-looking GPR (DLGPR) configurations position antennas perpendicular to the surface, offering advantages in detecting deeper targets while potentially obscuring shallow ones due to reflections at the air-soil interface [24,409,415–417]. Forward-looking GPR (FLGPR) orientations minimize clutter by reducing reflections from the air-ground interface through oblique antenna incidence [24,416,418,419]. Side-looking GPR (SLGPR) configurations utilize tilted antennas to mitigate specular reflection from the air-soil interface, often moving laterally or following circular paths for data capture [392,420–423].

The scanning architecture choice depends on the target depth and scenario. FLGPR or SLGPR configurations suit shallow targets, minimizing clutter and enhancing detection. DLGPR systems excel for deeper targets, despite increased clutter, offering extended dynamic range. DLGPR and FLGPR imaging capabilities are compared, with FLGPR optimizing transverse magnetic wave penetration, while DLGPR provides enhanced resolution but increased clutter [413,415].

UAV-based GPR methods are divided into fully-airborne and semi-airborne setups. In fully airborne configurations, both antennas are on one UAV or split between two UAVs for transmission and reception. Semi-airborne setups involve a ground-based vehicle with the transmission antenna and a UAV with the reception antenna, operating in down-looking mode (see Figure 15).

Preprints.org (www.preprints.org) | NOT PEER-REVIEWED | Posted: 1 November 2024 doi:10.20944/preprints202411.0058.v1

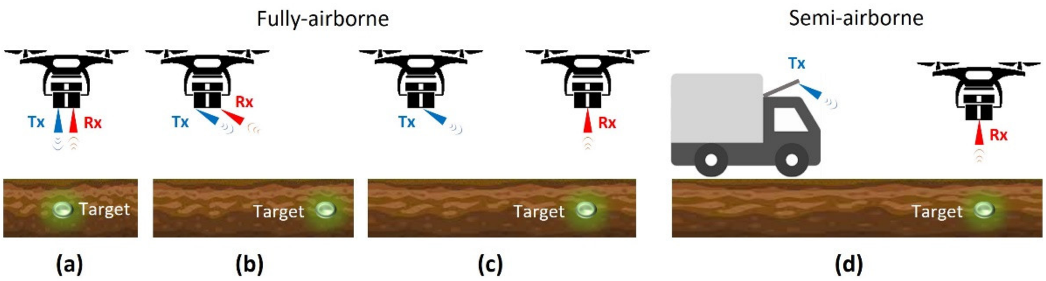

Figure 15. Fully/semi-airborne UAV-GPR: (**a, b**) Fully-airborne GPR using Tx and Rx onboard a single UAV operating in DLGPR and/or FLGPR modes, (**c**) Fully-airborne GPR using double UAVs, and (**d**) Semi-airborne scheme combining ground-based FLGPR and UAV-borne DLGPR (subfigure 'd' conceptualized from [415,424]).

Data processing in UAV-borne GPR, inspired by air-launched systems (e.g., [416]), involves two categories: Standard methods and Advanced algorithms (see Figure 16). Standard methods filter noise and correct motion errors, while advanced algorithms aim for high-resolution imaging [395].

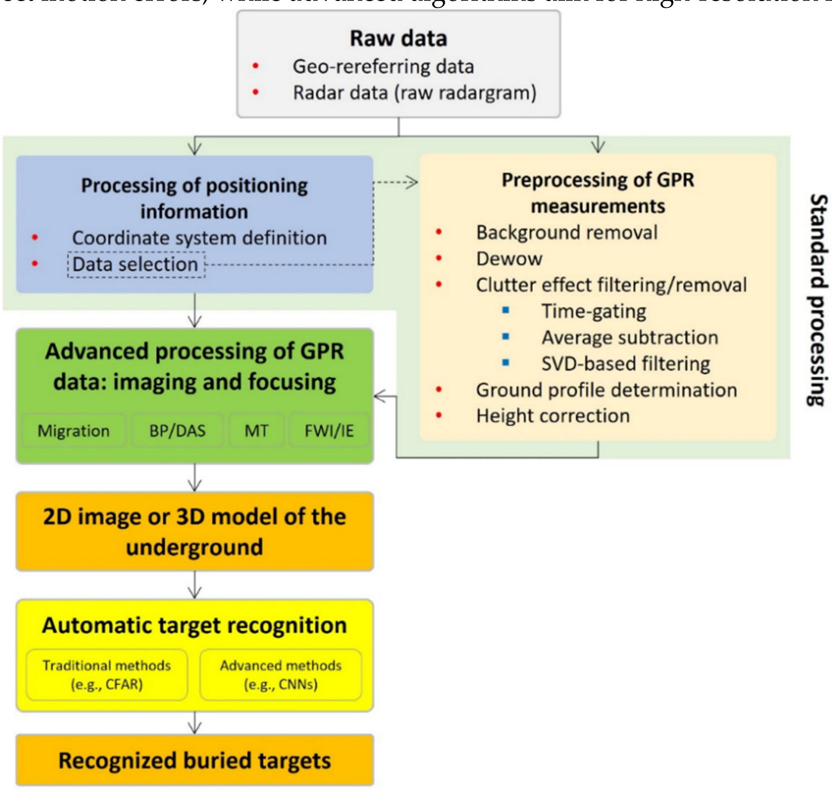

Figure 16. UAV-GPR data processing workflow (reconfigurated based on [24,425,426]).

In standard processing, data undergoes positioning management and preprocessing, including background removal [394], dewow [425], and clutter elimination. Techniques such as time-gating [427], average subtraction [428,429], and SVD-based filtering [430] are employed for clutter removal. Ground profile retrieval and height correction are also essential for data accuracy [426].

Focusing methods aim to enhance image resolution and interpretability by transforming diffraction hyperbolas into distinct bright spots [431,432]. Figure 17 depicts a UAV-mounted DL-GPR surveying a region of interest, capturing backscattered radar signals along its flight trajectory (Γ) across the angular frequency range $\Omega = [\omega_{min}, \omega_{max}]$. Each measured point (m) in the volumetric subsurface domain (D) is defined by the position vector $\vec{r}_m = x_m\hat{\imath} + y_m\hat{\jmath} + z_m\hat{k}$, representing various buried targets. The radar imaging process employs a simplified linear scattering model [433]. Equation (4) defines the scattered field at each point, with E_s representing the scattered field, E_i

denoting the incident field within domain D, χ(r) characterizing the unknown contrast function at any point r in D, G corresponding to Green's function, and k is the propagation constant.

$$E_s(r_m,\omega) = k^2 \iiint_D G(r_m,r,\omega)\, E_i(r,\omega)\chi(r)dr \qquad (4)$$

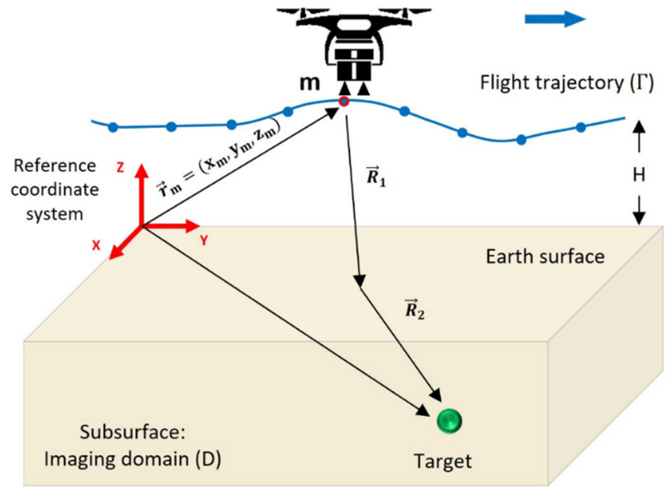

Figure 17. UAV-borne GPR imaging problem (reconfigured based on [417,434]).

Various algorithms were proposed to address the UAV-GPR imaging challenge, discussed as follows:

- *Migration Techniques:* Migration techniques like Kirchhoff's wave-equation and phase-shift migration (PSM) algorithms, commonly used in GPR, are applied in UAV-based GPR data processing for efficient analysis [435–439]. However, PSM requires data interpolation to a regular grid, which may pose challenges in irregular survey trajectories. Newer approaches like Piecewise SAR (P-SAR) address these limitations by considering the reflection and transmission coefficients of EM waves through diverse subsurface layers [440].
- *Back-projection (BP) or Delayand-and-Sum (DAS) Method:* UAV-based GPR often employs beam-forming or SAR-like Back-projection (BP) or Delay-and-Sum (DAS) methods due to non-rectilinear measurement trajectories [414]. They integrate radar echoes from the flight path to generate a reflectivity map using Equation (5).

$$\chi(r) = \int_\Gamma \int_\Omega E_s(r_m,\omega)\,(G(r_m,r,\omega)E_i(r,\omega)) * dr_m d\omega \qquad (5)$$

Where * represents the conjugation operator.

DAS involves summation of measurements at focal points across the target area [441]. Reflectivity ρ(r) is determined using scattered field data from N acquisition points and M discrete frequencies (Equation (6)), considering phase shifts from wave propagation (Equation (7)).

$$\rho(r) = \sum_{n=1}^{N}\sum_{m=1}^{M} E_s(r_n, f_m)\, e^{+j2(\phi_0+\phi_1)} \qquad (6)$$

$$\phi_0 + \phi_1 = k_{0,m}\|r' - r_n\|_2 \qquad (7)$$

Where r_n represents the position where the n-th measurement was acquired, f_m stands for the m-th discrete frequency (it is related to angular frequency), and ϕ_0 and ϕ_1 correspond to the phase shifts resulting from wave propagation. $k_{0,m}$ represents the free-space wavenumber for the m-th discrete frequency, while $r_{i,n}$ signifies the refraction point on the air-ground interface. The refraction point position ($r_{i,n}$) is determine using Snell's law [441].

DAS, suitable for irregular flight trajectories, are comparable to PSM techniques in performance for UAV-based GPR processing. They find application in various UAV-based GPR studies [392,394,397,406,414,428,429,442].

- *Microwave Tomography (MT):* MT focusing algorithms, using inverse filtering techniques, aim to solve the EM inverse scattering problem [432,443]. Unlike SAR-like methods, MT directly inverts the linear integral equation [24,395], addressing the imaging problem through a solution to the linear inverse problem (Equation (8)).

$$E_s = L_\chi \qquad (8)$$

Preprints.org (www.preprints.org) | NOT PEER-REVIEWED | Posted: 1 November 2024 doi:10.20944/preprints202411.0058.v1

$L: \mathcal{L}^2(D) \rightarrow \mathcal{L}^2(\Gamma \times \Omega)$ maps unknown to data space, both being square-integrable function spaces. Regularization, often through truncated SVD, stabilizes the ill-posed inverse problem [444]. MT's resilience to noise surpasses SAR-like methods, promoting its widespread adoption in UAV-based GPR imaging across various data collection scenarios and environments [24,395,425].

- *Full-waveform Inversion (FWI) or Integral Equation (IE)-based Methods:* FWI or IE GPR processing links radar backscattered fields with soil EM properties [404]. It estimates soil conductivity and permittivity by minimizing a cost function comparing the model and observed data [24]. In UAV-based GPR, FWI estimates soil permittivity, facilitating SWC mapping [395,406,434].

The mentioned methods reconstruct 2D images or 3D models of the subsurface and potential buried targets. These results can be refined using automatic target detection and recognition techniques, from traditional CFAR detectors [445] to advanced DL-based methods [446,447].

In this part the state-of-the-art UAV-compatible GPR antennas are reviewed. UAV-borne GPR systems rely on antennas to convert guided waves [424,448]. Modern UAV-compatible antennas include Vivaldi-like antennas, Archimedean spiral antennas, and helix antennas, as reported in [24,393,413,414,422], detailed in Table 18. Antennas in UAV-based GPR systems prioritize weight, dimensions, and radiation performance, often favoring horn-like or planar designs. These antennas are commonly featured in UAV-based GPR systems developed by [402,406,413,422,426,449,450]. Table 19 provides a comprehensive inspection of cutting-edge UAV-based radar and GPR systems, extracting detailed technical specifications from published works.

Table 18. Review of cutting-edge UAV-compatible GPR antennas.

Antenna	Specifications	Figures	References
Vivaldi Antennas	Vivaldi antennas, known for wide bandwidth and directional radiation, are popular in UAV applications due to their compact design and high performance. They come in two types: horn and planar. While horn antennas offer excellent radiofrequency characteristics, planar Vivaldi antennas are smaller and more suitable for UAV integration. Common models include IS-AV-0106G, TSA-600, and TC930-83 (dual-polarized Vivaldi), which provide versatility for different UAV-GPR applications.		[24,406,413,448,451]
Helix Antenna	Traditional cavity-backed antennas, like sinuous and helix types, offer high directivity and bandwidth but are limited by their weight, often >1 kg, making them less suitable for airborne GPR systems. Recent studies have addressed this issue by employing miniature helix antennas mounted on lightweight rotary-wing drones for UAV-based GPR surveys.	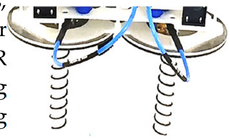	[24,414,451]
Spiral Antenna	A miniature spiral antenna has been successfully employed for GPR surveys in snow and ice. Archimedean spiral antennas, used in UAV systems with absorbing material, offer consistent gain and nearly frequency-independent input impedance. They may distort wideband signals, necessitating dechirping during post-processing to correct antenna group delay fluctuations across the frequency band.		[24,393]

Table 19. Review of the cutting-edge UAV-Radar/GPR systems.

Sys.	Platform	Specifications and Parameters	Purpose/Application	References
1	A drone non-specified type	Model/antenna: Linear array; Technology: Pulsed; Frequency: 100 MHz; Penetration ability: None	Environment monitoring	[396]
2	Small fixed-wing unmanned	Model/antenna: Linear array; Technology: FMCW; Frequency: Ka band; Measurement configuration: MIMO; Penetration ability: none	Environment monitoring	[397]

	airplane (ARTINO)			
3	The NASA SIERRA UAS	Model/antenna: Patch array; Technology: FMCW (LFM-CW SAR system); Frequency: 80–200 MHz; Penetration depth: A few meters	Sea ice experiments/ monitoring	[398]
4	Fixed-wing drone	Model/antenna: Log periodic; Technology: Pulsed; Frequency: 250-350 and 9,400-9,800 MHz; System type: InSAR; Penetration ability: None	Forest mapping and environmental monitoring	[399]
5	Fixed-wing drone	Model/antenna: Patch array; Technology: FMCW; Sensor: CW/FM SAR; Frequency: 5.3-9.65 GHz; Penetration ability: None	Environment monitoring	[400]
6	Quadcopter	Model/antenna: Horn and helix antennas; Technology: SFCW and Pulsed; Frequency: 350 MHz at 5 GHz; Penetration depth: A few cm for landmine and UXO detection task	Landmine and UXO detection; security and Earth observation	[401]
7	A mini multi-rotor UAV	Antenna: Two Logarithmic-periodic dipole antennas (LPDA) and one Raspberry Pi; Technology: Portable FMCW Radar; Frequency: 745 MHz with a bandwidth of 510 MHz; Penetration depth: <20 m; Processing technique: SAR; Flight height: 1.5 m	Archeological and geological applications	[452]
8	Rotary-wing hexacopter drone	Antanna: Vivaldi antipodal; Technology: Pulsed; Frequency: 1.5-6 GHz; Measurement config.: Bistatic config. with a 45° inclination; Penetration depth: <0.2 m; Radar technology: Bistatic SDR; Flight height: ~0.5 m	Landmine and UXO detection	[402,449]
9	Self-assembled DJI F550 hexacopter	Antenna: LPDA (two log-periodic PCB antennas named Ramsey LPY26); Technology: Pulsed Pulson P440; Frequency: 3.1-4.8 GHz; Measurement config.: Quasi monostatic in DL mode; Penetration depth: Not specified	Archaeology and infrastructure monitoring	[391]
10	DJI Matrice 600 Pro hexacopter	Antenna: Horn (1 Tx and 2 Rx orthogonal arranged antennas); Technology: FMCW; Architecture: SLGPR; Frequency: 1-4 GHz; Measurement configuration: Bistatic or quasi-monostatic; Flight height: 3-4 m; Radius: 7.5 m; Penetration depth: objects buried at 5 cm depth; SAR processing: polarimetric CSAR; GPR payload: Independent	Several: Infrastructure inspection, archaeological surveys, geological surveys, landmine and UXO detection	[405,421,422,442]
11	Octocopter (Kraken)	Antenna: One Spiral (Tx) and two Vivaldi (Rx) antennas with orthogonal arrangement and DL mode; Technology: Pulsed; Frequency: 0.95-6 GHz (M-Sequence UWB Radar); Penetration depth: A few meters (up to 1.7 m)	Snow and ice monitoring (retrieval of snowpack properties)	[393]

Preprints.org (www.preprints.org) | NOT PEER-REVIEWED | Posted: 1 November 2024 doi:10.20944/preprints202411.0058.v1

12	Multicopter: X8 model, made of 8 motors and 4 arms	Antenna: Hybrid horn-dipole antenna in DL mode; Technology: SFCW Planar R60 VNA; Frequency: 0.25-2.8 and 0.5-0.7 GHz; Measurement config.: Monostatic SFCW; Penetration depth: operation from 10-20 cm depth in bare agricultural fields; Flight height: 1-5 m	Soil moisture measurement (mapping)	[404]
13	Rotary-wing drone	Antenna: Ultrahigh frequency-UWB Radar; Technology: FMCW; Frequency: 0.5-3 GHz; Penetration depth: Not specified	Buried IEDs (e.g., landmine) detection	[453]
14	DJI Spreading Wings S1000+ octocopter	Antenna: Helix with DL mode; Tech.: Pulsed (Pulson P410); Frequency: 3.1-4.8 GHz; Measurement config.: Quasi-monostatic; Penetration depth: <1.5 m; SAR processing: able (DAS); Flight height: ~ 1.5 m	Landmine and UXO detection	[414]
15	DJI Matrice (M) 600 Pro	Frequency: 1.5 GHz; Survey velocity: 1.2 m/s; Flight height: ~1 m.	Snow hydrology	[454]
16	DJI Matrice 600 Pro hexacopter	Antenna: Hybrid Vivaldi-Horn antennas with DL mode; Technology: SFCW; Frequency: 0.55-2.7 GHz; Measurement config.: Bistatic or quasi-monostatic; Penetration depth: <0.5 m (objects in 0.2 m deep); Flight height: ≤ 0.5 m	Landmine detection	[406]
17	Octocopter	Antenna: UWB Vivaldi; Technology: SFCW; Frequency: 150-309 MHz; Penetration depth: < 3 m	Buried object detection	[455]
18	Rotary-wing mini-UAV	Antenna: 1 Tx antenna and 3 Rx with DL mode; Technology: SFCW; Frequency: 0.5-2 GHz; SAR processing: available; Flight height: ~ 1.5 m; Penetration depth: detection of objects 5-15 cm deep	Detection of buried objects (mines, explosive objects, and concealed targets)	[450]
19	Hexacopter	Antenn: Vivaldi patch antennas; Technology: FMCW; Frequency: 0.5-3 GHz; Architecture of Radar technology: SLGPR; Measurement config.: Bistatic or quasi-monostatic; SAR processing: available	Landmine detection	[392]
20	DJI Matrice 600 Pro hexacopter	Antenna: horn; Technology: FMCW; Frequency: 1-4 GHz; SAR processing: SLGPR-CSAR; Flight height and Radius: 2.5-5 m and 7.7 m; Penetration depth: < 1 m	Landmine detection	[422]
21	Hexacopter	Frequency: 3.1-4.8 GHz; Observation mode: DLGPR; Technology: Pulsed; SAR processing: MT; Flight height: 7.6-10.5 m	Archaeological surveys	[395,425]
22	Quadcopter (Cryocopter FOX)	Antenna: Dual Vivaldi; Configuration: DLGPR pseudo-random radar (1 Tx and 2 Rx); Frequency: 0.7-4.5 GHz; SAR processing: frequency-	Snow and ice studies (snow water equivalent content measurement and	[456,457]

doi:10.20944/preprints202411.0058.v1

		wavenumber for velocity estimation; Penetration depth: snow depth from 1.5 5.5 m.	snowpack properties retrieval)	
23	Ground vehicles and UAVs	Configuration: semi-airborne (an FL transmitter mounted on a ground vehicle and a drone-borne DL receiver); Frequency: 3.5-5.5 GHz; Survey schemes: Multimonostatic, multistatic, and multi-bistatic	Landmine and IED detection	[415]
24	DJI S1000 octocopter	Sensor: UWB SDRadar; Tx/Rx antennas: UWB Vivaldi; Frequency: 0.6-6 GHz; Flight height: ~2 m	Landmine detection	[458]
25	DJI M600 hexacopter	System name: IGPR-30; Central frequency: 0.4 GHz; Penetration depth: able to detect ice thickness of 6 m; Flight endurance: 30 min	Revealing morphology dynamics of ice cover	[459]
26	Hexacopter	Antenna: Gekko-80; Central frequency: 80 MHz; Data processing unit: RTS1600; Flight height: ~ 1 m	Mapping inland water bathymetry	[460]
27	DJI Matrix 600 Pro hexacopter	Antenna: COBRA plug-in SE-150 monostatic antenna; Frequency: 0.5-260 MHz; Technology: DLGPR pulsed radar; Measurement config.: Monostatic; Flight height: 6 m; Penetration depth: <40m; Vertical resolution: 0.27 m	Excavation area characterization	[408]
28	Quadcopter	Antenna: Horn; Technology: FMCW; Frequency: 5.4-6 MHz; System type: SAR; Penetration ability: None	A wide variety of applications	[461]
29	Unmanned helicopter	System name: SIR-3000 (GSSI); Antennas frequency: 400 MHz; Positioning devices: Onboard DGPS and Garmin handheld receiver	Feasibility test of UAV-based geophysical (EM and GPR) measurements	[462]
30	Hexacopter	Technology: SFCW (SDR-USRP); Frequency: 0.55-2.7 GHz (UWB principle); SAR processing: available	Anti-tank landmine detection	[463]
31	Hexacopter	System config.: array-based GPR SAR; Radar subsystem composition: UWB module with 1 Tx and 2 Rx, Frequency: 0.6-6 GHz	Enhanced buried threats (IEDs and landmines) detection	[464]
32	Hexacopter	Technology and architecture: DLGPR impulsed radar; SAR processing: available (PSM); Flight height: ~1.5 m; Frequency: C-band (3.1-5.1 GHz); Range resolution: 7.5 cm	Non-destructive identification of buried objects, such as landmines	[403,439]
33	Hexacopter	Antenna: UWB Vivaldi; Config.: DL pseudo-random radar (1 Tx and 2 Rx); Frequency: 0.6-6 GHz; SAR processing: available; Flight height: 1.2-2.3 m; Penetration depth: 0.25-1.5 m	Landmine and IED detection	[413,426,451]
34	Hexacopter	A GPR drone (GPRD) system with independent design: drone + GPR module	Search and rescue (SaR)	[412]
35	DJI M600 hexacopter	Antenna: *Drone it* GmbH cylindrical-shape radar antenna; Central frequency: 80 MHz; Survey endurance: 15 min	Archaeological prospection	[465]

36	Hexacopter	Technology: SLGPR FMCW; SAR processing: CSAR; Frequency: 1-4 GHz; Flight height: 2-4 m in 40 cm steps; Radius: 7.5 m; Penetration depth: <0.4 m	Detection of snow avalanche victims	[423]
37	DJI Spreading Wings S1000+	Radar technology: M-sequence UWB radar; Frequency: 0.1–6 GHz; Antenna: 2 UWB Vivaldi or two log-periodic antennas; Measurement configuration: Quasi-monostatic	Landmine and IED detection	[429]
38	Venture VFF-H01	Radar technology: Pulsed K2 IDS; Carrier frequency: 900 MHz; Antenna: Not specified; Measurement config.: Monostatic	Snow cover mapping	[407]
39	DJI Matrice 600/Pro	Radar technology: Pulsed Cobra Plug In GPR Cobra CBD Zond-12e; Frequency: 0.5–1000 MHz; Antenna: COBRA Plug-in SE-70 COBRA Plug-in SE-150 Cobra CBD 200/400/800; Measurement config.: Monostatic	A variety of potential applications	[417,466]
40	DJI Phantom 2	Radar technology: Pulsed PulsON P410; Frequency: 3.1-5.3 GHz; Antenna: Helix; Measurement configuration: Bistatic or quasi-monostatic in DL mode; Penetration ability: None	Radar imaging of the environment	[390]

In this part, applications of the UAV-borne GPR survey are reviewed. Table 20 provides an outline of the key application domains in which the previously discussed UAV-borne GPR prototypes find utility.

Table 20. Review of UAV-borne GPR applications.

Application	Descriptions	References
Buried Threats Object (Landmines, IDEs, and UXOs) Detection	UAV technology advancements have revolutionized buried threat object detection, particularly in landmine detection systems, where safety is paramount. UAVs offer faster scanning, access to remote areas, and increased safety by avoiding ground contact. This progress has made UAV- GPR surveys a primary tool for detecting buried threat objects.	[392,401–403,406,413–415,421,422,426,442,449–451,453,455,458,464]
Snow and Ice Studies	In snow regions, UAV-GPR surveys prove valuable. Researchers in Quebec, Canada, used UWB radar-equipped UAVs for snowpack data collection during 2020-2021, enhancing safety and coverage. They achieved precise estimation of Snow Water Equivalent by integrating airborne snow density and depth measurements with UAV-mounted UWB pseudo-noise radar. Additionally, a UAV-GPR system demonstrated promising results in snow depth measurement quality, resolution, and accuracy.	[393,454,456,457]
Archaeological Mapping	UAV-GPR is widely used in archaeology for non-invasive surveys. Researchers employ drone-borne surveys, showcasing GPR's detailed prospection capabilities. Despite shallow penetration depth, they achieve high resolution and develop imaging strategies using Mini-UAV sounders for robust 3D representations of investigated volumes.	[395,465]

Preprints.org (www.preprints.org) | NOT PEER-REVIEWED | Posted: 1 November 2024 doi:10.20944/preprints202411.0058.v1

Agricultural Applications	In precision farming, drones give detailed information about crops and soil but are more expensive than satellites. Research on GPR in farming and studies related to AI prepare the ground for combining GPR with drones in farming, showing great potential.	[467]
Soil Moisture Mapping	In Belgium's loess belt, UAV GPR mapped soil moisture across three fields, employing full-wave inverse modeling. This generated high-resolution soil moisture maps aligned with topography and aerial observations, showcasing UAV GPR's efficiency in rapid, precise soil moisture mapping for agriculture and environmental monitoring.	[404]
Bathymetry	UAV-GPR holds potential for inland water bathymetry, rivaling water-coupled GPR accuracy in Danish research. Despite constraints like minimum depth prerequisites (80-110 cm) and antenna height (~ 50 cm) above water, UAV-GPR surpassed sonar measurements in specific water body analyses.	[460]
SaR (e.g., victim detection)	A groundbreaking approach utilizes UAV-GPR for avalanche victim detection, eliminating the need for avalanche beacons. Operating as a SAR with FMCW modulation, the system was empirically validated in detecting buried mannequin torsos across varied snow conditions.	[423,468]

3.2.3. Unmanned Aerial LiDARgrammetry

A UAV-based LiDAR system consists of an aerial section with a UAV platform and sensors, including compact LiDAR, GNSS receiver, and IMU, while the ground section comprises a control terminal, flight control system, and ground control points [469–471]. LiDAR emits laser pulses to the Earth's surface, measuring distances based on pulse travel time. Integration of timing, LiDAR orientation, and location data determines point cloud accuracy [469]. For further details, interested readers are referred to [472,473].

When discussing UAV-compatible LiDAR sensors, it is important to distinguish between their mechanisms: Mechanical Scanning-based Sensors, Solid-state Technique-based Sensors, and Solid-state Hybrid Sensors [214,470,474,475]. The cutting-edge survey-grade UAV LiDAR sensors include Riegl VUX-1 UAV, Riegl mini VUX-1 UAV, Riegl mini VUX-1DL, Riegl VUX-240, Velodyne Puck LITE VLP-16, Quanergy M8, and Livox Mid-40. For more information, readers are referred to the relevant references (e.g., [470]).

To provide an overview of data processing and corrections in UAV-borne LiDARgrammetry, a comprehensive workflow comprising three main parts was proposed in [470]: point cloud production, point cloud refinement, and DEM generation. The initial phase involves calibration [476] and a combination of laser data and trajectory for initial point cloud generation [477]. Point cloud refinement includes removal of LiDAR point noises and outliers [478], as well as ground point classification [479]. Finally, DEM generation encompasses ground point filtering, followed by visualization and analysis. For further details, interested readers are referred to the provided reference.

Alongside the applications of UAV-borne LiDARgrammetry in urban mapping [28], this RS method are increasingly used in geoscientific studies for mapping inaccessible terrain and generating 3D models of geological features like cliffs, coasts, and volcanoes. This section explores UAV-borne LiDARgrammetry applications in geoscience, emphasizing its distinct utility from airborne LiDARgrammetry despite shared feasibility (Table 21). The applications mainly focus on capturing the surface geometry of the Earth's exterior.

Preprints.org (www.preprints.org) | NOT PEER-REVIEWED | Posted: 1 November 2024 doi:10.20944/preprints202411.0058.v1

Table 21. Review of UAV-LiDAR geoscientific applications.

Application	Descriptions	References
Fine-detailed digital terrain modeling	UAV-LiDAR is crucial for generating detailed DEMs essential for landform research. Eagle Geosciences used UAV surveys integrating magnetic and LiDAR technologies in the Miakadow project, aiding geological and structural mapping. Despite challenges like noise filtering, UAVs offer cost-effective and detailed DEM generation, foundational for various geophysical applications, including morphometric analysis and geomorphological mapping.	[480–485]
Fault zone mapping	Near Burwash Landing, YT, UAV-LiDAR was used to map fault zones and assess geothermal potential adjacent to the Eastern Denali fault (EDF). The system generated 30 cm resolution bare-earth DTMs of EDF segments, surpassing the resolution and canopy penetration of photogrammetric DSMs and DTMs. Analysis revealed dextral offsets along the fault, with the geothermal drill site strategically positioned at a minor releasing bend.	[486]
Landslide mapping and monitoring	UAV-LiDAR plays a crucial role in landslide mapping and monitoring, particularly in hazardous or inaccessible terrains like Ystalyfera, Wales. In this project, the technology penetrated dense vegetation, enabling the creation of high-resolution DTMs for detailed analysis. Regular surveys facilitated the understanding of landslide dynamics, with results integrated into risk maps for informed decision-making by the local community.	[487–495]
Land subsidence and fissure mapping	UAV-LiDAR has become instrumental in monitoring subsidence. Studies have validated its accuracy and compared its performance against traditional methods. Techniques like Digital Subsidence Models (DSuMs) and algorithms such as Local Flat Point Extraction (LFPE) have improved subsidence monitoring in mining areas. UAV-LiDAR has also been used to map road subsidence, highlighting its versatility beyond mining contexts. These findings underscore its importance in environmental management and risk mitigation efforts.	[30,495–500]
Geological mapping—geological structure measurement	LiDAR enables precise measurement of geological structures, crucial for assessing hazards like rockfalls and pre-earthquake indicators. These structures, including folds and fault planes, influence slope stability and rock mass behavior. Traditionally, studying rock discontinuities required manual methods, limiting assessments in hazardous areas. Integration of UAV-LiDAR allows remote 3D investigation of slopes, facilitating detailed structural measurements. Recent studies highlight its efficacy in geological structure analysis.	[501–505]
Geological mapping—geological catalogue production	Geological cataloging is vital in geological applications, including mapping, prospecting, and sampling. Laser scanners, especially when integrated with UAVs, are invaluable for creating detailed geological maps efficiently. They replace traditional surveying methods, reducing workload and enabling comprehensive database creation for mining areas.	[506]
Geological mapping—structural planes measurement	In geological surveys, assessing structural planes, especially extended faults, is challenging due to variations and topographical factors. 3D laser scanning has emerged as a valuable solution. The associated software features a fitting plane tool that determines structural plane occurrences, overcoming limitations of single-point	[506]

	measurements with geological compasses. This approach yields highly satisfactory results in determining geological structures.	
Glaciological investigations: characterization of ice morphology evolution	UAV-based technologies revolutionize the study of ice dolines, unique formations in remote ice streams. Researchers used specialized UAV systems to analyze the spatiotemporal evolution of an ice doline during Antarctic expeditions. They found that a collapse event in 2017 was induced by surface melting, with the doline growing in area and volume by early 2018. Photogrammetry proved cost-effective for large-scale surveys, while LiDAR excelled in detailing intricate ice features. They recommend an integrated approach for optimal performance.	[507]
Groundwater level mapping (hydrogeological studies)	In a geoscientific RS project, a UAV-LiDAR efficiently acquired piezometric information from traditional large-diameter wells. Tested in a coastal aquifer, it provided high vertical accuracies (RMSE of 5 cm), surpassing official DTMs in Spain. This method eliminated the need for laborious leveling work and proved effective for monitoring extensive or inaccessible areas, filling gaps in hydrogeological databases.	[508]
Topographic mapping for precision land leveling	An innovative method using a low-altitude UAV with LiDAR and PPK-GNSS technology mapped elevation variations on farmland in Henan Province, China. PPK-GNSS data ensured accurate ground survey point elevations, factoring installation height and nadir distance. Over 2,300 sets of mapping data per field were interpolated, yielding precise topographic maps for precision land leveling.	[509]
Volcanological studies	UAV-LiDAR is revolutionizing volcano mapping by providing precise topographic data collection, and overcoming obstacles like vegetation, gas emissions, or water bodies. This technology enhances RS capabilities, enabling comprehensive volcano studies.	[510]
Soil mapping—estimation of soil organic carbon (SOC)	Integrated UAV LiDAR/HS enhances soil mapping in forests. Using 40 HS visible and 101 LiDAR-derived variables, the study selected robust variables with the RRelieff algorithm to estimate forest SOC. Effective vegetation indices (VIs) included carotenoid reflectance index 2, non-linear index, and carotenoid reflectance index 1, while optimal LiDAR features were the canopy height model and DEM. Combining VI and LiDAR variables significantly improved estimation accuracy, with LiDAR features outperforming VIs.	[511,512]

3.3. UAV-Borne Geophysical Survey: Integrated Approach

Sensor integration and data fusion are hot topics in traditional geophysical methods, encompassing ground-based methods [513–524], as well as spaceborne and manned airborne methods [525–530]. Even fusion scenarios involving ground-based geophysical data and spaceborne imageries are explored [531]. Extending into UAV-based geophysical surveys, sensor integration and data fusion continue to be of interest. Table 22 offers a comprehensive review of studies in this domain.

Table 22. Sensor integration and data fusion in UAV-borne geophysical survey.

Integration/Fusion Method	Descriptions	References
Fusion of UAV Images and Magnetic Data	Integrating magnetic data with RGB, MS, and HS images enhances mineral exploration efficiency. This fusion combines RGB photogrammetry for surface analysis, HS imaging for mineral signatures, and magnetometers for detecting magnetic minerals. Likewise, integrating MS photogrammetry with magnetometry and radiometry enables detailed	[47,532,533]

Preprints.org (www.preprints.org) | NOT PEER-REVIEWED | Posted: 1 November 2024 doi:10.20944/preprints202411.0058.v1

	geological mapping and mineralization modeling. This integration produces a realistic model of magnetic mineralization within its geological context.	
Fusion of UAV Images and GPR Data	Integrating photogrammetry with GPR enhances quarry characterization and archaeological prospection. This fusion approach enables comprehensive subsurface investigation, aiding in identifying optimal areas for railway ballast production in quarries. Moreover, combining MS imagery and GPR survey facilitates precise archaeological anomaly detection and enables detailed 3D reconstruction, supporting interpretation in archaeological investigations.	[408,534]
Integration of UAV Magnetic and GPR Data	A UAV-based system combining GPR and magnetometer (MAG) for landmine detection was developed. Advanced methods like finite-difference time-domain simulations, SVD, Kirchhoff migration, and matched filtering were used for GPR signal identification and focusing. Magnetic dipole models with de-trending and spatial median filtering methods were employed for MAGs. Integration of the UAV GPR and MAG systems enabled experimental validation, crucial for parameter acquisition in landmine detection systems.	[535]
Integration of UAV Images with Magnetic and GPR Data	UAV images, magnetic, and GPR data were simultaneously surveyed at the Grumentum archaeological site. The integrated approach fused VNIR MS and infrared thermography with GPR and geomagnetic data, revealing Roman-era urban blocks and late antique/early medieval church features. The study underscores the potential and limitations of image fusion in enhancing archaeological insights, urging further experimentation across diverse case studies.	[536]
Integrated UAV Magnetic and Gravity Survey System	Integration of gravimetry with other methods is rare, but a system was developed involving the modification of a CH-4 medium-range drone. This work involved integrating a strapdown airborne gravimeter with a UAV-compatible aeromagnetic recorder, marking significant progress in this field.	[23]
Integration of UAV-borne Magnetic, Gamma Radiometric, and Spectrometric Surveys	The SibGIS UAS is a notable example of an integrated geophysical survey system, incorporating gamma radiometric, spectrometric, and magnetic surveys through integrated spectrometry-magnetometry systems. Experimental surveys demonstrate the feasibility of integrating gamma surveys with other geophysical surveys on a single UAV, offering rich information for geological and geophysical mapping.	[171]
Integration of UAV-borne Gamma and EM Survey Methods	TDEM offers promising capabilities to complement gamma surveys on UAVs. Lightweight TDEM systems can integrate seamlessly with gamma survey systems, enhancing geological information without significant impact on productivity or costs.	[347]
Integration of UAV-borne Magnetic and EM Survey Methods	In the Smart Exploration initiative, SGU and Uppsala University developed two UAV-based systems to jointly measure the total magnetic field and EM signals. Tests showed high-quality data collection with a strong signal-to-noise ratio. SGU applies the systems in projects like the FUTURE project, mapping and modeling mineral resources.	[537]
Integration of UAV-borne Magnetometry System and Ground-based TDEM System	A joint detection system was introduced, integrating UAVMAG and TDEM-Cart for UXO detection. The approach fuses magnetic field and EM data, yielding accurate positioning and enhanced UXO detection. Successful detection of various targets was demonstrated in field tests, with improved efficiency in cued survey mode and positioning accuracy of <10 cm achieved in joint interpretation.	[538]
Fusion of UAV photogrammetry and TLS Data for Geophysical Applications	UAV photogrammetry and laser scanning data fusion enhances geological mapping precision. It addresses the limitations of laser scanners by merging UAV photogrammetry point clouds, filling blind spots. Researchers employ algorithms like ICP for merging, retaining laser scanning precision. This method offers an approach for precise geological hazard assessment, yielding high-resolution DEMs for geomorphological studies.	[539,540]

 doi:10.20944/preprints202411.0058.v1

Integration of UAV LiDARgrammetry and Photogrammetry for the Characterization of Ice Morphology Evolution	During consecutive Chinese Antarctic expeditions in 2017 and 2018, specialized UAV systems were used for glaciological investigations. The UAV-LiDAR system, named Polar Elf, characterized the spatiotemporal evolution of an ice doline using multi-temporal and multi-modal UAV RS, employing an analysis of DTM of Differences.	[507]
Fusion of UAV HS-LiDAR, UAV MS-photogrammetry, and Ground-based LiDAR-digital Photography for Soil Mapping	UAV RS accurately maps soil nutrients, detecting changes in rangelands. Combining multispectral imagery and photogrammetry achieved 95% accuracy in bare soil cover classification. Fusion with LiDAR improved classification to 87%, revealing carbon and nitrogen loss post-fire. Insights into post-fire plant-soil-nutrient interactions were gained, favoring grasses in shrub-affected rangelands, illuminating soil surface carbon and nutrient dynamics.	[541]
Integration of UAV Imaging (MS and Thermal) and GPR for SWC Estimation	UAV-based data enhanced SWC predictions using thousands of GPR-derived SWC measurements pre and post precipitation events. The RF method predicted SWC in a central US vineyard employing MS and thermal UAV data. Combining thermal data with MS data notably improved SWC estimation accuracy, while reflectance data showed comparable significance to VIs.	[542]
Integration of UAV RGB, TIR, and MS Imageries for Biocrust Ecology Mapping	In Spain's dryland environment, UAV imagery mapped biocrust distribution. RGB and MS imagery delineated terrain attributes and ecosystem components. Thermal infrared data correlated with soil moisture levels. Analysis linked biocrusts to terrain attributes, highlighting apparent thermal inertia, elevation, and potential solar incoming radiation as influencers. Integrated UAV RS enhances dryland ecosystem understanding.	[543]
Integration of UAV Magnetometry and LiDARgrammetry	Eagle Geosciences applied UAV surveys with magnetic and LiDAR technologies for geological and structural mapping in the Miakadow project. Integrated data identified structures and favorable contexts for lithium-bearing pegmatite formations, enhancing insights alongside magnetic survey results.	[483]
Fusion of UAV and Satellite Imageries for Geoscientific Applications	Integrated satellite and UAV data enhance understanding of natural Earth processes. Researchers combine diverse data sources, such as historic aerial photographs and modern satellite imagery, to study archaeological sites and historical land use patterns. Additionally, studies use integrated approaches like D-InSAR and UAV photogrammetry to map surface subsidence in mining areas, providing insights into deformation patterns and land subsidence.	[243,244,247,544]

4. Discussions and Conclusions

This study presents a comprehensive review of cutting-edge geophysical survey techniques applicable via UAVs. To the best our knowledge, this is the first review to systematically compile and evaluate these methods. The reviewed methods encompass traditional geophysical approaches such as magnetometry, gravimetry, EM survey, GPR, gamma spectrometry, and radiometry, as well as non-geophysical methods like photogrammetry and LiDARgrammetry. The collected papers were categorized based on sensor type (active or passive) and another category explores sensor integration and data fusion concepts in UAV-based geophysical surveys.

While our study initially focused on geophysical survey methods, we also observed a significant rise in the use of UAV-based RS methods for various geoscientific applications, including geological mapping. The number of research conducted in these areas has increased dramatically, leading to the emergence of numerous UAV-based geophysical RS systems worldwide, with their numbers continuing to grow. This growing interest can be attributed to the cost-efficiency and effectiveness of UAVs, sensors, and related devices, which strike a balance between traditional RS-based (satellite-based and manned aerial) geophysical methods and ground-based methods. Additionally, the unmanned nature of UAVs reduces risks and challenges associated with traditional surveying

Preprints.org (www.preprints.org) | NOT PEER-REVIEWED | Posted: 1 November 2024 doi:10.20944/preprints202411.0058.v1

methods, making them a groundbreaking tool in geoscience and related disciplines, which usually deal with rough terrains.

Upon reviewing the literature, it became evident that UAV-based magnetometry and GPR survey methods are the most commonly utilized among standard geophysical survey techniques. In contrast, UAV-based gravimetry receives less attention due to the challenges associated with deploying gravimetric instruments on lightweight drones. Our observations also revealed a variety of options for UAV platform types suitable for unmanned aerial geophysical RS. Rotary-wing multi-rotor drones, known for their high maneuverability, are the most commonly used platform type, with unmanned helicopters showing similar applicability. Fixed-wing UAVs are better suited for surveying larger areas, and the addition of VTOL capability enhances their applicability in scenarios where traditional runways are unavailable. However, unmanned airships are not as favored as the other three drone types. Regarding sensors, magnetometry benefits from a wide variety of sensor types among standard geophysical methods, while photogrammetry, as a non-standard method, exhibits the most variability in this regard.

Discussions on applications revealed that mineral exploration, detection of near-surface ferrous objects (primarily in magnetometry and GPR), soil contamination mapping (mainly using gamma survey), and landslide/subsidence mapping (mainly in photogrammetry and LiDARgrammetry) were the most prevalent applications. While some methods such as photogrammetry and LiDARgrammetry were primarily used for spatial and geometric analysis of the Earth's crust (e.g., deformation mapping), others like MS imaging and HS spectroscopy found various applications related to soil mapping and analysis. Interestingly, certain applications such as mine or UXO detection were shared between different geophysical methods, illustrating the versatility of UAV-based geophysical techniques.

Although UAV-based RS is unmanned, it does not eliminate the need for fieldwork entirely. While certain survey methods like GPR require less fieldwork, others such as spectrometry/radiometry (for collecting ground-truth samples for laboratory analysis) and photogrammetry (for establishing ground control points) necessitate more extensive fieldwork. Thus, despite advancements, fieldwork remains essential in many UAV-borne survey methods.

The reviewed literature highlights significant attention to sensor integration in UAV-based geophysical RS. This integration involves deploying multiple geophysical sensors on a single or multiple UAV platforms. The benefits are evident, as it reduces costs, time, and human resources by enabling the collection of diverse data modalities in a single sortie. Notably, while individual sensors offer limited insights, combining data from multiple sensors can uncover novel perspectives not achievable with a single sensor. For instance, while an optical camera captures surface information, magnetometers delve into subsurface details, enhancing our understanding of the study area. However, sensor integration and data fusion pose several challenges, including differences in data modalities, acquisition time, misregistration, varying viewpoints, and spatial resolutions. These challenges become more pronounced when integrating UAV-based data with data from different sources such as space-borne, airborne, and ground-based platforms, as observed in our review. Consequently, careful consideration is essential when fusing different types of geophysical data to ensure accurate and meaningful results.

In conclusion, the reviewed studies unanimously affirm that UAV-borne geophysical RS methods offer comparable results to traditional ground-based and aerial methods. The cost-effectiveness and unmanned nature of UAVs, sensors, and related devices have revolutionized geoscience and related disciplines, bridging the gap between satellite-based, aerial, and ground-based geophysical methods. Despite significant progress, ongoing efforts are essential for further advancement in sensors, platforms, and methods. In terms of sensors, there is a need for more options capable of deployment on lightweight UAVs, similar to the variety available for traditional methods. Platforms are also evolving to become lighter and more endurance-focused, benefiting not only UAV-borne geophysical RS but also all domains of unmanned aerial RS. Methodologies require tailored development to suit UAV-specific requirements, such as customized processing methods.

The contribution of this review study extends to researchers across geoscience disciplines, providing a comprehensive and systematic overview of the possibilities offered by UAV RS in geophysical surveying. For instance, it aids researchers in selecting suitable methods, sensors, and UAV platforms for their desired applications. Overall, this review acts as a valuable resource, much like a mini-handbook, for the geoscience community.

Author Contributions: Conceptualization, F.S., F.D.J., and A.T.; methodology, F.S, F.D.J., and A.T.; software, A.T.; investigation, A.T.; data curation, A.T.; writing—original draft preparation, A.T.; writing—review and editing, F.S., F.D.J., and M.V.D.M; visualization, A.T.; supervision, F.S. and F.D.J.; project administration, F.S.; funding acquisition, F.D.J. All authors have read and agreed to the published version of the manuscript.

Funding: The APC was funded by the University of Twente.

Data Availability Statement: No new data were created or analyzed in this study. Data sharing is not applicable to this article.

Conflicts of Interest: The authors declare no conflicts of interest.

References

1. Windley, F.; Albritton, C. Earth sciences. *Encyclopedia Britannica* **2024**.
2. Lowrie, W.; Fichtner, A. *Fundamentals of geophysics*; Cambridge university press: 2020.
3. Fossen, H. *Structural geology*; Cambridge university press: 2016.
4. Vanicek, P.; Krakiwsky, E.J. *Geodesy: the concepts*; Elsevier: 2015.
5. Holt-Jensen, A. Geography: history and concepts. **2018**.
6. Hasan, M.; Shang, Y.; Yi, X.; Shao, P.; He, M. Determination of rock mass integrity coefficient using a non-invasive geophysical approach. *Journal of Rock Mechanics and Geotechnical Engineering* **2023**, *15*, 1426-1440.
7. Nabighian, M.N.; Grauch, V.; Hansen, R.; LaFehr, T.; Li, Y.; Peirce, J.W.; Phillips, J.D.; Ruder, M. The historical development of the magnetic method in exploration. *Geophysics* **2005**, *70*, 33ND-61ND.
8. Hinze, W.J.; Von Frese, R.R.; Von Frese, R.; Saad, A.H. *Gravity and magnetic exploration: Principles, practices, and applications*; Cambridge University Press: 2013.
9. Nabighian, M.N. *Electromagnetic methods in applied geophysics: Voume 1, theory*; Society of Exploration Geophysicists: 1988.
10. Xing, K.; Li, S.; Qu, Z.; Gao, M.; Gao, Y.; Zhang, X. UAV Time-Domain Electromagnetic System and a Workflow for Subsurface Targets Detection. *Remote Sensing* **2024**, *16*, 330.
11. McCay, A.T.; Harley, T.L.; Younger, P.L.; Sanderson, D.C.; Cresswell, A.J. Gamma-ray spectrometry in geothermal exploration: State of the art techniques. *Energies* **2014**, *7*, 4757-4780.
12. Conyers, L.B. *Ground-penetrating radar for archaeology*; Rowman & Littlefield: 2023.
13. Zhao, D.; Liu, X.; Wang, Z.; Gou, T. Seismic anisotropy tomography and mantle dynamics. *Surveys in Geophysics* **2023**, *44*, 947-982.
14. Perrone, A.; Lapenna, V.; Piscitelli, S. Electrical resistivity tomography technique for landslide investigation: A review. *Earth-Science Reviews* **2014**, *135*, 65-82.
15. Foley, C.P.; Leslie, K.; Binks, R.; Lewis, C.; Murray, W.; Sloggett, G.; Lam, S.; Sankrithyan, B.; Savvides, N.; Katzaros, A. Field trials using HTS SQUID magnetometers for ground-based and airborne geophysical applications. *IEEE transactions on applied superconductivity* **1999**, *9*, 3786-3792.
16. Siemon, B.; Costabel, S.; Voß, W.; Meyer, U.; Deus, N.; Elbracht, J.; Günther, T.; Wiederhold, H. Airborne and ground geophysical mapping of coastal clays in Eastern Friesland, Germany. *Geophysics* **2015**, *80*, WB21-WB34.
17. Planke, S.; Svensen, H.; Myklebust, R.; Bannister, S.; Manton, B.; Lorenz, L. Geophysics and remote sensing. *Physical Geology of Shallow Magmatic Systems: Dykes, Sills and Laccoliths* **2018**, 131-146.
18. Kaloshin, I.; Kuznetsov, V.; Skripachev, V.; Surovceva, I. Capabilities evaluation of spaceborne scientific equipment for geophysical applications. In Proceedings of the MATEC Web of Conferences, 2017; p. 01024.
19. Cummings, A.R.; McKee, A.; Kulkarni, K.; Markandey, N. The rise of UAVs. *Photogrammetric Engineering & Remote Sensing* **2017**, *83*, 317-325.
20. Stewart, R.R.; Chang, L.; Sudarshan, S.; Becker, A.; Alfataierge, E. A New Buzz in the Air: Seismic Drones. *Geophysical Society of Houston P* **2016**, *22*.
21. Levell, J.; Clow, A.; van Duijn, B.; Franken, P.; Campman, X. Drones for deploying seismic nodes: for those hard to reach places. In Proceedings of the 80th EAGE Conference and Exhibition 2018, 2018; pp. 1-5.
22. Zheng, Y.; Li, S.; Xing, K.; Zhang, X. Unmanned aerial vehicles for magnetic surveys: A review on platform selection and interference suppression. *Drones* **2021**, *5*, 93.
23. Luo, K.; Cao, J.; Wang, C.; Cai, S.; Yu, R.; Wu, M.; Yang, B.; Xiang, W. First unmanned aerial vehicle airborne gravimetry based on the CH-4 UAV in China. *Journal of Applied Geophysics* **2022**, *206*, 104835.

24. López, Y.Á.; Garcia-Fernandez, M.; Alvarez-Narciandi, G.; Andrés, F.L.-H. Unmanned aerial vehicle-based ground-penetrating radar systems: A review. *IEEE Geoscience and Remote Sensing Magazine* **2022**, *10*, 66-86.
25. Altfelder, S.; Preugschat, B.; Matos, M.; Kandzia, F.; Wiens, B.; Eshmuradov, O.; Kunze, C. Upscaling ground-based backpack gamma-ray spectrometry to spatial resolution of UAV-based gamma-ray spectrometry for system validation. *Journal of Environmental Radioactivity* **2024**, *273*, 107382.
26. Sudarshan, S.K.; Huang, L.; Li, C.; Stewart, R.; Becker, A.T. Seismic surveying with drone-mounted geophones. In Proceedings of the 2016 IEEE International Conference on Automation Science and Engineering (CASE), 2016; pp. 1354-1359.
27. Gerke, M. Developments in UAV-photogrammetry. *Journal of Digital Landscape Architecture* **2018**, *3*, 262-272.
28. Kovanič, Ľ.; Topitzer, B.; Peťovský, P.; Blišťan, P.; Gergeľová, M.B.; Blišťanová, M. Review of photogrammetric and Lidar applications of UAV. *Applied Sciences* **2023**, *13*, 6732.
29. Mohamad, N.; Ahmad, A.; Din, A.H.M. A Review of UAV Photogrammetry Application in Assessing Surface Elevation Changes. *Journal of Information System and Technology Management7* **2022**, 195-204.
30. Zheng, J.; Yao, W.; Lin, X.; Ma, B.; Bai, L. An accurate digital subsidence model for deformation detection of coal mining areas using a UAV-based LiDAR. *Remote Sensing* **2022**, *14*, 421.
31. Pranckutė, R. Web of Science (WoS) and Scopus: The titans of bibliographic information in today's academic world. *Publications* **2021**, *9*, 12.
32. Singh, V.K.; Singh, P.; Karmakar, M.; Leta, J.; Mayr, P. The journal coverage of Web of Science, Scopus and Dimensions: A comparative analysis. *Scientometrics* **2021**, *126*, 5113-5142.
33. Page, M.J.; McKenzie, J.E.; Bossuyt, P.M.; Boutron, I.; Hoffmann, T.C.; Mulrow, C.D.; Shamseer, L.; Tetzlaff, J.M.; Akl, E.A.; Brennan, S.E. The PRISMA 2020 statement: an updated guideline for reporting systematic reviews. *Bmj* **2021**, *372*.
34. Fingas, M.F.; Brown, C.E. Review of oil spill remote sensing. *Spill Science & Technology Bulletin* **1997**, *4*, 199-208.
35. Shahsavani, H. An aeromagnetic survey carried out using a rotary-wing UAV equipped with a low-cost magneto-inductive sensor. *International Journal of Remote Sensing* **2021**, *42*, 8805-8818.
36. Caron, R.M.; Samson, C.; Straznicky, P.; Ferguson, S.; Sander, L. Aeromagnetic surveying using a simulated unmanned aircraft system. *Geophysical Prospecting* **2014**, *62*, 352-363.
37. Gavazzi, B.; Le Maire, P.; Munschy, M.; Dechamp, A. Fluxgate vector magnetometers: A multisensor device for ground, UAV, and airborne magnetic surveys. *The Leading Edge* **2016**, *35*, 795-797.
38. Dai, J.; Huang, K.; Xu, C.; Zhang, S.; Yi, Z.; Meng, L.; Xiao, Q.; Liu, C.; Zhang, C. UAV magnetic measurement system for regional geomagnetic survey. In Proceedings of the IOP Conference Series: Earth and Environmental Science, 2019; p. 032019.
39. Jiang, D.; Zeng, Z.; Zhou, S.; Guan, Y.; Lin, T. Integration of an aeromagnetic measurement system based on an unmanned aerial vehicle platform and its application in the exploration of the Ma'anshan magnetite deposit. *IEEE Access* **2020**, *8*, 189576-189586.
40. Mu, Y.; Zhang, X.; Xie, W.; Zheng, Y. Automatic detection of near-surface targets for unmanned aerial vehicle (UAV) magnetic survey. *Remote Sensing* **2020**, *12*, 452.
41. Døssing, A.; Lima Simoes da Silva, E.; Martelet, G.; Maack Rasmussen, T.; Gloaguen, E.; Thejll Petersen, J.; Linde, J. A high-speed, light-weight scalar magnetometer bird for km scale UAV magnetic surveying: On sensor choice, bird design, and quality of output data. *Remote Sensing* **2021**, *13*, 649.
42. Lev, E.; Arie, M. Unmanned airborne magnetic and VLF investigations: Effective geophysical methodology for the near future. *Positioning* **2011**, *2011*.
43. Krishna, V.; Lima Simões da Silva, E.; Døssing, A. Experiments on magnetic interference for a portable airborne magnetometry system using a hybrid unmanned aerial vehicle (UAV). *Geoscientific Instrumentation, Methods and Data Systems* **2021**, *10*, 25-34.
44. Walker, B. Developing high sensitivity magnetometers for unmanned aircraft. **2016**.
45. AirBIRD & AirGRAD UAV Systems. Available online: https://www.gemsys.ca/uav-systems/
46. MagArrow II UAV-Enabled Magnetometer. Available online: https://www.geometrics.com/product/magarrow/
47. Jackisch, R.; Madriz, Y.; Zimmermann, R.; Pirttijärvi, M.; Saartenoja, A.; Heincke, B.H.; Salmirinne, H.; Kujasalo, J.-P.; Andreani, L.; Gloaguen, R. Drone-borne hyperspectral and magnetic data integration: Otanmäki Fe-Ti-V deposit in Finland. *Remote sensing* **2019**, *11*, 2084.
48. Zheng, Y.; Zhang, X.; Liu, H.; Xing, K. A Fast Position Estimation Method of Near-Surface Targets Detection for Unmanned Aerial Vehicle Magnetic Surveys. In Proceedings of the Advances in Intelligent Automation and Soft Computing, 2022; pp. 936-945.
49. Cherkasov, S.; Kapshtan, D. Unmanned aerial systems for magnetic survey. *Drones Appl* **2018**, 135-148.
50. Macharet, D.G.; Perez-Imaz, H.I.; Rezeck, P.A.; Potje, G.A.; Benyosef, L.C.; Wiermann, A.; Freitas, G.M.; Garcia, L.G.; Campos, M.F. Autonomous aeromagnetic surveys using a fluxgate magnetometer. *Sensors* **2016**, *16*, 2169.

51. Malehmir, A.; Dynesius, L.; Paulusson, K.; Paulusson, A.; Johansson, H.; Bastani, M.; Wedmark, M.; Marsden, P. The potential of rotary-wing UAV-based magnetic surveys for mineral exploration: A case study from central Sweden. *The Leading Edge* **2017**, *36*, 552-557.
52. Nikulin, A.; de Smet, T.S. A UAV-based magnetic survey method to detect and identify orphaned oil and gas wells. *The Leading Edge* **2019**, *38*, 447-452.
53. Parshin, A.V.; Morozov, V.A.; Blinov, A.V.; Kosterev, A.N.; Budyak, A.E. Low-altitude geophysical magnetic prospecting based on multirotor UAV as a promising replacement for traditional ground survey. *Geo-spatial information science* **2018**, *21*, 67-74.
54. Cunningham, M. Aeromagnetic surveying with unmanned aircraft systems. Carleton University, 2016.
55. Cunningham, M.; Samson, C.; Wood, A.; Cook, I. Aeromagnetic surveying with a rotary-wing unmanned aircraft system: A case study from a zinc deposit in Nash Creek, New Brunswick, Canada. *Pure and Applied Geophysics* **2018**, *175*, 3145-3158.
56. Parvar, K. Development and evaluation of unmanned aerial vehicle (UAV) magnetometry systems. Queen's University (Canada), 2016.
57. Acoustic and magnetic signatures management naval forces. Available online: https://www.ecagroup.com/en/defence-security/acoustic-magnetic-signatures-management-naval-forces/
58. Stoll, J.; Moritz, D. Unmanned aircraft systems for rapid near surface geophysical measurements. In Proceedings of the 75th EAGE Conference & Exhibition-Workshops, 2013; pp. cp-349-00062.
59. Flying robots in combination with onboard geophysical sensors. Available online: https://www.mgt-geo.com/technology.html/
60. Walter, C.; Braun, A.; Fotopoulos, G. Spectral analysis of magnetometer swing in high-resolution UAV-borne aeromagnetic surveys. In Proceedings of the 2019 IEEE Systems and Technologies for Remote Sensing Applications Through Unmanned Aerial Systems (STRATUS), 2019; pp. 1-4.
61. QIAO, Z.; MA, G.; ZHOU, W.; YU, P.; ZHOU, S.; WANG, T.; TANG, S.; DAI, W.; MENG, Z.; ZHANG, Z. Research on the comprehensive compensation of aeromagnetic system error of multi-rotor UAV. *Chinese Journal of Geophysics* **2020**, *63*, 4604-4612.
62. de Smet, T.S.; Nikulin, A.; Romanzo, N.; Graber, N.; Dietrich, C.; Puliaiev, A. Successful application of drone-based aeromagnetic surveys to locate legacy oil and gas wells in Cattaraugus county, New York. *Journal of Applied Geophysics* **2021**, *186*, 104250.
63. Nikulin, P.D.; deSmet, P.D.; Puliaiev, A.; Zhurakhov, V.; Fasullo, S.; Chen, G.; Spiegel, I.; Cappuccio, K. Automated UAS aeromagnetic surveys to detect MBRL unexploded ordnance. *The Journal of Conventional Weapons Destruction* **2020**, *24*, 13.
64. Le Maire, P.; Bertrand, L.; Munschy, M.; Diraison, M.; Géraud, Y. Aerial magnetic mapping with an unmanned aerial vehicle and a fluxgate magnetometer: A new method for rapid mapping and upscaling from the field to regional scale. *Geophysical prospecting* **2020**, *68*, 2307-2319.
65. Gailler, L.; Labazuy, P.; Régis, E.; Bontemps, M.; Souriot, T.; Bacques, G.; Carton, B. Validation of a new UAV magnetic prospecting tool for volcano monitoring and geohazard assessment. *Remote Sensing* **2021**, *13*, 894.
66. Pisciotta, A.; Vitale, G.; Scudero, S.; Martorana, R.; Capizzi, P.; D'Alessandro, A. A lightweight prototype of a magnetometric system for unmanned aerial vehicles. *Sensors* **2021**, *21*, 4691.
67. Walter, C.; Braun, A.; Fotopoulos, G. High-resolution unmanned aerial vehicle aeromagnetic surveys for mineral exploration targets. *Geophysical Prospecting* **2020**, *68*, 334-349.
68. Lum, C.; Rysdyk, R.; Pongpunwattana, A. Autonomous airborne geomagnetic surveying and target identification. In *Infotech@ Aerospace*; 2005; p. 7039.
69. Dion-Ortega, A. Abitibi Géophysique lance le tout premier drone magnétométrique. *Montreal, QC, Canada. Retrieved November* **2015**, *9*, 2015.
70. ScanEagle – Mini-UAV (Unmanned Aerial Vehicle). Available online: https://www.naval-technology.com/projects/scaneagle-uav/
71. Funaki, M.; Hirasawa, N. Outline of a small unmanned aerial vehicle (Ant-Plane) designed for Antarctic research. *Polar Science* **2008**, *2*, 129-142.
72. Funaki, M.; Higashino, S.-I.; Sakanaka, S.; Iwata, N.; Nakamura, N.; Hirasawa, N.; Obara, N.; Kuwabara, M. Small unmanned aerial vehicles for aeromagnetic surveys and their flights in the South Shetland Islands, Antarctica. *Polar Science* **2014**, *8*, 342-356.
73. Barnard, J. The use of unmanned aircraft in oil, gas and mineral exploration and production activities. In Proceedings of the Proceedings of the 23rd Bristol International UAV Systems Conference, 2008.
74. Glen, J.M.; Egger, A.E.; Ippolito, C.; Athens, N. Correlation of geothermal springs with sub-surface fault terminations revealed by high-resolution, UAV-acquired magnetic data. In Proceedings of the Proceedings of the 38th Workshop on Geothermal Reservoir Engineering: Stanford Geothermal Program Workshop Report SGP-TR-198, 2013; pp. 1233-1242.

75. Li, W.; Qin, X.; Gan, X. The IGGE UAV aero magnetic and radiometric survey system. In Proceedings of the Near Surface Geoscience 2014-20th European Meeting of Environmental and Engineering Geophysics, 2014; pp. 1-5.
76. Jackisch, R.; Lorenz, S.; Kirsch, M.; Zimmermann, R.; Tusa, L.; Pirttijärvi, M.; Saartenoja, A.; Ugalde, H.; Madriz, Y.; Savolainen, M. Integrated geological and geophysical mapping of a carbonatite-hosting outcrop in siilinjärvi, finland, using unmanned aerial systems. *Remote Sensing* **2020**, *12*, 2998.
77. UAV based magnetic survey system. Available online: https://radai.fi/uav-based-magnetic-survey-system/
78. JU, X.; NIU, H.-b.; GUO, H.; HAN, S.; WANG, Y.-z.; LÜ, C.; ZHENG, Q. Safety analysis and quality evaluation of the aeromagnetic measurement system of CH-4 UAV. *Progress in Geophysics* **2020**, *35*, 1565-1571.
79. Gradient Magnetometer UAV. Available online: https://www.gemsys.ca/wp-content/themes/gemsystems/pdf/GEM_MONARCH_UAV.pdf
80. Parshin, A.; Savin, A.; Morozov, V.; Badmayev, M.-J. Development of low-cost unmanned aerogeophysical system based on light VTOL aircraft. In Proceedings of the International Conference on Aviamechanical Engineering and Transport (AviaENT 2019), 2019; pp. 271-276.
81. Hansen, C.R.D. Magnetic signature characterization of a fixed-wing vertical take-off and landing (VTOL) unmanned aerial vehicle (UAV). 2018.
82. Industrial drone TD100 series. Available online: https://www.aeroexpo.online/prod/brican-flight-systems/product-181537-19049.html
83. Drone Magnetic Survey for Mineral Exploration in Gansu. Available online: https://www.jouav.com/case-study/drone-magnetic-survey-for-minning.html
84. Koyama, T.; Kaneko, T.; Ohminato, T.; Yanagisawa, T.; Watanabe, A.; Takeo, M. An aeromagnetic survey of Shinmoe-dake volcano, Kirishima, Japan, after the 2011 eruption using an unmanned autonomous helicopter. *Earth, Planets and Space* **2013**, *65*, 657-666.
85. Hashimoto, T.; Koyama, T.; Kaneko, T.; Ohminato, T.; Yanagisawa, T.; Yoshimoto, M.; Suzuki, E. Aeromagnetic survey using an unmanned autonomous helicopter over Tarumae Volcano, northern Japan. *Exploration Geophysics* **2014**, *45*, 37-42.
86. Pei, Y.; Liu, B.; Hua, Q.; Liu, C.; Ji, Y. An aeromagnetic survey system based on an unmanned autonomous helicopter: Development, experiment, and analysis. *International journal of remote sensing* **2017**, *38*, 3068-3083.
87. Eck, C.; Imbach, B. Aerial magnetic sensing with an UAV helicopter. *The International Archives of the Photogrammetry, Remote Sensing and Spatial Information Sciences* **2012**, *38*, 81-85.
88. GEM Hawk Available online: https://www.gemsys.ca/wp-content/themes/gemsystems/pdf/GEM_UAV_Solutions-GEM%20HAWK_Feb2017_web.pdf
89. Versteeg, R.; McKay, M.; Anderson, M.; Johnson, R.; Selfridge, B.; Bennett, J. Feasibility study for an Autonomous UAV-Magnetometer system. *Idaho National Laboratory* **2007**, 1-53.
90. McKay, M.D.; Anderson, M.O. *Development of Autonomous Magnetometer Rotorcraft for Wide Area Assessment*; Idaho National Lab.(INL), Idaho Falls, ID (United States): 2011.
91. Xi, Y.; Lu, N.; Zhang, L.; Li, J.; Zhang, F.; Wu, S.; Liao, G.; Beng, F.; Huang, W. Integration and application of an aeromagnetic survey system based on unmanned helicopter platform. *Geophysical and Geochemical Exploration* **2019**, *43*, 125-131.
92. ZHANG, F.-m.; WEN, J.-l.; ZHAO, X.-h.; FANG, W.-l. Development and application of aeromagnetic measurement system for unmanned helicopter. *Progress in Geophysics* **2019**, *34*, 1694-1699.
93. Xu, Q.; Liu, L.; Huang, S.; Wu, F. Research and test of compensation method for cesium optical pump aeromagnetic system of domestic UAV helicopter. *J. Nav. Inst. Aeronaut. Eng* **2020**, *35*, 141-148.
94. Noriega, G. Performance measures in aeromagnetic compensation. *The Leading Edge* **2011**, *30*, 1122-1127.
95. Dou, Z.; Han, Q.; Niu, X.; Peng, X.; Guo, H. An adaptive filter for aeromagnetic compensation based on wavelet multiresolution analysis. *IEEE Geoscience and Remote Sensing Letters* **2016**, *13*, 1069-1073.
96. Accomando, F.; Vitale, A.; Bonfante, A.; Buonanno, M.; Florio, G. Performance of two different flight configurations for drone-borne magnetic data. *Sensors* **2021**, *21*, 5736.
97. Leliak, P. Identification and evaluation of magnetic-field sources of magnetic airborne detector equipped aircraft. *IRE Transactions on Aerospace and Navigational Electronics* **1961**, 95-105.
98. Tuck, L. Characterization and compensation of magnetic interference resulting from unmanned aircraft systems. Carleton University, 2019.
99. Reeves, C. *Aeromagnetic surveys: principles, practice and interpretation*; Geosoft Washington (DC): 2005; Volume 155.
100. Samson, C.; Straznicky, P.; Laliberté, J.; Caron, R.; Ferguson, S.; Archer, R. Designing and building an unmanned aircraft system for aeromagnetic surveying. In Proceedings of the SEG International Exposition and Annual Meeting, 2010; pp. SEG-2010-1167.
101. Wood, A.; Cook, I.; Doyle, B.; Cunningham, M.; Samson, C. Experimental aeromagnetic survey using an unmanned air system. *The Leading Edge* **2016**, *35*, 270-273.

Preprints.org (www.preprints.org) | NOT PEER-REVIEWED | Posted: 1 November 2024 doi:10.20944/preprints202411.0058.v1

102. Nasyrtdinov, B.; Latipov, R.; Khassanov, D.; Popov, M.; Usmanov, A. Assessment of the impact of unmanned aerial vehicles with different engine types on the MMPOS-1 magnetometer. *International Multidisciplinary Scientific GeoConference: SGEM* **2020**, *20*, 475-482.
103. Anderson, D.; Pita, A. Geophysical surveying with georanger uav. In *Infotech@ Aerospace*; 2005; p. 6952.
104. Gee, J.S.; Cande, S.C.; Kent, D.V.; Partner, R.; Heckman, K. Mapping geomagnetic field variations with unmanned airborne vehicles. *Eos, Transactions American Geophysical Union* **2008**, *89*, 178-179.
105. Rodgers, M.; Malservisi, R.; Connor, C.; Wang, P.; Connor, L.; Van Alphen, R.; Vallée, M.; Hastings, M.S.; McIlrath, J. From beaches to volcanoes: UAV applications in geoscience using high-resolution topography and aerial magnetic surveys. In Proceedings of the AGU Fall Meeting Abstracts, 2019; pp. EP11C-2127.
106. Durfeld, R. *GEOPHYSICAL REPORT AIRBORNE MAGNETIC SURVEY ON THE BIRCH PROPERTY*; 2012.
107. Wells, M. Attenuating magnetic interference in a UAV system. Carleton University, 2008.
108. Forrester, R.W. Magnetic signature control strategies for an unmanned aircraft system. Carleton University, 2011.
109. LI, Z.; GAO, S.; WANG, X. New method of aeromagnetic surveys with rotorcraft UAV in particular areas. *Chinese Journal of Geophysics* **2018**, *61*, 3825-3834.
110. Calou, P.; Munschy, M. Airborne magnetic surveying with a drone and determination of the total magnetization of a dipole. *IEEE Transactions on Magnetics* **2020**, *56*, 1-9.
111. Hammack, R.; Veloski, G.; Schlagenhauf, M.; Lowe, R.; Zorn, A.; Wylie, L. Using drone-mounted geophysical sensors to map legacy oil and gas infrastructure. In Proceedings of the Unconventional Resources Technology Conference, 20–22 July 2020, 2020; pp. 3517-3528.
112. Nikulin, A.; de Smet, T.S. UAV-based aeromagnetic surveys for orphaned well location: Emerging best practices. *The Leading Edge* **2023**, *42*, 817-823.
113. de Smet, T.S.; Nikulin, A.; Balrup, N.; Graber, N. Successful integration of UAV aeromagnetic mapping with terrestrial methane emissions surveys in orphaned well remediation. *Remote Sensing* **2023**, *15*, 5004.
114. Luoma, S.; Zhou, X. Construction of a fluxgate magnetic gradiometer for integration with an unmanned aircraft system. *Remote Sensing* **2020**, *12*, 2551.
115. Fernandez Romero, S.; Morata Barrado, P.; Rivero Rodriguez, M.A.; Vazquez Yañez, G.A.; De Diego Custodio, E.; Michelena, M.D. Vector magnetometry using remotely piloted aircraft systems: An example of application for planetary exploration. *Remote Sensing* **2021**, *13*, 390.
116. Schmidt, V.; Becken, M.; Schmalzl, J. A UAV-borne magnetic survey for archaeological prospection of a Celtic burial site. *First Break* **2020**, *38*, 61-66.
117. Porras, D.; Carrasco, J.; Carrasco, P.; Alfageme, S.; Gonzalez-Aguilera, D.; Lopez Guijarro, R. Drone magnetometry in mining research. An application in the study of Triassic Cu–Co–Ni mineralizations in the Estancias Mountain Range, Almería (Spain). *Drones* **2021**, *5*, 151.
118. Kim, B.; Lee, S.; Park, G.; Cho, S.-J. Development of an unmanned airship for magnetic exploration. *Exploration Geophysics* **2021**, *52*, 462-467.
119. Efrem, R.; Coutu, A.; Saeedi, S. Suspended Magnetometer Survey for Mineral Data Acquisition with Vertical Take-off and Landing Fixed-wing Aircraft. *arXiv preprint arXiv:2402.11797* **2024**.
120. Parvar, K.; Braun, A.; Layton-Matthews, D.; Burns, M. UAV magnetometry for chromite exploration in the Samail ophiolite sequence, Oman. *Journal of Unmanned Vehicle Systems* **2017**, *6*, 57-69.
121. Cunningham, M.; Samson, C.; Laliberté, J.; Goldie, M.; Wood, A.; Birkett, D. Inversion of magnetic data acquired with a rotary-wing unmanned aircraft system for gold exploration. *Pure and Applied Geophysics* **2021**, *178*, 501-516.
122. Yoo, L.-S.; Lee, J.-H.; Lee, Y.-K.; Jung, S.-K.; Choi, Y. Application of a drone magnetometer system to military mine detection in the demilitarized zone. *Sensors* **2021**, *21*, 3175.
123. Kolster, M.E.; Wigh, M.D.; Lima Simoes da Silva, E.; Bjerg Vilhelmsen, T.; Døssing, A. High-speed magnetic surveying for unexploded ordnance using UAV systems. *Remote Sensing* **2022**, *14*, 1134.
124. Wang, Y.M.D., T. . Measuring Earth's gravity field from the air. Available online: https://eos.org/science-updates/measuring-earths-gravity-field-from-the-air (accessed on 10 January).
125. Francke, J. *Developing UAV - Mounted Geophysical Sensor Arrays*; July 2020.
126. Alkan, R.M.; Erol, S.; Ozulu, I.M.; Ilci, V. Accuracy comparison of post-processed PPP and real-time absolute positioning techniques. *Geomatics, Natural Hazards and Risk* **2020**, *11*, 178-190.
127. Nordin, A.F.; Jamil, H.; Isa, M.N.; Mohamed, A.; Tahir, S.H.; Musta, B.; Forsberg, R.; Olesen, A.V.; Nielsen, J.E.; Abd Majid, A.K. Geological mapping of Sabah, Malaysia, using airborne gravity survey. *Borneo Science, The Journal of Science and Technology* **2016**, *37*, 14-27.
128. Termens, A. airborne gravimetry. Available online: https://www.slideshare.net/slideshow/airborne-gravimetry/75797480 (accessed on May 9).
129. Dransfield, M. Requirements for airborne gravity gradient terrain corrections. *ASEG Extended Abstracts* **2010**, *2010*, 1-4.
130. Kaub, L.; Seruge, C.; Chopra, S.D.; Glen, J.M.; Teodorescu, M. Developing an autonomous unmanned aerial system to estimate field terrain corrections for gravity measurements. *The Leading Edge* **2018**, *37*, 584-591.

131. Dransfield, M.; Zeng, Y. Airborne gravity gradiometry: Terrain corrections and elevation error. *Geophysics* **2009**, *74*, I37-I42.
132. Navigation, I. iCORUS. Available online: https://www.imarnavigation.de/downloads/iCORUS.pdf
133. Jensen, T.E.; Olesen, A.V.; Forsberg, R.; Olsson, P.-A.; Josefsson, Ö. New results from strapdown airborne gravimetry using temperature stabilisation. *Remote sensing* **2019**, *11*, 2682.
134. Grover, G.; Forsberg, R.; Jensen, T.; Müller, F.; Hoss, M.; Bourne, T.; Wright, O. World's First Fixed Wing UAV Gravity Data Collection Flight. Less cost & less carbon. In Proceedings of the Second EAGE Workshop on Unmanned Aerial Vehicles, 2021; pp. 1-3.
135. Lin, C.; Chiang, K.; Kuo, C. Integration of INS and GNSS for gravimetric application with UAS. *The International Archives of the Photogrammetry, Remote Sensing and Spatial Information Sciences* **2018**, *42*, 263-268.
136. Middlemiss, R.P.; Bramsiepe, S.G.; Douglas, R.; Hough, J.; Paul, D.J.; Rowan, S.; Hammond, G.D. Field tests of a portable MEMS gravimeter. *Sensors* **2017**, *17*, 2571.
137. Passey, E.; Hammond, G.; Bramsiepe, S.; Prasad, A.; Middlemiss, R.; Paul, D.; Walker, R.; Noack, A.; Anastasiou, K. Development of a MEMs gravimeter for drone-based field surveys. In Proceedings of the EGU General Assembly Conference Abstracts, 2020; p. 20906.
138. Byrne, M. New Gravimeter Technology Will Enable High-Res Drone-Based Gravity Mapping. Available online: https://www.vice.com/en/article/8q8xak/gravimeter-technology-drone-based-gravity-mapping-geologists-volcano-detection.
139. Pike, W.; Standley, I.; Calcutt, S.; Mukherjee, A. A broad-band silicon microseismometer with 0.25 NG/rtHz performance. In Proceedings of the 2018 IEEE Micro Electro Mechanical Systems (MEMS), 2018; pp. 113-116.
140. Tang, S.; Liu, H.; Yan, S.; Xu, X.; Wu, W.; Fan, J.; Liu, J.; Hu, C.; Tu, L. A high-sensitivity MEMS gravimeter with a large dynamic range. *Microsystems & nanoengineering* **2019**, *5*, 45.
141. Du, Z.; Topham, A.; Lofts, J.J.C.; Seshia, A.A. Brazil Pre-Salt, Santos Basin: Feasibility study for the application of borehole gravity to improve reservoir monitoring. In Proceedings of the Offshore Technology Conference, 2020; p. D031S034R001.
142. Zhao, C.; Pandit, M.; Sobreviela, G.; Steinmann, P.; Mustafazade, A.; Zou, X.; Seshia, A. A resonant MEMS accelerometer with 56ng bias stability and 98ng/Hz 1/2 noise floor. *Journal of Microelectromechanical Systems* **2019**, *28*, 324-326.
143. Anastasiadis, K. Gravimeters prospecting for aerial surveys using drones. **2016**.
144. Middlemiss, R.; Samarelli, A.; Paul, D.; Hough, J.; Rowan, S.; Hammond, G. Measurement of the Earth tides with a MEMS gravimeter. *Nature* **2016**, *531*, 614-617.
145. RG-1 REMOTE OPERATING GRAVITY METER. Available online: https://scintrexltd.com/product/rg-1-remote-operating-gravity-meter/
146. Deurloo, R.; Bastos, M.; Geng, Y.; Yan, W. Evaluation of low-and medium-cost IMUs for Airborne Gravimetry with UAVs. In Proceedings of the AGU Fall Meeting Abstracts, 2011; pp. G12A-01.
147. Tokue, S.; Ogura, Y.; Morikawa, H.; Matsuda, S.; Yokoi, I.; Suda, H.; Kima, S.; Kusumoto, S.; Noguchi, T.; Komazawa, M. Developments of airborne survey on an unmanned helicopter for quick observation of gravity and magnetic. In Proceedings of the 11th International Conference on Structural Safety and Reliability, ICOSSAR 2013, 2013; pp. 1363-1368.
148. Morikawa, H.; Tokue, S.; Ogura, Y.; Matsuda, S.; Saeki, M.; Ohsawa, E.; Suzuki, T.; Yokoi, I.; Kusumoto, S.; Noguchi, T. A development of airborne survey of gravity and magnetics on an unmanned helicopter and its data processing. In Proceedings of the Japan Geoscience Meeting, 2013.
149. Becker, D. *Advanced calibration methods for strapdown airborne gravimetry*; Technische Universität Darmstadt: 2016.
150. DRONES FOR GEOPHYSICS TAKING OFF. Available online: https://brasilminingsite.com.br/drones-for-geophysics-taking-off/
151. Lin, C.-A. The Performance Analysis of an UAV Borne Vector Gravimetry System. In Proceedings of the Proceedings of the 29th International Technical Meeting of the Satellite Division of The Institute of Navigation (ION GNSS+ 2016), 2016; pp. 857-871.
152. Ball, M. Aurora Centaur UAS Used in NOAA Gravity Measurement Program. Available online: https://www.unmannedsystemstechnology.com/2017/03/aurora-uas-centaur-used-noaa-gravity-measurement-program/ (accessed on 28 Mar).
153. Alaoui-Sosse, S.; Pastor, P.; Durand, P.; Medina, P.; Gavart, M.; Darrozes, J.; Lothon, M. Development and qualification of instrumented unmanned planes for turbulence observations in the atmospheric surface layer. **2018**.
154. Hammond, G. *MEMS Gravimeters*; Institute for Gravitational Research SUPA, University of Glasgow: 2018.
155. Wang, Y.; Cao, J.; Yu, R.; Xiang, W. Airborne gravimetry and error compensation based on the undulating flight of UAV. In Proceedings of the International Conference on Mechanical Engineering, Measurement Control, and Instrumentation, 2021; pp. 435-445.

156. BAS-200 of Russian Helicopters was the first ever UAV at MAKS-2021. Available online: https://www.helihub.com/2021/07/26/bas-200-of-russian-helicopters-was-the-first-ever-uav-at-maks-2021/ (accessed on 26 Jul).
157. New BAS-200 Drone for Geophysical Explorations in Arctic. Available online: https://www.helihub.com/2022/02/21/new-bas-200-drone-for-geophysical-explorations-in-arctic/ (accessed on 21 Feb).
158. Sediles Martinez, A.J. Unmanned Aerial Vehicles (UAVs) As a Non-invasive Optimization Tool for the Exploration and Management of Raw Materials. **2022**.
159. DroneSOM – Drone Geophysics and Self-Organizing Maps. Available online: https://www.gtk.fi/en/research-project/dronesom/
160. DroneSOM – more precise, efficient, and environmentally friendly mineral exploration. Available online: https://dronesom.com/
161. Koomans, R.; Limburg, H. Drone-borne gamma-ray spetrometry–a dream come true. **2020**.
162. Limburg, H.; van der Veeke, S.; Koomans, R. Towards drone-borne gammaray mapping of soils. *First Break* **2019**, *37*, 55-61.
163. Van Der Veeke, S.; Koomans, R.; Van Egmond, F.; Limburg, J. A drone as platform for airborne gamma-ray surveys to characterize soil and monitor contaminations. In Proceedings of the 24th European Meeting of Environmental and Engineering Geophysics, 2018; pp. 1-5.
164. Royo, P.; Vargas, A.; Guillot, T.; Saiz, D.; Pichel, J.; Rabago, D.; Duch, M.A.; Grossi, C.; Luchkov, M.; Dangendorf, V. The Mapping of Alpha-Emitting Radionuclides in the Environment Using an Unmanned Aircraft System. *Remote Sensing* **2024**, *16*, 848.
165. Gabrlik, P.; Lazna, T. Simulation of gamma radiation mapping using an unmanned aerial system. *IFAC-PapersOnLine* **2018**, *51*, 256-262.
166. Geelen, S.; Camps, J.; Olyslaegers, G.; Ilegems, G.; Schroeyers, W. Radiological surveillance using a fixed-wing uav platform. *Remote Sensing* **2022**, *14*, 3908.
167. Koomans, R.L., Han; van der Veeke, Steven. THE USE OF GAMMA-RAY SPECTROMETERS IN AIRBORNE SURVEYS: Soil Mapping with Drones. **2022**.
168. MacFarlane, J.; Payton, O.; Keatley, A.; Scott, G.; Pullin, H.; Crane, R.; Smilion, M.; Popescu, I.; Curlea, V.; Scott, T. Lightweight aerial vehicles for monitoring, assessment and mapping of radiation anomalies. *Journal of environmental radioactivity* **2014**, *136*, 127-130.
169. van der Veeke, S.; Limburg, J.; Koomans, R.; Söderström, M.; van der Graaf, E. Optimizing gamma-ray spectrometers for UAV-borne surveys with geophysical applications. *Journal of Environmental Radioactivity* **2021**, *237*, 106717.
170. Erdi-Krausz, G.; Matolin, M.; Minty, B.; Nicolet, J.; Reford, W.; Schetselaar, E. *Guidelines for radioelement mapping using gamma ray spectrometry data: also as open access e-book*; International Atomic Energy Agency (IAEA): 2003.
171. Parshin, A.; Morozov, V.; Snegirev, N.; Valkova, E.; Shikalenko, F. Advantages of gamma-radiometric and spectrometric low-altitude geophysical surveys by unmanned aerial systems with small scintillation detectors. *Applied Sciences* **2021**, *11*, 2247.
172. Kazemeini, M.; Vargas, J.; Barzilov, A.; Yim, W. Gamma ray measurements using unmanned aerial systems. *Use of Gamma Radiation Techniques in Peaceful Applications* **2019**, 85.
173. Borbinha, J.; Romanets, Y.; Teles, P.; Corisco, J.; Vaz, P.; Carvalho, D.; Brouwer, Y.; Luís, R.; Pinto, L.; Vale, A. Performance analysis of geiger–müller and cadmium zinc telluride sensors envisaging airborne radiological monitoring in NORM sites. *Sensors* **2020**, *20*, 1538.
174. Briechle, S.; Sizov, A.; Tretyak, O.; Antropov, V.; Molitor, N.; Krzystek, P. UAV-based detection of unknown radioactive biomass deposits in Chernobyl's Exclusion Zone. *The International Archives of the Photogrammetry, Remote Sensing and Spatial Information Sciences* **2018**, *42*, 163-169.
175. Šálek, O.; Matolín, M.; Gryc, L. Mapping of radiation anomalies using UAV mini-airborne gamma-ray spectrometry. *Journal of environmental radioactivity* **2018**, *182*, 101-107.
176. Parshin, A.; Grebenkin, N.; Morozov, V.; Shikalenko, F. Research Note: First results of a low-altitude unmanned aircraft system gamma survey by comparison with the terrestrial and aerial gamma survey data. *Geophysical prospecting* **2018**, *66*, 1433-1438.
177. Parshin, A.; Budyak, A.; Chebokchinov, I.; Sapunov, V.; Bulnayev, A.; Morozov, V. Complex UAS-geophysical surveys at the first stages of geological prospecting: Case in the western Sayan (Russia). In Proceedings of the First EAGE Workshop on Unmanned Aerial Vehicles, 2019; pp. 1-5.
178. Kurvinen, K.; Smolander, P.; Pöllänen, R.; Kuukankorpi, S.; Kettunen, M.; Lyytinen, J. Design of a radiation surveillance unit for an unmanned aerial vehicle. *Journal of environmental radioactivity* **2005**, *81*, 1-10.
179. Heikonen, K.; Saaristo, T. You and Your TETRA RADIO, TETRA as a Tool for Public Safety. **2002**.
180. Kunze, C.; Preugschat, B.; Arndt, R.; Kandzia, F.; Wiens, B.; Altfelder, S. Development of a UAV-based gamma spectrometry system for natural radionuclides and field tests at central Asian Uranium legacy sites. *Remote Sensing* **2022**, *14*, 2147.

181. Widodo, S.; Abimanyu, A.; Apribra, R. Development of drone mounted aerial gamma monitoring system for environmental radionuclide surveillance in BATAN. In Proceedings of the Journal of Physics: Conference Series, 2020; p. 012126.
182. Van Egmond, F.; Van Der Veeke, S.; Knotters, M.; Koomans, R.; Walvoort, D.; Limburg, J. *Mapping soil texture with a gamma-ray spectrometer: comparison between UAV and proximal measurements and traditional sampling: validation study*; 2352-2739; WOT Natuur & Milieu: 2018.
183. Pirttijärvi, M.; Oy, R. Radai's UAV based radiometric measurements at Rautuvaara mine in Kolari. *Radai Survey Report (http://Www. Radai. Fi)* **2016**.
184. Hendriks, P.; Limburg, J.; De Meijer, R. Full-spectrum analysis of natural γ-ray spectra. *Journal of Environmental Radioactivity* **2001**, *53*, 365-380.
185. Grasty, R.; Glynn, J.; Grant, J. The analysis of multichannel airborne gamma-ray spectra. *Geophysics* **1985**, *50*, 2611-2620.
186. Minty, B.R.; McFadden, P.; Kennett, B.L. Multichannel processing for airborne gamma-ray spectrometry. *Geophysics* **1998**, *63*, 1971-1985.
187. Van der Graaf, E.; Limburg, J.; Koomans, R.; Tijs, M. Monte Carlo based calibration of scintillation detectors for laboratory and in situ gamma ray measurements. *Journal of environmental radioactivity* **2011**, *102*, 270-282.
188. Billings, S.D.; Minty, B.R.; Newsam, G.N. Deconvolution and spatial resolution of airborne gamma-ray surveys. *Geophysics* **2003**, *68*, 1257-1266.
189. Pfitzner, K.; Ryan, B.; Martin, P. *Airborne gamma survey of the Sleisbeck mine area*; January 2003.
190. Kock, P.; Samuelsson, C. Comparison of airborne and terrestrial gamma spectrometry measurements-evaluation of three areas in southern Sweden. *Journal of Environmental Radioactivity* **2011**, *102*, 605-613.
191. Xia, J.; Song, B.; Gu, Y.; Li, Z.; Xu, J.; Ge, L.; Zhang, Q.; Zeng, G.; Liu, Q.; Yang, X. Application of advanced spectral-ratio radon background correction in the UAV-borne gamma-ray spectrometry. *Nuclear Engineering and Technology* **2023**, *55*, 2927-2934.
192. Van der Veeke, S.; Limburg, J.; Koomans, R.; Söderström, M.; de Waal, S.; van der Graaf, E. Footprint and height corrections for UAV-borne gamma-ray spectrometry studies. *Journal of Environmental Radioactivity* **2021**, *231*, 106545.
193. Lowdon, M.; Martin, P.G.; Hubbard, M.W.; Taggart, M.P.; Connor, D.T.; Verbelen, Y.; Sellin, P.; Scott, T.B. Evaluation of scintillator detection materials for application within airborne environmental radiation monitoring. *Sensors* **2019**, *19*, 3828.
194. Woodbridge, E.; Connor, D.T.; Verbelen, Y.; Hine, D.; Richardson, T.; Scott, T.B. Airborne gamma-ray mapping using fixed-wing vertical take-off and landing (VTOL) uncrewed aerial vehicles. *Frontiers in Robotics and AI* **2023**, *10*.
195. Prokesch, M. CdZnTe for gamma and x-ray applications. *Solid-state radiation detectors: Technology and applications* **2015**, 17-48.
196. Aleotti, J.; Micconi, G.; Caselli, S.; Benassi, G.; Zambelli, N.; Bettelli, M.; Calestani, D.; Zappettini, A. Haptic teleoperation of UAV equipped with gamma-ray spectrometer for detection and identification of radio-active materials in industrial plants. *Factories of the Future: The Italian Flagship Initiative* **2019**, 197-214.
197. Hartman, J.; Barzilov, A.; Novikov, I. Remote sensing of neutron and gamma radiation using aerial unmanned autonomous system. In Proceedings of the 2015 IEEE nuclear science symposium and medical imaging conference (NSS/MIC), 2015; pp. 1-4.
198. Barzilov, A.; Kazemeini, M. Unmanned Aerial System Integrated Sensor for Remote Gamma and Neutron Monitoring. *Sensors* **2020**, *20*, 5529.
199. Molnar, A.; Domozi, Z.; Lovas, I. Drone-based gamma radiation dose distribution survey with a discrete measurement point procedure. *Sensors* **2021**, *21*, 4930.
200. Sanada, Y.; Torii, T. Aerial radiation monitoring around the Fukushima Dai-ichi nuclear power plant using an unmanned helicopter. *Journal of environmental radioactivity* **2015**, *139*, 294-299.
201. Parshin, A.; Gatilov, M.; Davidenko, Y.; Bashkeev, A.; Snegirev, N.; Milgunov, A. Using the "triad" of UAV-TEM, UAV-magnetic prospecting and UAV-gamma-spectrometry: Case of prospecting for blind ore deposits. In Proceedings of the NSG2022 3rd Conference on Airborne, Drone and Robotic Geophysics, 2022; pp. 1-5.
202. Mochizuki, S.; Kataoka, J.; Tagawa, L.; Iwamoto, Y.; Okochi, H.; Katsumi, N.; Kinno, S.; Arimoto, M.; Maruhashi, T.; Fujieda, K. First demonstration of aerial gamma-ray imaging using drone for prompt radiation survey in Fukushima. *Journal of Instrumentation* **2017**, *12*, P11014.
203. UAV Radiation Monitoring Solutions. Available online: https://www.aretasaerial.com/sites/default/files/Aretas-Aerial-UAV-Radiation-Monitoring-030817.pdf
204. Čerba, Š.; Lüley, J.; Vrban, B.; Osuský, F.; Nečas, V. Unmanned radiation-monitoring system. *IEEE Transactions on Nuclear Science* **2020**, *67*, 636-643.
205. Gong, P.; Tang, X.-B.; Huang, X.; Wang, P.; Wen, L.-S.; Zhu, X.-X.; Zhou, C. Locating lost radioactive sources using a UAV radiation monitoring system. *Applied radiation and isotopes* **2019**, *150*, 1-13.

206. Molnar, A. Three-Dimensional Detection of Gamma Radiation and Polluting Gases Using Quadrocopters. *Herald of Dagestan State Technical University Technical Sciences* **2020**, *47*, 102-116.
207. Pöllänen, R.; Toivonen, H.; Peräjärvi, K.; Karhunen, T.; Ilander, T.; Lehtinen, J.; Rintala, K.; Katajainen, T.; Niemelä, J.; Juusela, M. Radiation surveillance using an unmanned aerial vehicle. *Applied radiation and isotopes* **2009**, *67*, 340-344.
208. Preugschat, B.; Ibs-von Seht, M.; Kunze, C.; Arndt, R.; Kandzia, F.; Wiens, B.; Altfelder, S.; Walther, C. Drone-Based Investigation of Uranium Mining Legacies-Recent Developments in the DUB-GEM Project. In Proceedings of the EGU General Assembly Conference Abstracts, 2022; pp. EGU22-12872.
209. Adão, T.; Hruška, J.; Pádua, L.; Bessa, J.; Peres, E.; Morais, R.; Sousa, J.J. Hyperspectral imaging: A review on UAV-based sensors, data processing and applications for agriculture and forestry. *Remote sensing* **2017**, *9*, 1110.
210. Olson, D.; Anderson, J. Review on unmanned aerial vehicles, remote sensors, imagery processing, and their applications in agriculture. *Agronomy Journal* **2021**, *113*, 971-992.
211. Berra, E.; Peppa, M. Advances and challenges of UAV SFM MVS photogrammetry and remote sensing: Short review. In Proceedings of the 2020 ieee latin american grss & isprs remote sensing conference (lagirs), 2020; pp. 533-538.
212. Colomina, I.; Molina, P. Unmanned aerial systems for photogrammetry and remote sensing: A review. *ISPRS Journal of photogrammetry and remote sensing* **2014**, *92*, 79-97.
213. Greenwood, W.W.; Lynch, J.P.; Zekkos, D. Applications of UAVs in civil infrastructure. *Journal of infrastructure systems* **2019**, *25*, 04019002.
214. Zhang, Z.; Zhu, L. A review on unmanned aerial vehicle remote sensing: Platforms, sensors, data processing methods, and applications. *Drones* **2023**, *7*, 398.
215. Paraforos, D.S.; Sharipov, G.M.; Heiß, A.; Griepentrog, H.W. Position Accuracy Assessment of a UAV-mounted Sequoia+ Multispectral Camera Using a Robotic Total Station. *Agriculture* **2022**, *12*, 885.
216. Felipe-García, B.; Hernández-López, D.; Lerma, J.L. Analysis of the ground sample distance on large photogrammetric surveys. *Applied Geomatics* **2012**, *4*, 231-244.
217. Logie, G.S.; Coburn, C.A. An investigation of the spectral and radiometric characteristics of low-cost digital cameras for use in UAV remote sensing. *International Journal of Remote Sensing* **2018**, *39*, 4891-4909.
218. Kelcey, J.; Lucieer, A. Sensor correction and radiometric calibration of a 6-band multispectral imaging sensor for UAV remote sensing. *The International Archives of the Photogrammetry, Remote Sensing and Spatial Information Sciences* **2012**, *39*, 393-398.
219. DadrasJavan, F.; Samadzadegan, F.; Seyed Pourazar, S.H.; Fazeli, H. UAV-based multispectral imagery for fast Citrus Greening detection. *Journal of Plant Diseases and Protection* **2019**, *126*, 307-318.
220. Jiménez-Jiménez, S.I.; Ojeda-Bustamante, W.; Marcial-Pablo, M.d.J.; Enciso, J. Digital terrain models generated with low-cost UAV photogrammetry: Methodology and accuracy. *ISPRS International Journal of Geo-Information* **2021**, *10*, 285.
221. Niethammer, U.; James, M.; Rothmund, S.; Travelletti, J.; Joswig, M. UAV-based remote sensing of the Super-Sauze landslide: Evaluation and results. *Engineering Geology* **2012**, *128*, 2-11.
222. Lucieer, A.; Jong, S.M.d.; Turner, D. Mapping landslide displacements using Structure from Motion (SfM) and image correlation of multi-temporal UAV photography. *Progress in physical geography* **2014**, *38*, 97-116.
223. Lindner, G.; Schraml, K.; Mansberger, R.; Hübl, J. UAV monitoring and documentation of a large landslide. *Applied Geomatics* **2016**, *8*, 1-11.
224. Turner, D.; Lucieer, A.; De Jong, S.M. Time series analysis of landslide dynamics using an unmanned aerial vehicle (UAV). *Remote Sensing* **2015**, *7*, 1736-1757.
225. Al-Rawabdeh, A.; He, F.; Moussa, A.; El-Sheimy, N.; Habib, A. Using an unmanned aerial vehicle-based digital imaging system to derive a 3D point cloud for landslide scarp recognition. *Remote sensing* **2016**, *8*, 95.
226. Fernández, T.; Pérez, J.L.; Cardenal, J.; Gómez, J.M.; Colomo, C.; Delgado, J. Analysis of landslide evolution affecting olive groves using UAV and photogrammetric techniques. *Remote Sensing* **2016**, *8*, 837.
227. Peppa, M.; Mills, J.; Moore, P.; Miller, P.; Chambers, J. Accuracy assessment of a UAV-based landslide monitoring system. *The International Archives of the Photogrammetry, Remote Sensing and Spatial Information Sciences* **2016**, *41*, 895-902.
228. Ardi, N.; Iryanti, M.; Asmoro, C.; Nurhayati, N.; Agustine, E. Mapping landslide potential area using fault fracture density analysis on unmanned aerial vehicle (UAV) image. In Proceedings of the IOP Conference Series: Earth and Environmental Science, 2018; p. 012010.
229. Ma, S.; Xu, C.; Shao, X.; Zhang, P.; Liang, X.; Tian, Y. Geometric and kinematic features of a landslide in Mabian Sichuan, China, derived from UAV photography. *Landslides* **2019**, *16*, 373-381.
230. Rossi, G.; Tanteri, L.; Tofani, V.; Vannocci, P.; Moretti, S.; Casagli, N. Multitemporal UAV surveys for landslide mapping and characterization. *Landslides* **2018**, *15*, 1045-1052.
231. Barlow, J.; Gilham, J.; Ibarra Cofrã, I. Kinematic analysis of sea cliff stability using UAV photogrammetry. *International Journal of Remote Sensing* **2017**, *38*, 2464-2479.

232. Karantanellis, E.; Marinos, V.; Vassilakis, E.; Christaras, B. Object-based analysis using unmanned aerial vehicles (UAVs) for site-specific landslide assessment. *Remote Sensing* **2020**, *12*, 1711.
233. Godone, D.; Allasia, P.; Borrelli, L.; Gullà, G. UAV and structure from motion approach to monitor the maierato landslide evolution. *Remote Sensing* **2020**, *12*, 1039.
234. Xu, Q.; Li, W.-l.; Ju, Y.-z.; Dong, X.-j.; Peng, D.-l. Multitemporal UAV-based photogrammetry for landslide detection and monitoring in a large area: a case study in the Heifangtai terrace in the Loess Plateau of China. *Journal of mountain science* **2020**, *17*, 1826-1839.
235. Wang, Z.; Huang, T.; Bao, X.; Ma, S.; Sun, C.; Liu, G. Study on extraction of landslide information based on UAV survey. In Proceedings of the IOP Conference Series: Earth and Environmental Science, 2021; p. 012042.
236. Nikolakopoulos, K.G.; Kyriou, A.; Koukouvelas, I.K.; Tomaras, N.; Lyros, E. UAV, GNSS, and InSAR Data Analyses for Landslide Monitoring in a Mountainous Village in Western Greece. *Remote Sensing* **2023**, *15*, 2870.
237. Gasperini, D.; Allemand, P.; Delacourt, C.; Grandjean, P. Potential and limitation of UAV for monitoring subsidence in municipal landfills. *International Journal of Environmental Technology and Management* **2014**, *17*, 1-13.
238. Vrublová, D.; Kapica, R.; Jiránková, E.; Strus, A. Documentation of landslides and inaccessible parts of a mine using an unmanned UAV system and methods of digital terrestrial photogrammetry. *GeoScience Engineering* **2015**, *61*, 8.
239. Suh, J.; Choi, Y. Mapping hazardous mining-induced sinkhole subsidence using unmanned aerial vehicle (drone) photogrammetry. *Environmental Earth Sciences* **2017**, *76*, 1-12.
240. Haddon, E. Modeling Land-surface Deformation and Subsidence with UAV Photogrammetry. Available online: https://eros.usgs.gov/doi-remote-sensing-activities/2018/usgs/modeling-land-surface-deformation-and-subsidence-uav-photogrammetry
241. Ignjatović Stupar, D.; Rošer, J.; Vulić, M. Investigation of unmanned aerial vehicles-based photogrammetry for large mine subsidence monitoring. *Minerals* **2020**, *10*, 196.
242. Galeana-Pérez, V.M.; Chávez-Alegría, O.; Medellin-Aguilar, G. On the measure of land subsidence throughout DEM and orthomosaics using GPS and UAV. *Ingeniería, investigación y tecnología* **2021**, *22*, 0-0.
243. Tan, H.; Yu, X.; Zhu, M.; Guo, Z.; Chen, H. Deformation monitoring and spatiotemporal evolution of mining area with unmanned aerial vehicle and D-InSAR technology. *Mobile Information Systems* **2022**, *2022*.
244. Zhang, Y.; Lian, X.; Ge, L.; Liu, X.; Du, Z.; Yang, W.; Wu, Y.; Hu, H.; Cai, Y. Surface subsidence monitoring induced by underground coal mining by combining DInSAR and UAV photogrammetry. *Remote Sensing* **2022**, *14*, 4711.
245. Alamsyah, D.C. Simulating The Use of UAV Photogrammetry For Monitoring Land Subsidence at Urban Area. *Syntax Literate; Jurnal Ilmiah Indonesia* **2022**, *7*, 6656-6673.
246. Kim, N.; Macciotta, R.; Jun, B. Time series analysis of slope displacements using UAV photogrammetry and its relationship with rainfall intensity. *Landslides* **2024**, 1-17.
247. Zhao, J.; Yang, X.; Zhang, Z.; Niu, Y.; Zhao, Z. Mine Subsidence Monitoring Integrating DS-InSAR with UAV Photogrammetry Products: Case Studies on Hebei and Inner Mongolia. *Remote Sensing* **2023**, *15*, 4998.
248. Fu, Y.; Wu, Y.; Yin, X.; Zhang, Y. Mapping mining-induced ground fissures and their evolution using UAV photogrammetry. *Frontiers in Earth Science* **2023**, *11*, 1260913.
249. Vasterling, M.; Schloemer, S.; Fischer, C.; Ehrler, C. Thermal Imaging of Subsurface Coal Fires by means of an Unmanned Aerial Vehicle (UAV) in the Autonomous Province Xinjiang, PRC. In Proceedings of the EGU general assembly conference abstracts, 2010; p. 8664.
250. Harvey, M.C.; Luketina, K. Thermal infrared cameras and drones: a match made in heaven for cost-effective geothermal exploration, monitoring and development. In Proceedings of the 37th New Zealand Geothermal Workshop, 2015.
251. Harvey, M.; Rowland, J.; Luketina, K. Drone with thermal infrared camera provides high resolution georeferenced imagery of the Waikite geothermal area, New Zealand. *Journal of Volcanology and Geothermal Research* **2016**, *325*, 61-69.
252. Nishar, A.; Richards, S.; Breen, D.; Robertson, J.; Breen, B. Thermal infrared imaging of geothermal environments and by an unmanned aerial vehicle (UAV): A case study of the Wairakei–Tauhara geothermal field, Taupo, New Zealand. *Renewable Energy* **2016**, *86*, 1256-1264.
253. Lee, E.; Yoon, H.; Hyun, S.P.; Burnett, W.C.; Koh, D.C.; Ha, K.; Kim, D.j.; Kim, Y.; Kang, K.m. Unmanned aerial vehicles (UAVs)-based thermal infrared (TIR) mapping, a novel approach to assess groundwater discharge into the coastal zone. *Limnology and Oceanography: Methods* **2016**, *14*, 725-735.
254. Chio, S.-H.; Lin, C.-H. Preliminary study of UAS equipped with thermal camera for volcanic geothermal monitoring in Taiwan. *Sensors* **2017**, *17*, 1649.
255. Cherkasov, S.V.; Farkhutdinov, A.M.; Rykovanov, D.P.; Shaipov, A.A. The use of unmanned aerial vehicle for geothermal exploitation monitoring: Khankala field example. *Journal of Sustainable Development of Energy, Water and Environment Systems* **2018**, *6*, 351-362.

256. Kraaijenbrink, P.D.; Shea, J.M.; Litt, M.; Steiner, J.F.; Treichler, D.; Koch, I.; Immerzeel, W.W. Mapping surface temperatures on a debris-covered glacier with an unmanned aerial vehicle. *Frontiers in Earth Science* **2018**, *6*, 64.
257. Bjornsson, G.; Grimsson, G.; Sigurdsson, A.; Laenen, V.S. Thermal mapping of Icelandic geothermal surface manifestations with a drone. In Proceedings of the Proceedings of 44th Workshop on Geothermal Reservoir Engineering, 2019; pp. 1-8.
258. Dugdale, S.J.; Kelleher, C.A.; Malcolm, I.A.; Caldwell, S.; Hannah, D.M. Assessing the potential of drone-based thermal infrared imagery for quantifying river temperature heterogeneity. *Hydrological Processes* **2019**, *33*, 1152-1163.
259. Walter, T.R.; Jousset, P.; Allahbakhshi, M.; Witt, T.; Gudmundsson, M.T.; Hersir, G.P. Underwater and drone based photogrammetry reveals structural control at Geysir geothermal field in Iceland. *Journal of Volcanology and Geothermal Research* **2020**, *391*, 106282.
260. Silvestri, M.; Marotta, E.; Buongiorno, M.F.; Avvisati, G.; Belviso, P.; Bellucci Sessa, E.; Caputo, T.; Longo, V.; De Leo, V.; Teggi, S. Monitoring of surface temperature on Parco delle Biancane (Italian geothermal area) using optical satellite data, UAV and field campaigns. *Remote Sensing* **2020**, *12*, 2018.
261. Casas-Mulet, R.; Pander, J.; Ryu, D.; Stewardson, M.J.; Geist, J. Unmanned aerial vehicle (UAV)-based thermal infra-red (TIR) and optical imagery reveals multi-spatial scale controls of cold-water areas over a groundwater-dominated riverscape. *Frontiers in Environmental Science* **2020**, *8*, 64.
262. Bertalan, L.; Holb, I.; Pataki, A.; Négyesi, G.; Szabó, G.; Szalóki, A.K.; Szabó, S. UAV-based multispectral and thermal cameras to predict soil water content–A machine learning approach. *Computers and Electronics in Agriculture* **2022**, *200*, 107262.
263. Muanza, P.; Jónsdóttir, I.; Kristinsson, S.; Einarsson, G.; Björnsson, G. Geothermal mapping and remote sensing of thermal anomalies at Grændalur area, Hveragerði, SW Iceland.
264. Bahri, R.A.; Noviandy, T.R.; Suhendra, R.; Idroes, G.M.; Yanis, M.; Yandri, E.; Nizamuddin, N.; Irvanizam, I. Utilization of Drone with Thermal Camera in Mapping Digital Elevation Model for Ie Seu'um Geothermal Manifestation Exploration Security. *Leuser Journal of Environmental Studies* **2023**, *1*, 25-33.
265. Hassan-Esfahani, L.; Torres-Rua, A.; Jensen, A.; McKee, M. Assessment of surface soil moisture using high-resolution multi-spectral imagery and artificial neural networks. *Remote Sensing* **2015**, *7*, 2627-2646.
266. Ge, X.; Wang, J.; Ding, J.; Cao, X.; Zhang, Z.; Liu, J.; Li, X. Combining UAV-based hyperspectral imagery and machine learning algorithms for soil moisture content monitoring. *PeerJ* **2019**, *7*, e6926.
267. Lu, F.; Sun, Y.; Hou, F. Using UAV visible images to estimate the soil moisture of steppe. *Water* **2020**, *12*, 2334.
268. Ge, X.; Ding, J.; Jin, X.; Wang, J.; Chen, X.; Li, X.; Liu, J.; Xie, B. Estimating agricultural soil moisture content through UAV-based hyperspectral images in the arid region. *Remote Sensing* **2021**, *13*, 1562.
269. Sedano-Cibrián, J.; Pérez-Álvarez, R.; de Luis-Ruiz, J.M.; Pereda-García, R.; Salas-Menocal, B.R. Thermal water prospection with UAV, low-cost sensors and GIS. Application to the Case of La Hermida. *Sensors* **2022**, *22*, 6756.
270. Ismail, A.; Rashid, A.S.A.; Sa'ari, R.; Mustaffar, M.; Abdullah, R.A.; Kassim, A.; Yusof, N.M.; Abd Rahaman, N.; Apandi, N.M.; Kalatehjari, R. Application of UAV-based photogrammetry and normalised water index (NDWI) to estimate the rock mass rating (RMR): A case study. *Physics and Chemistry of the Earth, Parts A/B/C* **2022**, *127*, 103161.
271. Zhang, Y.; Han, W.; Zhang, H.; Niu, X.; Shao, G. Evaluating soil moisture content under maize coverage using UAV multimodal data by machine learning algorithms. *Journal of Hydrology* **2023**, *617*, 129086.
272. Park, S.; Choi, Y. Applications of unmanned aerial vehicles in mining from exploration to reclamation: A review. *Minerals* **2020**, *10*, 663.
273. Vasuki, Y.; Holden, E.-J.; Kovesi, P.; Micklethwaite, S. Semi-automatic mapping of geological Structures using UAV-based photogrammetric data: An image analysis approach. *Computers & Geosciences* **2014**, *69*, 22-32.
274. Jakob, S.; Zimmermann, R.; Gloaguen, R. The need for accurate geometric and radiometric corrections of drone-borne hyperspectral data for mineral exploration: Mephysto—A toolbox for pre-processing drone-borne hyperspectral data. *Remote Sensing* **2017**, *9*, 88.
275. Madjid, M.; Vandeginste, V.; Hampson, G.; Jordan, C.; Booth, A. Drones in carbonate geology: Opportunities and challenges, and application in diagenetic dolomite geobody mapping. *Marine and Petroleum Geology* **2018**, *91*, 723-734.
276. Kirsch, M.; Lorenz, S.; Zimmermann, R.; Tusa, L.; Möckel, R.; Hödl, P.; Booysen, R.; Khodadadzadeh, M.; Gloaguen, R. Integration of terrestrial and drone-borne hyperspectral and photogrammetric sensing methods for exploration mapping and mining monitoring. *Remote Sensing* **2018**, *10*, 1366.
277. Heincke, B.; Jackisch, R.; Saartenoja, A.; Salmirinne, H.; Rapp, S.; Zimmermann, R.; Pirttijärvi, M.; Sörensen, E.V.; Gloaguen, R.; Ek, L. Developing multi-sensor drones for geological mapping and mineral exploration: Setup and first results from the MULSEDRO project. *GEUS Bulletin* **2019**, *43*.

278. Jackisch, R.; Madriz, Y.; Zimmermann, R.; Pirttijärvi, M.; Saartenoja, A.; Salmirinne, H.; Heincke, B.H.; Gloaguen, R. Integration of UAS-borne hyperspectral remote-sensing and geophysics in mineral exploration under sub-polar conditions in Finland. In Proceedings of the Geophysical Research Abstracts, 2019.
279. Flores, H.; Lorenz, S.; Jackisch, R.; Tusa, L.; Contreras, I.C.; Zimmermann, R.; Gloaguen, R. UAS-based hyperspectral environmental monitoring of acid mine drainage affected waters. *Minerals* **2021**, *11*, 182.
280. Cramer, A.S.; Calvin, W.M.; McCoy, S.W.; Breitmeyer, R.J.; Haagsma, M.; Kratt, C. Mapping potentially acid generating material on abandoned mine lands using remotely piloted aerial systems. *Minerals* **2021**, *11*, 365.
281. Pérez-Álvarez, R.; Sedano-Cibrián, J.; de Luis-Ruiz, J.M.; Fernández-Maroto, G.; Pereda-García, R. Mining exploration with UAV, low-cost thermal cameras and GIS tools—application to the specific case of the complex sulfides hosted in Carbonates of Udías (Cantabria, Spain). *Minerals* **2022**, *12*, 140.
282. Sinaice, B.B.; Owada, N.; Ikeda, H.; Toriya, H.; Bagai, Z.; Shemang, E.; Adachi, T.; Kawamura, Y. Spectral angle mapping and AI methods applied in automatic identification of Placer deposit magnetite using multispectral camera mounted on UAV. *Minerals* **2022**, *12*, 268.
283. Jackisch, R.; Heincke, B.H.; Zimmermann, R.; Sørensen, E.V.; Pirttijärvi, M.; Kirsch, M.; Salmirinne, H.; Lode, S.; Kuronen, U.; Gloaguen, R. Drone-based magnetic and multispectral surveys to develop a 3D model for mineral exploration at Qullissat, Disko Island, Greenland. *Solid Earth Discussions* **2021**, *2021*, 1-51.
284. Salgado, L.; López-Sánchez, C.A.; Colina, A.; Baragaño, D.; Forján, R.; Gallego, J. Hg and As pollution in the soil-plant system evaluated by combining multispectral UAV-RS, geochemical survey and machine learning. *Environmental Pollution* **2023**, *333*, 122066.
285. Eskandari, A.; Hosseini, M.; Nicotra, E. Application of Satellite Remote Sensing, UAV-Geological Mapping, and Machine Learning Methods in the Exploration of Podiform Chromite Deposits. *Minerals* **2023**, *13*, 251.
286. McLeod, T.; Samson, C.; Labrie, M.; Shehata, K.; Mah, J.; Lai, P.; Wang, L.; Elder, J. Using video acquired from an unmanned aerial vehicle (UAV) to measure fracture orientation in an open-pit mine. *Geomatica* **2013**, *67*, 173-180.
287. Wang, Q.; Wu, L.; Chen, S.; Shu, D.; Xu, Z.; Li, F.; Wang, R. Accuracy evaluation of 3d geometry from low-attitude uav collections a case at zijin mine. *The International Archives of the Photogrammetry, Remote Sensing and Spatial Information Sciences* **2014**, *40*, 297-300.
288. Cho, S.-J.; Bang, E.-S.; Kang, I.-M. Construction of precise digital terrain model for nonmetal open-pit mine by using unmanned aerial photograph. *Economic and Environmental Geology* **2015**, *48*, 205-212.
289. Lee, S.; Choi, Y. Topographic survey at small-scale open-pit mines using a popular rotary-wing unmanned aerial vehicle (drone). *Tunnel and underground space* **2015**, *25*, 462-469.
290. Chen, J.; Li, K.; Chang, K.-J.; Sofia, G.; Tarolli, P. Open-pit mining geomorphic feature characterisation. *International Journal of Applied Earth Observation and Geoinformation* **2015**, *42*, 76-86.
291. Blistan, P.; Kovanič, Ľ.; Zelizňaková, V.; Palková, J. Using UAV photogrammetry to document rock outcrops. *Acta Montanistica Slovaca* **2016**, *21*.
292. Ge, L.; Li, X.; Ng, A.H.-M. UAV for mining applications: A case study at an open-cut mine and a longwall mine in New South Wales, Australia. In Proceedings of the 2016 IEEE International Geoscience and Remote Sensing Symposium (IGARSS), 2016; pp. 5422-5425.
293. Rossi, P.; Mancini, F.; Dubbini, M.; Mazzone, F.; Capra, A. Combining nadir and oblique UAV imagery to reconstruct quarry topography: methodology and feasibility analysis. *European Journal of Remote Sensing* **2017**, *50*, 211-221.
294. Mitchell, J.; Marshall, J.A. Design of a novel auto-rotating uav platform for underground mine cavity surveying. **2017**.
295. Freire, G.; Cota, R. Capture of images in inaccessible areas in an underground mine using an unmanned aerial vehicle. In Proceedings of the UMT 2017: Proceedings of the First International Conference on Underground Mining Technology, 2017.
296. Turner, R.; Bhagwat, N.; Galayda, L.; Knoll, C.; Russell, E.; MacLaughlin, M. Geotechnical characterization of underground mine excavations from UAV-captured photogrammetric & thermal imagery. In Proceedings of the ARMA US Rock Mechanics/Geomechanics Symposium, 2018; pp. ARMA-2018-2508.
297. Beretta, F.; Rodrigues, A.; Peroni, R.; Costa, J. Automated lithological classification using UAV and machine learning on an open cast mine. *Applied Earth Science* **2019**, *128*, 79-88.
298. Katuruza, M.; Birch, C. The use of unmanned aircraft system technology for highwall mapping at Isibonelo Colliery, South Africa. *Journal of the Southern African Institute of Mining and Metallurgy* **2019**, *119*, 291-295.
299. Stead, D.; Donati, D.; Wolter, A.; Sturzenegger, M. Application of remote sensing to the investigation of rock slopes: Experience gained and lessons learned. *ISPRS international journal of geo-information* **2019**, *8*, 296.
300. Raj, P. Use of Drones in an Underground Mine for Geotechnical Monitoring. The University of Arizona, 2019.

301. Turner, R.M.; MacLaughlin, M.M.; Iverson, S.R. Identifying and mapping potentially adverse discontinuities in underground excavations using thermal and multispectral UAV imagery. *Engineering geology* **2020**, *266*, 105470.
302. Honarmand, M.; Shahriari, H. Geological mapping using drone-based photogrammetry: An application for exploration of vein-type Cu mineralization. *Minerals* **2021**, *11*, 585.
303. Wakeford, Z.E.; Chmielewska, M.; Hole, M.J.; Howell, J.A.; Jerram, D.A. Combining thermal imaging with photogrammetry of an active volcano using UAV: an example from Stromboli, Italy. *The Photogrammetric Record* **2019**, *34*, 445-466.
304. Gracchi, T.; Tacconi Stefanelli, C.; Rossi, G.; Di Traglia, F.; Nolesini, T.; Tanteri, L.; Casagli, N. UAV-based multitemporal remote sensing surveys of volcano unstable flanks: a case study from stromboli. *Remote Sensing* **2022**, *14*, 2489.
305. Granados-Bolaños, S.; Quesada-Román, A.; Alvarado, G.E. Low-cost UAV applications in dynamic tropical volcanic landforms. *Journal of Volcanology and Geothermal Research* **2021**, *410*, 107143.
306. Swift, C.M. Fundamentals of the electromagnetic method. *Electromagnetic methods in applied geophysics* **1988**, *1*, 5-10.
307. Frequency-Domain Electromagnetics. Available online: https://olsonengineering.com/methods/geophysical-methods/electromagnetics/frequency-domain-em/
308. Ward, S.H.; Hohmann, G.W. Electromagnetic theory for geophysical applications. In *Electromagnetic methods in applied geophysics: Voume 1, theory*; Society of Exploration Geophysicists: 1988; pp. 130-311.
309. Pirttijärvi, M.; Saartenoja, A.; Korkeakangas, P. Drone-based electromagnetic survey system for geophysical applications. *Open Research Europe* **2022**, *2*, 3.
310. Korus, J. Combining hydraulic head analysis with airborne electromagnetics to detect and map impermeable aquifer boundaries. *Water* **2018**, *10*, 975.
311. Wu, X.; Xue, G.; Fang, G.; Li, X.; Ji, Y. The development and applications of the semi-airborne electromagnetic system in China. *Ieee Access* **2019**, *7*, 104956-104966.
312. Fountain, D. years of airborne EM–focus on the last decade: AEM 2008. In Proceedings of the 5th International Conference on Airborne Electromagnetics, conference abstracts, 2008.
313. Legault, J.M. Airborne electromagnetic systems–state of the art and future directions. *CSEG Recorder* **2015**, *40*, 38-49.
314. McNeil, J.; Labson, V. Geological mapping using VLF radio field. *Electromagnetic methods in applied geophysics* **1991**, *2*.
315. Smith, R.; Fountain, D.; Allard, M. The MEGATEM fixed-wing transient EM system applied to mineral exploration: a discovery case history. *First Break* **2003**, *21*.
316. Lane, R.; Green, A.; Golding, C.; Owers, M.; Pik, P.; Plunkett, C.; Sattel, D.; Thorn, B. An example of 3D conductivity mapping using the TEMPEST airborne electromagnetic system. *Exploration Geophysics* **2000**, *31*, 162-172.
317. Sørensen, K.I.; Auken, E. SkyTEM-A new high-resolution helicopter transient electromagnetic system. *Exploration Geophysics* **2004**, *35*, 191-199.
318. Vallee, M.A.; Smith, R.S.; Keating, P. Metalliferous mining geophysics—State of the art after a decade in the new millennium. *Geophysics* **2011**, *76*, W31-W50.
319. Lin, J.; Chen, J.; Liu, F.; Zhang, Y. The helicopter time-domain electromagnetic technology advances in China. *Surveys in Geophysics* **2021**, *42*, 585-624.
320. Thomson, S.; Fountain, D.; Watts, T. Airborne geophysics–evolution and revolution. In Proceedings of the Proceedings of Exploration, 2007; pp. 19-37.
321. Doll, W.E.; Gamey, T.J.; Holladay, J.S.; Sheehan, J.R.; Norton, J.; Beard, L.P.; Lee, J.L.; Hanson, A.E.; Lahti, R.M. Results of a high-resolution airborne TEM system demonstration for unexploded ordnance detection. *Geophysics* **2010**, *75*, B211-B220.
322. Lo, B.; Zang, M. Numerical modeling of Z-TEM (airborne AFMAG) responses to guide exploration strategies. In *SEG Technical Program Expanded Abstracts 2008*; Society of Exploration Geophysicists: 2008; pp. 1098-1102.
323. Holtham, E.; Oldenburg, D.W. Three-dimensional forward modelling and inversion of Z-TEM data. In *SEG Technical Program Expanded Abstracts 2008*; Society of Exploration Geophysicists: 2008; pp. 564-568.
324. Vovenko, T.; Moilanen, E.; Volkovitsky, A.; Karshakov, E. New abilities of quadrature EM systems. In Proceedings of the 6th International AEM Conference & Exhibition, 2013; pp. cp-383-00067.
325. Abedi, M.; Fournier, D.; Devriese, S.G.; Oldenburg, D.W. Integrated inversion of airborne geophysics over a structural geological unit: A case study for delineation of a porphyry copper zone in Iran. *Journal of Applied Geophysics* **2018**, *152*, 188-202.
326. Delsman, J.R.; Van Baaren, E.S.; Siemon, B.; Dabekaussen, W.; Karaoulis, M.C.; Pauw, P.S.; Vermaas, T.; Bootsma, H.; De Louw, P.G.; Gunnink, J.L. Large-scale, probabilistic salinity mapping using airborne electromagnetics for groundwater management in Zeeland, the Netherlands. *Environmental research letters* **2018**, *13*, 084011.

327. Steuer, A.; Smirnova, M.; Becken, M.; Schiffler, M.; Günther, T.; Rochlitz, R.; Yogeshwar, P.; Mörbe, W.; Siemon, B.; Costabel, S. Comparison of novel semi-airborne electromagnetic data with multi-scale geophysical, petrophysical and geological data from Schleiz, Germany. *Journal of Applied Geophysics* **2020**, *182*, 104172.
328. Rankka, K.; Andersson-Sköld, Y.; Hultén, C.; Larsson, R.; Leroux, V.; Dahlin, T. Quick clay in Sweden. **2004**.
329. Pfaffhuber, A.A.; Persson, L.; Lysdahl, A.O.; Kåsin, K.; Anschütz, H.; Bastani, M.; Bazin, S.; Löfroth, H. Integrated scanning for quick clay with AEM and ground-based investigations. *First Break* **2017**, *35*.
330. Auken, E.; Boesen, T.; Christiansen, A.V. A review of airborne electromagnetic methods with focus on geotechnical and hydrological applications from 2007 to 2017. *Advances in geophysics* **2017**, *58*, 47-93.
331. Pfaffhuber, A.A.; Lysdahl, A.O.; Sørmo, E.; Skurdal, G.H.; Thomassen, T.; Anschütz, H.; Scheibz, J. Delineating hazardous material without touching—AEM mapping of Norwegian alum shale. *First Break* **2017**, *35*.
332. Pedersen, J.B.; Schaars, F.W.; Christiansen, A.V.; Foged, N.; Schamper, C.; Rolf, H.; Auken, E. Mapping the fresh-saltwater interface in the coastal zone using high-resolution airborne electromagnetics. *First Break* **2017**, *35*.
333. Siemon, B.; Steuer, A. *Airborne geophysical investigation of groundwater resources in Northern Sumatra after the Tsunami of 2004*; INTECH Open Access Publisher: 2011.
334. Minsley, B.; Wellman, T.; Walvoord, M.A.; Revil, A. Sensitivity of airborne geophysical data to sublacustrine and near-surface permafrost thaw. *Cryosphere* **2015**, *9*.
335. Pastick, N.J.; Jorgenson, M.T.; Wylie, B.K.; Minsley, B.J.; Ji, L.; Walvoord, M.A.; Smith, B.D.; Abraham, J.D.; Rose, J.R. Extending airborne electromagnetic surveys for regional active layer and permafrost mapping with remote sensing and ancillary data, Yukon Flats Ecoregion, Central Alaska. *Permafrost and Periglacial Processes* **2013**, *24*, 184-199.
336. Mikucki, J.A.; Auken, E.; Tulaczyk, S.; Virginia, R.; Schamper, C.; Sørensen, K.; Doran, P.; Dugan, H.; Foley, N. Deep groundwater and potential subsurface habitats beneath an Antarctic dry valley. *Nature communications* **2015**, *6*, 6831.
337. Podgorski, J.E.; Auken, E.; Schamper, C.; Vest Christiansen, A.; Kalscheuer, T.; Green, A.G. Processing and inversion of commercial helicopter time-domain electromagnetic data for environmental assessments and geologic and hydrologic mapping. *Geophysics* **2013**, *78*, E149-E159.
338. Siemon, B.; Ibs-von Seht, M.; Steuer, A.; Deus, N.; Wiederhold, H. Airborne electromagnetic, magnetic, and radiometric surveys at the German North Sea coast applied to groundwater and soil investigations. *Remote Sensing* **2020**, *12*, 1629.
339. Airborne Electromagnetic (AEM) Survey 2022. Available online: https://www.usgs.gov/centers/upper-midwest-water-science-center/science/airborne-electromagnetic-aem-survey-2022 (accessed on January 26).
340. Høyer, A.-S.; Jørgensen, F.; Sandersen, P.; Viezzoli, A.; Møller, I. 3D geological modelling of a complex buried-valley network delineated from borehole and AEM data. *Journal of Applied Geophysics* **2015**, *122*, 94-102.
341. Finn, C.A.; Deszcz-Pan, M.; Anderson, E.D.; John, D.A. Three-dimensional geophysical mapping of rock alteration and water content at Mount Adams, Washington: Implications for lahar hazards. *Journal of Geophysical Research: Solid Earth* **2007**, *112*.
342. Legault, J.; Orta, M.; Kaminski, V.; Prikhodko, A.; Kumar, H. Helicopter Electromagnetic (VTEM™ AND ZTEM™) Applications for Gold Exploration. In Proceedings of the Kegs-Pdac Symposium, Toronto, Canadá, 2010.
343. Mahmoodi, O.; Morelli, R. Using magnetic and electromagnetic data processing to map sub-Phanerozoic basement features in the Flin Flon area. *Summary of Investigations* **2017**, *2*, 2017-2014.2012.
344. Fraser, D.C. Magnetite ore tonnage estimates from an aerial electromagnetic survey. *Geoexploration* **1973**, *11*, 97-105.
345. Roach, I.C. The Frome airborne electromagnetic survey, South Australia. *ASEG Extended Abstracts* **2012**, *2012*, 1-3.
346. Crowe, M.; Heinson, G.; Dhu, T. Magnetotellurics and Airborne Electromagnetics? a combined method for assessing basin structure and exploring for unconformity related uranium. *ASEG extended abstracts* **2013**, *2013*, 1-5.
347. Parshin, A.; Bashkeev, A.; Davidenko, Y.; Persova, M.; Iakovlev, S.; Bukhalov, S.; Grebenkin, N.; Tokareva, M. Lightweight unmanned aerial system for time-domain electromagnetic prospecting—The next stage in applied UAV-Geophysics. *Applied Sciences* **2021**, *11*, 2060.
348. Mitsuhata, Y.; Ueda, T.; Kamimura, A.; Kato, S.; Takeuchi, A.; Aduma, C.; Yokota, T. Development of a drone-borne electromagnetic survey system for searching for buried vehicles and soil resistivity mapping. *Near Surface Geophysics* **2022**, *20*, 16-29.
349. Vilhelmsen, T.B.; Døssing, A. Drone-towed CSEM system for near-surface geophysical prospecting: On instrument noise, temperature drift, transmission frequency and survey setup. *EGUsphere* **2022**, *2022*, 1-32.

350. Spies, B.R.; Frischknecht, F.C. Electromagnetic sounding. **1991**.
351. Kotowski, P.O.; Becken, M.; Thiede, A.; Schmidt, V.; Schmalzl, J.; Ueding, S.; Klingen, S. Evaluation of a semi-airborne electromagnetic survey based on a multicopter aircraft system. *Geosciences* **2022**, *12*, 26.
352. Stoll*, J.B.; Noellenburg, R.; Kordes, T.; Becken, M.; Tezkan, B.; Yogeshwar, P.; Bergers, R.; Matzander, U. Semi-Airborne electromagnetics using a multicopter. In Proceedings of the International Workshop on Gravity, Electrical & Magnetic Methods and Their Applications, Xi'an, China, May 19–22, 2019, 2019; pp. 363-366.
353. Stoll, J.B.; Kordes, T.; Noellenburg, R. Semi-Airborne Electromagnetics Using a Multicopter. Available online: https://www.per.co.id/2021/09/07/semi-airborne-electromagnetics-using-a-multicopter/
354. Di, Q.; Xue, G.; Yin, C.; Li, X. New methods of controlled-source electromagnetic detection in China. *Science China Earth Sciences* **2020**, *63*, 1268-1277.
355. Kipfinger, R. Unmanned airborne vehicle (UAV): Flight testing and evaluation of two-channel E-field very low frequency (VLF) instrument. *United States Geological Survey* **1998**, 1-4.
356. Eröss, R.; Tezkan, B.; Stoll, J.B.; Bergers, R. Interpretation of very low frequency measurements carried out with an unmanned aerial system by 2D conductivity models. *Journal of Environmental and Engineering Geophysics* **2017**, *22*, 83-94.
357. Telford, W.M.; Geldart, L.P.; Sheriff, R.E. *Applied geophysics*; Cambridge university press: 1990.
358. Tezkan, B. A review of environmental applications of quasi-stationary electromagnetic techniques. *Surveys in Geophysics* **1999**, *20*, 279-308.
359. Pedersen, L.B.; Persson, L.; Bastani, M.; Byström, S. Airborne VLF measurements and mapping of ground conductivity in Sweden. *Journal of applied geophysics* **2009**, *67*, 250-258.
360. Vozoff, K. The magnetotelluric method in the exploration of sedimentary basins. *Geophysics* **1972**, *37*, 98-141.
361. Pedersen, L.B.; Qian, W.; Dynesius, L.; Zhang, P. An airborne tensor VLF system. From concept to realization 1. *Geophysical Prospecting* **1994**, *42*, 863-883.
362. Eröss, R. Very Low Frequency Measurements carried out with an Unmanned Aircraft System. Universität zu Köln, 2015.
363. Harris, F.J. On the use of windows for harmonic analysis with the discrete Fourier transform. *Proceedings of the IEEE* **1978**, *66*, 51-83.
364. Macnae, J. Low Noise, Lightweight EM and AMT sensors for Unmanned Airborne Systems (UAS). **2021**.
365. Qi, Z.-p.; Li, X.; Li, H.; Zhang, Y.-y.; Zhou, J. Drone-borne transient electromagnetic system and its application in UXO detection. In Proceedings of the SEG International Exposition and Annual Meeting, 2018; pp. SEG-2018-2997180.
366. Karaoulis, M.; Ritsema, I.; Bremmer, C.; De Kleine, M.; Oude Essink, G.; Ahlrichs, E. Drone-Borne Electromagnetic (DR-EM) Surveying in The Netherlands: Lab and Field Validation Results. *Remote Sensing* **2022**, *14*, 5335.
367. Barrowes, B.E.; Glaser, D.R.; Quinn, B.G.; Prishvin, M.; Shubitidze, F.; RESEARCH, C.R.; States, E.L.H.N.H.U. *Unmanned Aerial Systems Electromagnetic Induction Sensor Development: Evaluation of Commercial-off-the-Shelf Unmanned Aerial System Motor Interference and Mitigation in Airborne Electromagnetic Induction Sensors*; US Army Engineer Research and Development Center, Cold Regions Research and …: 2019.
368. Tang, P.; Chen, F.; Jiang, A.; Zhou, W.; Wang, H.; Leucci, G.; de Giorgi, L.; Sileo, M.; Luo, R.; Lasaponara, R. Multi-frequency electromagnetic induction survey for archaeological prospection: Approach and results in Han Hangu Pass and Xishan Yang in China. *Surveys in Geophysics* **2018**, *39*, 1285-1302.
369. Bastani, M.; Johansson, H.; Paulusson, A.; Paulusson, K.; Dynesius, L. Unmanned Aerial Vehicles (UAV) and ground-based electromagnetic (EM) systems. *First Break* **2020**, *38*, 87-89.
370. Bobarika, I.; Parshin, A. Lightweight UAV Variant of Unconventional Design as a Carrier for Performing Complex Airborne Geophysical Surveying. In Proceedings of the First EAGE Workshop on Unmanned Aerial Vehicles, 2019; pp. 1-4.
371. Parshin, A.; Iakovlev, S.; Davidenko, Y.A.; Bashkeev, A.; Vinokurov, V.; Bukhalov, S. Two Variants of Lightweight Unmanned Systems for Low-Altitude Electromagnetic Soundings. In Proceedings of the Engineering and Mining Geophysics 2021, 2021; pp. 1-6.
372. Parshin, A.; Davidenko, Y.; Yakovlev, S.; Vinokurov, V.; Bashkeev, A. Lightweight TEM and VLF systems for low-altitude UAV-based geophysical. In Proceedings of the NSG2021 27th European Meeting of Environmental and Engineering Geophysics, 2021; pp. 1-5.
373. Hallbauer-Zadorozhnaya, V.D., Yu. A.; Parshin, A.V.; Stettler, E. Drone based experimental TEM surveys over Lake Baikal and a uranium occurrence. In Proceedings of the 25th EM Induction Workshop, Çeşme, Turkey, September 11-17, 2022.
374. Moreno, W.F.; Nogueira, F.C.; Shiguemori, E.H.; Kux, H.J. Electromagnetic Sensor Onboard Drones for the Detectin of Land Mines. **2018**.

375. Morifuji, Y.; Kubota, K.; Tanaka, S.; Suenaga, H.; Jomori, A.; Jomori, A.; Toyama, T. Drone electromagnetic survey for slope subsurface structure investigation—Flight along steep slope. In Proceedings of the Proceedings of the 14th SEGJ International Symposium, Tokyo, Japan, 18–21 October 2021, 2021; pp. 38-41.
376. Davydenko, Y.; Tereshkin, S.; Bashkeev, A.; Iakovlev, S.; Shkirya, M.; Parshin, A.; Persova, M. The Results of Experimental and Methodological Work With the New Uav-Tem Technology on Lake Baikal. In Proceedings of the NSG2022 3rd Conference on Airborne, Drone and Robotic Geophysics, 2022; pp. 1-5.
377. Bjerg, T.; da Silva, E.L.S.; Døssing, A. Investigation of UAV noise reduction for electromagnetic induction surveying. In Proceedings of the NSG2020 3rd Conference on Geophysics for Mineral Exploration and Mining, 2020; pp. 1-5.
378. Unmanned Aerial Vehicle Geophysics. Available online: https://discogeo.com/expertise/uav/
379. DronEM (Drone for Electromagnetic fields Measurements). Available online: https://www.geo-k.co/2017/05/29/dronem-drone-for-electromagnetic-fields-measurements/
380. UAV VLF-EM SYSTEM: Resistivity Mapping Solution. Available online: https://www.gemsys.ca/uav-vlf/
381. Electromagnetic Drone. Available online: https://www.per.co.id/services/geophysical/drone-electromagnetic/
382. Siemon, B.; Christiansen, A.V.; Auken, E. A review of helicopter-borne electromagnetic methods for groundwater exploration. *Near Surface Geophysics* **2009**, *7*, 629-646.
383. Frischknecht, F.C. Field about an oscillating magnetic dipole over a two-layer earth and application to ground and airborne electromagnetic surveys. *Quart. Colorado School of Mines* **1967**, *62*, 1-370.
384. Auken, E.; Christiansen, A.V. Layered and laterally constrained 2D inversion of resistivity data. *Geophysics* **2004**, *69*, 752-761.
385. Minsley, B.J. A trans-dimensional Bayesian Markov chain Monte Carlo algorithm for model assessment using frequency-domain electromagnetic data. *Geophysical Journal International* **2011**, *187*, 252-272.
386. Viezzoli, A.; Christiansen, A.V.; Auken, E.; Sørensen, K. Quasi-3D modeling of airborne TEM data by spatially constrained inversion. *Geophysics* **2008**, *73*, F105-F113.
387. Bosch, F.; Müller, I. Improved karst exploration by VLF-EM-gradient survey: comparison with other geophysical methods. *Near Surface Geophysics* **2005**, *3*, 299-310.
388. Johmori, A.; Johmori, A.; Kondou, T.; Yuuki, Y.; Kawase, M. Development of grounded electrical-source airborne transient electromagnetics (GREATEM) system using a multicopter. In Proceedings of the Proceedings of the 138th Society of Exploration Geophysicists of Japan Conference, Tokyo, 2018; pp. 120-123.
389. Sun, H.; Zhang, N.; Li, D.; Liu, S.; Ye, Q. The first semi-airborne transient electromagnetic survey for tunnel investigation in very complex terrain areas. *Tunnelling and Underground Space Technology* **2023**, *132*, 104893.
390. Li, C.J.; Ling, H. High-resolution, downward-looking radar imaging using a small consumer drone. In Proceedings of the 2016 IEEE International Symposium on Antennas and Propagation (APSURSI), 2016; pp. 2037-2038.
391. Ludeno, G.; Catapano, I.; Renga, A.; Vetrella, A.R.; Fasano, G.; Soldovieri, F. Assessment of a micro-UAV system for microwave tomography radar imaging. *Remote Sensing of Environment* **2018**, *212*, 90-102.
392. Schreiber, E.; Heinzel, A.; Peichl, M.; Engel, M.; Wiesbeck, W. Advanced buried object detection by multichannel, UAV/drone carried synthetic aperture radar. In Proceedings of the 2019 13th European Conference on Antennas and Propagation (EuCAP), 2019; pp. 1-5.
393. Jenssen, R.O.R.; Eckerstorfer, M.; Jacobsen, S. Drone-mounted ultrawideband radar for retrieval of snowpack properties. *IEEE Transactions on Instrumentation and Measurement* **2019**, *69*, 221-230.
394. Catapano, I.; Gennarelli, G.; Ludeno, G.; Noviello, C.; Esposito, G.; Renga, A.; Fasano, G.; Soldovieri, F. Small multicopter-UAV-based radar imaging: Performance assessment for a single flight track. *Remote Sensing* **2020**, *12*, 774.
395. Noviello, C.; Esposito, G.; Catapano, I.; Soldovieri, F. Multilines imaging approach for mini-UAV radar imaging system. *IEEE Geoscience and Remote Sensing Letters* **2021**, *19*, 1-5.
396. Giret, R.; Jeuland, H.; Enert, P. A study of a 3D-SAR concept for a millimeter wave imaging radar onboard an UAV. In Proceedings of the First European Radar Conference, 2004. EURAD., 2004; pp. 201-204.
397. Weib, M.; Ender, J. A 3D imaging radar for small unmanned airplanes-ARTINO. In Proceedings of the European Radar Conference, 2005. EURAD 2005., 2005; pp. 209-212.
398. Zaugg, E.; Long, D.; Edwards, M.; Fladeland, M.; Kolyer, R.; Crocker, I.; Maslanik, J.; Herzfeld, U.; Wallin, B. Using the microASAR on the NASA SIERRA UAS in the characterization of Arctic sea ice experiment. In Proceedings of the 2010 IEEE Radar Conference, 2010; pp. 271-276.
399. Remy, M.A.; de Macedo, K.A.; Moreira, J.R. The first UAV-based P-and X-band interferometric SAR system. In Proceedings of the 2012 IEEE International Geoscience and Remote Sensing Symposium, 2012; pp. 5041-5044.
400. Aguasca, A.; Acevo-Herrera, R.; Broquetas, A.; Mallorqui, J.J.; Fabregas, X. ARBRES: Light-weight CW/FM SAR sensors for small UAVs. *Sensors* **2013**, *13*, 3204-3216.

401. Amiri, A.; Tong, K.; Chetty, K. Feasibility study of multi-frequency Ground Penetrating Radar for rotary UAV platforms. **2012**.
402. Colorado, J.; Perez, M.; Mondragon, I.; Mendez, D.; Parra, C.; Devia, C.; Martinez-Moritz, J.; Neira, L. An integrated aerial system for landmine detection: SDR-based Ground Penetrating Radar onboard an autonomous drone. *Advanced Robotics* **2017**, *31*, 791-808.
403. Garcia-Fernandez, M.; Alvarez-Lopez, Y.; Las Heras, F.; Gonzalez-Valdes, B.; Rodriguez-Vaqueiro, Y.; Pino, A.; Arboleya-Arboleya, A. GPR system onboard a UAV for non-invasive detection of buried objects. In Proceedings of the 2018 IEEE International Symposium on Antennas and Propagation & USNC/URSI National Radio Science Meeting, 2018; pp. 1967-1968.
404. Wu, K.; Rodriguez, G.A.; Zajc, M.; Jacquemin, E.; Clément, M.; De Coster, A.; Lambot, S. A new drone-borne GPR for soil moisture mapping. *Remote Sensing of Environment* **2019**, *235*, 111456.
405. Burr, R.; Schartel, M.; Grathwohl, A.; Mayer, W.; Walter, T.; Waldschmidt, C. UAV-borne FMCW InSAR for focusing buried objects. *IEEE Geoscience and Remote Sensing Letters* **2021**, *19*, 1-5.
406. Šipoš, D.; Gleich, D. A lightweight and low-power UAV-borne ground penetrating radar design for landmine detection. *Sensors* **2020**, *20*, 2234.
407. Vergnano, A.; Franco, D.; Godio, A. Drone-borne ground-penetrating radar for snow cover mapping. *Remote Sensing* **2022**, *14*, 1763.
408. Saponaro, A.; Dipierro, G.; Cannella, E.; Panarese, A.; Galiano, A.M.; Massaro, A. A UAV-GPR fusion approach for the characterization of a quarry excavation area in Falconara Albanese, Southern Italy. *Drones* **2021**, *5*, 40.
409. Rosen, E.M.; Ayers, E. Assessment of down-looking GPR sensors for landmine detection. In Proceedings of the Detection and Remediation Technologies for Mines and Minelike Targets X, 2005; pp. 423-434.
410. Rosen, E.M.; Rotondo, F.S.; Ayers, E. Testing and evaluation of forward-looking GPR countermine systems. In Proceedings of the Detection and Remediation Technologies for Mines and Minelike Targets X, 2005; pp. 901-911.
411. Diamanti, N.; Annan, A.P. Air-launched and ground-coupled GPR data. In Proceedings of the 2017 11th European Conference on Antennas and Propagation (EUCAP), 2017; pp. 1694-1698.
412. Ristmae, T.; Dionysiou, D.D.; Koutsokeras, M.; Douklias, A.; Ouzounoglou, E.; Amditis, A.; Fotopoulos, A.; Diles, G.; Linardatos, P.; Smanis, K. The CURSOR Search and Rescue (SaR) Kit: an innovative solution for improving the efficiency of Urban SaR Operations. In Proceedings of the ISCRAM, 2021; pp. 867-880.
413. Garcia-Fernandez, M.; López, Y.Á.; Andrés, F.L.-H. Airborne multi-channel ground penetrating radar for improvised explosive devices and landmine detection. *IEEE Access* **2020**, *8*, 165927-165943.
414. Fernández, M.G.; López, Y.Á.; Arboleya, A.A.; Valdés, B.G.; Vaqueiro, Y.R.; Andrés, F.L.-H.; García, A.P. Synthetic aperture radar imaging system for landmine detection using a ground penetrating radar on board a unmanned aerial vehicle. *IEEE Access* **2018**, *6*, 45100-45112.
415. Garcia-Fernandez, M.; Morgenthaler, A.; Alvarez-Lopez, Y.; Las Heras, F.; Rappaport, C. Bistatic landmine and IED detection combining vehicle and drone mounted GPR sensors. *Remote Sensing* **2019**, *11*, 2299.
416. Catapano, I.; Gennarelli, G.; Ludeno, G.; Noviello, C.; Esposito, G.; Soldovieri, F. Contactless ground penetrating radar imaging: State of the art, challenges, and microwave tomography-based data processing. *IEEE Geoscience and Remote Sensing Magazine* **2021**, *10*, 251-273.
417. Noviello, C.; Gennarelli, G.; Esposito, G.; Ludeno, G.; Fasano, G.; Capozzoli, L.; Soldovieri, F.; Catapano, I. An overview on down-looking UAV-based GPR systems. *Remote Sensing* **2022**, *14*, 3245.
418. Comite, D.; Ahmad, F.; Amin, M.G.; Dogaru, T. Forward-looking ground-penetrating radar: Subsurface target imaging and detection: A review. *IEEE Geoscience and Remote Sensing Magazine* **2021**, *9*, 173-190.
419. Comite, D.; Ahmad, F.; Dogaru, T.; Amin, M.G. Adaptive detection of low-signature targets in forward-looking GPR imagery. *IEEE Geoscience and Remote Sensing Letters* **2018**, *15*, 1520-1524.
420. Chandra, M.; Tanzi, T. On the Design of a side-looking Drone-borne GPR and its Physical Basis. In Proceedings of the URSI. AT-RASC 2018. Second URSI Atlantic Radio Science Meeting-2018., 2018.
421. Burr, R.; Schartel, M.; Mayer, W.; Walter, T.; Waldschmidt, C. UAV-based polarimetric synthetic aperture radar for mine detection. In Proceedings of the IGARSS 2019-2019 IEEE International Geoscience and Remote Sensing Symposium, 2019; pp. 9208-9211.
422. Schartel, M.; Burr, R.; Bähnemann, R.; Mayer, W.; Waldschmidt, C. An experimental study on airborne landmine detection using a circular synthetic aperture radar. *arXiv preprint arXiv:2005.02600* **2020**.
423. Grathwohl, A.; Hinz, P.; Burr, R.; Steiner, M.; Waldschmidt, C. Experimental study on the detection of avalanche victims using an airborne ground penetrating synthetic aperture radar. In Proceedings of the 2021 IEEE Radar Conference (RadarConf21), 2021; pp. 1-6.
424. Karthikeyan, R.; Chandramouli, A.; Srivatsun, G. Ground Penetrating Radar (GPR) Antenna Design: A Comparative Study. *International Journal of Engineering and Advanced Technology (IJEAT)* **2018**, *8*, 168-176.
425. Noviello, C.; Esposito, G.; Fasano, G.; Renga, A.; Soldovieri, F.; Catapano, I. Small-UAV radar imaging system performance with GPS and CDGPS based motion compensation. *Remote Sensing* **2020**, *12*, 3463.

426. García-Fernández, M.; Álvarez-Narciandi, G.; López, Y.Á.; Andrés, F.L.-H. Improvements in GPR-SAR imaging focusing and detection capabilities of UAV-mounted GPR systems. *ISPRS Journal of Photogrammetry and Remote Sensing* **2022**, *189*, 128-142.
427. Vuksanovic, B.; Bostanudin, N.; Hidzir, H.; Parchizadeh, H. Discarding Unwanted Features from GPR Images Using2DPCA and ICA Techniques. *International Journal of Information and Electronics Engineering* **2013**, *3*, 317.
428. Gonzalez-Diaz, M.; Garcia-Fernandez, M.; Alvarez-Lopez, Y.; Las-Heras, F. Improvement of GPR SAR-based techniques for accurate detection and imaging of buried objects. *IEEE Transactions on Instrumentation and measurement* **2019**, *69*, 3126-3138.
429. Garcia-Fernandez, M.; Alvarez-Lopez, Y.; Las Heras, F. Autonomous airborne 3D SAR imaging system for subsurface sensing: UWB-GPR on board a UAV for landmine and IED detection. *Remote Sensing* **2019**, *11*, 2357.
430. Garcia-Fernandez, M.; Alvarez-Lopez, Y.; Arboleya-Arboleya, A.; Las-Heras, F.; Rodriguez-Vaqueiro, Y.; Gonzalez-Valdes, B.; Pino-Garcia, A. SVD-based clutter removal technique for GPR. In Proceedings of the 2017 IEEE International Symposium on Antennas and Propagation & USNC/URSI National Radio Science Meeting, 2017; pp. 2369-2370.
431. Daniels, D.J. *Ground penetrating radar*; Iet: 2004; Volume 1.
432. Persico, R. *Introduction to ground penetrating radar: inverse scattering and data processing*; John Wiley & Sons: 2014.
433. Curlander, J.C.; McDonough, R.N. *Synthetic aperture radar*; Wiley, New York: 1991; Volume 11.
434. Catapano, I.; Noviello, C.; Soldovieri, F. Down-Looking Airborne Radar Imaging Performance: The Multi-Line and Multi-Frequency. *Remote Sensing* **2021**, *13*, 4897.
435. Schneider, W.A. Integral formulation for migration in two and three dimensions. *Geophysics* **1978**, *43*, 49-76.
436. Gazdag, J. Wave equation migration with the phase-shift method. *Geophysics* **1978**, *43*, 1342-1351.
437. Marpaung, D.H.; Lu, Y. A comparative study of migration algorithms for UWB GPR images in SISO-SAR and MIMO-array configurations. In Proceedings of the 2014 15th International Radar Symposium (IRS), 2014; pp. 1-4.
438. Özdemir, C.; Demirci, Ş.; Yiğit, E.; Yilmaz, B. A review on migration methods in B-scan ground penetrating radar imaging. *Mathematical Problems in Engineering* **2014**, *2014*.
439. Garcia-Fernandez, M.; Alvarez-Lopez, Y.; Gonzalez-Valdes, B.; Rodriguez-Vaqueiro, Y.; Arboleya-Arboleya, A.; Las Heras, F. Recent advances in high-resolution Ground Penetrating Radar on board an Unmanned Aerial Vehicle. In Proceedings of the 2019 13th European Conference on Antennas and Propagation (EuCAP), 2019; pp. 1-5.
440. Fallahpour, M.; Case, J.T.; Ghasr, M.T.; Zoughi, R. Piecewise and Wiener filter-based SAR techniques for monostatic microwave imaging of layered structures. *IEEE Transactions on Antennas and Propagation* **2013**, *62*, 282-294.
441. Johansson, E.M.; Mast, J.E. Three-dimensional ground-penetrating radar imaging using synthetic aperture time-domain focusing. In Proceedings of the Advanced Microwave and Millimeter-Wave Detectors, 1994; pp. 205-214.
442. Burr, R.; Schartel, M.; Schmidt, P.; Mayer, W.; Walter, T.; Waldschmidt, C. Design and Implementation of a FMCW GPR for UAV-based Mine Detection. In Proceedings of the 2018 IEEE MTT-S International Conference on Microwaves for Intelligent Mobility (ICMIM), 2018; pp. 1-4.
443. Catapano, I.; Gennarelli, G.; Ludeno, G.; Soldovieri, F.; Persico, R. Ground-penetrating radar: operation principle and data processing. *Wiley encyclopedia of electrical and electronics engineering* **1999**, 1-23.
444. Bertero, M.; Boccacci, P.; De Mol, C. *Introduction to inverse problems in imaging*; CRC press: 2021.
445. Gader, P.; Lee, W.-H.; Wilson, J.N. Detecting landmines with ground-penetrating radar using feature-based rules, order statistics, and adaptive whitening. *IEEE Transactions on Geoscience and Remote Sensing* **2004**, *42*, 2522-2534.
446. Hou, F.; Lei, W.; Li, S.; Xi, J. Deep learning-based subsurface target detection from GPR scans. *IEEE sensors journal* **2021**, *21*, 8161-8171.
447. Alpdemir, M.N.; Sezgin, M. A reinforcement learning (RL)-based hybrid method for ground penetrating radar (GPR)-driven buried object detection. *Neural Computing and Applications* **2024**, *36*, 8199-8219.
448. Maruddani, B.; Sandi, E.; Salam, M.F.N. Design and Implementation of Low-cost Wideband Vivaldi Antenna for Ground Penetrating Radar. *KnE Social Sciences* **2019**, 498–506-498–506.
449. Cerquera, M.R.P.; Montaño, J.D.C.; Mondragón, I.; Canbolat, H. UAV for landmine detection using SDR-based GPR technology. *Robots Operating in Hazardous Environments* **2017**, 26-55.
450. Roussi, C.; Xique, I.; Burns, J.; Hart, B. Buried object imaging using a small UAS-based GPR. In Proceedings of the Detection and Sensing of Mines, Explosive Objects, and Obscured Targets XXIV, 2019; pp. 146-154.

Preprints.org (www.preprints.org) | NOT PEER-REVIEWED | Posted: 1 November 2024 doi:10.20944/preprints202411.0058.v1

451. Fernández, M.G.; Narciandi, G.Á.; Arboleya, A.; Antuña, C.V.; Andrés, F.L.-H.; López, Y.Á. Development of an airborne-based GPR system for landmine and IED detection: Antenna analysis and intercomparison. *IEEE Access* **2021**, *9*, 127382-127396.
452. Yarlequé, M.A.; Alvarez, S.; Martínez, H.J.; Canelo, A.C. FMCW GPR radar for archaeological applications: First analytical and measurement results. In Proceedings of the 2017 Xxxiind General Assembly and Scientific Symposium of the International Union of Radio Science (Ursi Gass), 2017; pp. 1-3.
453. Dill, S.; Schreiber, E.; Engel, M.; Heinzel, A.; Peichl, M. A drone carried multichannel Synthetic Aperture Radar for advanced buried object detection. In Proceedings of the 2019 IEEE Radar Conference (RadarConf), 2019; pp. 1-6.
454. Valence, E.; Baraer, M.; Rosa, E.; Barbecot, F.; Monty, C. Drone-based ground-penetrating radar (GPR) application to snow hydrology. *The Cryosphere* **2022**, *16*, 3843-3860.
455. Wu, S.; Wang, L.; Zeng, X.; Wang, F.; Liang, Z.; Ye, H. UAV-Mounted GPR for Object Detection Based on Cross-Correlation Background Subtraction Method. *Remote Sensing* **2022**, *14*, 5132.
456. Jenssen, R.O.R.; Jacobsen, S.K. Measurement of snow water equivalent using drone-mounted ultra-wide-band radar. *Remote Sensing* **2021**, *13*, 2610.
457. Jenssen, R.O.R.; Jacobsen, S. Drone-mounted UWB snow radar: technical improvements and field results. *Journal of Electromagnetic Waves and Applications* **2020**, *34*, 1930-1954.
458. Prager, S.; Moghaddam, M. Application of ultra-wideband synthesis in software defined radar for UAV-based landmine detection. In Proceedings of the IGARSS 2019-2019 IEEE International Geoscience and Remote Sensing Symposium, 2019; pp. 10115-10118.
459. Li, C.; Li, Z.; Huang, W.; Zhang, B.; Deng, Y.; Li, G. Morphology dynamics of ice cover in a river bend revealed by the UAV-GPR and sentinel-2. *Remote Sensing* **2023**, *15*, 3180.
460. Bandini, F.; Kooij, L.; Mortensen, B.K.; Caspersen, M.B.; Thomsen, L.G.; Olesen, D.; Bauer-Gottwein, P. Mapping inland water bathymetry with ground penetrating radar (GPR) on board unmanned aerial systems (UASs). *Journal of Hydrology* **2023**, *616*, 128789.
461. Svedin, J.; Bernland, A.; Gustafsson, A.; Claar, E.; Luong, J. Small UAV-based SAR system using low-cost radar, position, and attitude sensors with onboard imaging capability. *International Journal of Microwave and Wireless Technologies* **2021**, *13*, 602-613.
462. Altdorff, D.; Schliffke, N.; Riedel, M.; Schmidt, V.; van der Kruk, J.; Vereecken, H.; Stoll, J.; Becken, M. UAV-borne electromagnetic induction and ground-penetrating radar measurements: a feasibility test. *Water Resour. Res* **2014**, *42*, W11403.
463. Building a ground penetrating radar for drones with Red Pitaya. Available online: https://content.redpitaya.com/blog/building-a-ground-penetrating-radar-with-red-pitaya
464. García-Fernández, M.; Álvarez-Narciandi, G.; López, Y.Á.; Las-Heras, F. Array-based ground penetrating synthetic aperture radar on board an unmanned aerial vehicle for enhanced buried threats detection. *IEEE Transactions on Geoscience and Remote Sensing* **2023**.
465. Linck, R.; Kaltak, A. Drone radar: A new survey approach for Archaeological Prospection. In Proceedings of the Proceedings of the 3th International Conference on Archaeological Prospection, Sligo, Ireland, 2019; pp. 268-271.
466. Francke, J.; Dobrovolskiy, A. Challenges and opportunities with drone-mounted GPR. In Proceedings of the First International Meeting for Applied Geoscience & Energy, 2021; pp. 3043-3047.
467. Linna, P.; Halla, A.; Narra, N. Ground-penetrating radar-mounted drones in agriculture. In Proceedings of the New Developments and Environmental Applications of Drones: Proceedings of FinDrones 2020, 2022; pp. 139-156.
468. Molina, C.M.; Wisniewski, K.D.; Salamanca, A.; Saumett, M.; Rojas, C.; Gómez, H.; Baena, A.; Pringle, J.K. Monitoring of simulated clandestine graves of victims using UAVs, GPR, electrical tomography and conductivity over 4-8 years post-burial to aid forensic search investigators in Colombia, South America. *Forensic Science International* **2024**, *355*, 111919.
469. Guan, S.; Zhu, Z.; Wang, G. A review on UAV-based remote sensing technologies for construction and civil applications. *Drones* **2022**, *6*, 117.
470. Zhou, W.; Chen, F.; Guo, H.; Hu, M.; Li, Q.; Tang, P.; Zheng, W.; Liu, J.a.; Luo, R.; Yan, K. UAV Laser scanning technology: A potential cost-effective tool for micro-topography detection over wooded areas for archaeological prospection. *International Journal of Digital Earth* **2020**, *13*, 1279-1301.
471. Riemersma, G. Improving UAV LiDAR survey accuracy using Ground Control Targets. Available online: https://www.routescene.com/resources/ground-control-targets-for-uav-lidar-accuracy/#:~:text=Setting%20Ground%20Control%20Points%20(GCP,the%20accuracy%20of%20the%20survey. (accessed on January 10).
472. Ravi, R.; Shamseldin, T.; Elbahnasawy, M.; Lin, Y.-J.; Habib, A. Bias impact analysis and calibration of UAV-based mobile LiDAR system with spinning multi-beam laser scanner. *Applied Sciences* **2018**, *8*, 297.

473. Del Savio, A.A.; Luna Torres, A.; Chicchón Apaza, M.A.; Vergara Olivera, M.A.; Llimpe Rojas, S.R.; Urday Ibarra, G.T.; Reyes Ñique, J.L.; Macedo Arevalo, R.I. Integrating a LiDAR Sensor in a UAV Platform to Obtain a Georeferenced Point Cloud. *Applied Sciences* **2022**, *12*, 12838.
474. Fernandez-Diaz, J.C.; Carter, W.E.; Shrestha, R.L.; Glennie, C.L. Now you see it… now you don't: Understanding airborne mapping LiDAR collection and data product generation for archaeological research in Mesoamerica. *Remote Sensing* **2014**, *6*, 9951-10001.
475. Abediasl, H.; Hashemi, H. Monolithic optical phased-array transceiver in a standard SOI CMOS process. *Optics express* **2015**, *23*, 6509-6519.
476. Habib, A.; Bang, K.I.; Kersting, A.P.; Chow, J. Alternative methodologies for LiDAR system calibration. *Remote Sensing* **2010**, *2*, 874-907.
477. Kaňuk, J.; Gallay, M.; Eck, C.; Zgraggen, C.; Dvorný, E. Technical report: unmanned helicopter solution for survey-grade LiDAR and hyperspectral mapping. *Pure and Applied Geophysics* **2018**, *175*, 3357-3373.
478. Meng, X.; Currit, N.; Zhao, K. Ground filtering algorithms for airborne LiDAR data: A review of critical issues. *Remote Sensing* **2010**, *2*, 833-860.
479. Chen, Z.; Gao, B.; Devereux, B. State-of-the-art: DTM generation using airborne LIDAR data. *Sensors* **2017**, *17*, 150.
480. Chang, K.-J.; Hsieh, Y.-C.; Chan, Y.-C.; Huang, M.-J. UAS LiDAR data processing, quality assessment and geosciences prospects. In Proceedings of the Geophysical Research Abstracts, 2019.
481. VanValkenburgh, P.; Cushman, K.; Butters, L.J.C.; Vega, C.R.; Roberts, C.B.; Kepler, C.; Kellner, J. Lasers without lost cities: Using drone lidar to capture architectural complexity at Kuelap, Amazonas, Peru. *Journal of Field Archaeology* **2020**, *45*, S75-S88.
482. MacDonell, C.J.; Williams, R.D.; Maniatis, G.; Roberts, K.; Naylor, M. Consumer-grade UAV solid-state LiDAR accurately quantifies topography in a vegetated fluvial environment. *Earth Surface Processes and Landforms* **2023**, *48*, 2211-2229.
483. Demers, M. *UAV Magnetic and Lidar surveys on the Miakadow Property*; Eagle Geosciences: October 12 2021.
484. Esin, A.İ.; Akgul, M.; Akay, A.O.; Yurtseven, H. Comparison of LiDAR-based morphometric analysis of a drainage basin with results obtained from UAV, TOPO, ASTER and SRTM-based DEMs. *Arabian Journal of Geosciences* **2021**, *14*, 1-15.
485. Luo, D.; Lin, H.; Jin, Z.; Zheng, H.; Song, Y.; Feng, L.; Guo, Q. Applications of UAV digital aerial photogrammetry and LiDAR in geomorphology and land cover research. *Journal of Earth Environment* **2019**, *10*, 213-226.
486. Finley, T.; Salomon, G.; Nissen, E.; Stephen, R.; Cassidy, J.; Menounos, B. Preliminary results and structural interpretations from drone lidar surveys over the Eastern Denali fault, Yukon. *Yukon Exploration and Geology* **2021**, 83-105.
487. Using UAV LiDAR mapping to monitor landslides safely. Available online: https://www.routescene.com/case-studies/uav-lidar-mapping-landslides-safely/ (accessed on April 28).
488. Jones, L.; Hobbs, P. The application of terrestrial LiDAR for geohazard mapping, monitoring and modelling in the British Geological Survey. *Remote Sensing* **2021**, *13*, 395.
489. Liu, C.; Li, W.; Lei, W.; Liu, L.; Wu, H. Architecture planning and geo-disasters assessment mapping of landslide by using airborne LiDAR data and UAV images. In Proceedings of the International Symposium on Lidar and Radar Mapping 2011: Technologies and Applications, 2011; pp. 468-474.
490. Casagli, N.; Frodella, W.; Morelli, S.; Tofani, V.; Ciampalini, A.; Intrieri, E.; Raspini, F.; Rossi, G.; Tanteri, L.; Lu, P. Spaceborne, UAV and ground-based remote sensing techniques for landslide mapping, monitoring and early warning. *Geoenvironmental Disasters* **2017**, *4*, 1-23.
491. Kowalski, A.; Wajs, J.; Kasza, D. MONITORING OF ANTHROPOGENIC LANDSLIDE ACTIVITY WITH COMBINED UAV AND LIDAR-DERIVED DEMS-A CASE STUDY OF THE CZERWONY WAWOZ LANDSLIDE (SW POLAND, WESTERN SUDETES). *Acta Geodynamica et Geromaterialia* **2018**, *15*, 117-130.
492. Hussain, Y.; Schlögel, R.; Innocenti, A.; Hamza, O.; Iannucci, R.; Martino, S.; Havenith, H.-B. Review on the geophysical and UAV-based methods applied to landslides. *Remote Sensing* **2022**, *14*, 4564.
493. França Pereira, F.; Sussel Gonçalves Mendes, T.; Jorge Coelho Simões, S.; Roberto Magalhães de Andrade, M.; Luiz Lopes Reiss, M.; Fortes Cavalcante Renk, J.; Correia da Silva Santos, T. Comparison of LiDAR-and UAV-derived data for landslide susceptibility mapping using Random Forest algorithm. *Landslides* **2023**, *20*, 579-600.
494. Petrovič, D.; Kozmus Trajkovski, K.; Grigillo, D. Use of LiDAR drone data for O-mapping and change detection in mountainous areas. *Abstracts of the ICA* **2023**, *6*, 200.
495. Wang, K.; Yao, L.; Lin, J. Ground Surface Deformation Detection from Far Satellite SAR to UAV LiDAR and Terrestrial Lidar. In Proceedings of the 5th Asia Pacific Meeting on Near Surface Geoscience & Engineering, 2023; pp. 1-5.
496. Yongting, Z.; Youning, X.; Wei, L.; Caiyong, W.; Qiaomin, L.; Xueru, Y.; Jianhong, B. Technical methods for colliery subsidence disaster monitoring using UAV LiDAR: a case study of the Maliantai colliery, Ningdong coal base, Ningxia. *Geological Bulletin of China* **2018**, *37*, 2270-2277.

497. Jóźków, G.; Walicka, A.; Borkowski, A. Monitoring terrain deformations caused by underground mining using UAV data. *The International Archives of the Photogrammetry, Remote Sensing and Spatial Information Sciences* **2021**, *43*, 737-744.
498. Dong, Y.; Wang, D.; Liu, F.; Wang, J. A new data processing method for high-precision mining subsidence measurement using airborne LiDAR. *Frontiers in Earth Science* **2022**, *10*, 858050.
499. Yang, Q.; Tang, F.; Wang, F.; Tang, J.; Fan, Z.; Ma, T.; Su, Y.; Xue, J. A new technical pathway for extracting high accuracy surface deformation information in coal mining areas using UAV LiDAR data: An example from the Yushen mining area in western China. *Measurement* **2023**, *218*, 113220.
500. An, S.; Yuan, L.; Xu, Y.; Wang, X.; Zhou, D. Ground subsidence monitoring in based on UAV-LiDAR technology: a case study of a mine in the Ordos, China. *Geomechanics and Geophysics for Geo-Energy and Geo-Resources* **2024**, *10*, 57.
501. Abellán, A.; Oppikofer, T.; Jaboyedoff, M.; Rosser, N.J.; Lim, M.; Lato, M.J. Terrestrial laser scanning of rock slope instabilities. *Earth surface processes and landforms* **2014**, *39*, 80-97.
502. Akturk, E.; Altunel, A.O. Accuracy assessment of a low-cost UAV derived digital elevation model (DEM) in a highly broken and vegetated terrain. *Measurement* **2019**, *136*, 382-386.
503. Sturzenegger, M.; Willms, D.; Pate, K.; Johnston, B. Experience using terrestrial remote sensing techniques for rock slope performance assessment. In Proceedings of the Slope Stability 2013: Proceedings of the 2013 International Symposium on Slope Stability in Open Pit Mining and Civil Engineering, 2013; pp. 775-782.
504. Fernández-Lozano, J.; Gutiérrez-Alonso, G. The use of UAVs (unmanned air vehicles) in geology. In Proceedings of the Conference Paper. Available at: The Future of Mining in South Africa: Sunset or Sunrise, 2016.
505. Lin, M.-L.; Chen, Y.-C.; Tseng, Y.-H.; Chang, K.-J.; Wang, K.-L. Investigation of geological structures using UAV LiDAR and its effects on the failure mechanism of deep-seated landslide in Lantai Area, Taiwan. *Applied Sciences* **2021**, *11*, 10052.
506. Application of UAV Lidar in Mining Survey. Available online: https://www.dronefromchina.com/new/Application-of-UAV-Lidar-in-Mining-Survey.html
507. Li, T.; Zhang, B.; Xiao, W.; Cheng, X.; Li, Z.; Zhao, J. UAV-based photogrammetry and LiDAR for the characterization of ice morphology evolution. *IEEE Journal of Selected Topics in Applied Earth Observations and Remote Sensing* **2020**, *13*, 4188-4199.
508. García-López, S.; Vélez-Nicolás, M.; Zarandona-Palacio, P.; Curcio, A.; Ruiz-Ortiz, V.; Barbero, L. UAV-borne LiDAR revolutionizing groundwater level mapping. *Science of the Total Environment* **2023**, *859*, 160272.
509. Du, M.; Li, H.; Roshanianfard, A. Design and experimental study on an innovative UAV-LiDAR topographic mapping system for precision land levelling. *Drones* **2022**, *6*, 403.
510. James, M.R.; Carr, B.; D'Arcy, F.; Diefenbach, A.; Dietterich, H.; Fornaciai, A.; Lev, E.; Liu, E.; Pieri, D.; Rodgers, M. Volcanological applications of unoccupied aircraft systems (UAS): Developments, strategies, and future challenges. *Volcanica* **2020**, *3*, 67-114.
511. Chen, Z.; Chen, Y.; Shi, T.; Chen, X.; Pan, X.; Lei, J.; Wu, T.; Li, Y.; Liu, Q.; Liu, X. Estimation of Soil Organic Carbon in Tropical Rainforest Regions by Combining Uav Hyperspectral and Lidar Data. *Available at SSRN 4547030*.
512. Pouladi, N.; Gholizadeh, A.; Khosravi, V.; Borůvka, L. Digital mapping of soil organic carbon using remote sensing data: A systematic review. *Catena* **2023**, *232*, 107409.
513. Rey, J.; Martínez, J.; Mendoza, R.; Hidalgo, C.; Florez Rodríguez, C. Combining Geophysical Techniques (Eri, Ip, Tdem and Gpr) for the Characterization of Mining Waste. *Available at SSRN 4127252*.
514. Oliveira, R.J.; Caldeira, B.; Teixidó, T.; Borges, J.F.; Bezzeghoud, M. Geophysical data fusion of ground-penetrating radar and magnetic datasets using 2D wavelet transform and singular value decomposition. *Frontiers in Earth Science* **2022**, *10*, 1011999.
515. Ghezzi, A. A New Approach to data integration in Archaeological Geophysics. **2020**.
516. Khalil, M.H.; Hassan, N.A. Ground magnetic, GPR, and dipole-dipole resistivity for landfill investigation. *International Journal of Geosciences* **2016**, *7*, 828.
517. Ukaegbu, I.K.; Gamage, K.A.; Aspinall, M.D. Integration of Ground-Penetrating Radar and Gamma-Ray Detectors for Nonintrusive Characterisation of Buried Radioactive Objects. *Sensors* **2019**, *19*, 2743.
518. Coelho, B.Z.; Karaoulis, M. Data fusion of geotechnical and geophysical data for three-dimensional subsoil schematisations. *Advanced Engineering Informatics* **2022**, *53*, 101671.
519. Tian, G.; Shaikh, S.A.; Lizan, A.; Chen, R.; Wang, Y. Geophysical Data Fusions for Resolution Improvement. In Proceedings of the International Conference on Engineering Geophysics, Al Ain, United Arab Emirates, 15-18 November 2015, 2015; pp. 42-42.
520. Grandjean, G.; Malet, J.-P.; Bitri, A.; Méric, O. Geophysical data fusion by fuzzy logic for imaging the mechanical behaviour of mudslides. *Bulletin de la société géologique de France* **2007**, *178*, 127-136.
521. Casa, R.; Castaldi, F.; Pascucci, S.; Basso, B.; Pignatti, S. Geophysical and hyperspectral data fusion techniques for in-field estimation of soil properties. *Vadose Zone Journal* **2013**, *12*, vzj2012. 0201.

522. Bakuła, K.; Lejzerowicz, A.; Pilarska-Mazurek, M.; Ostrowski, W.; Górka, J.; Biernat, P.; Czernic, P.; Załęgowski, K.; Kleszczewska, K.W.; Węzka, K. Sensor integration and application of low-sized mobile mapping platform equipped with lidar, gpr and photogrammetric sensors. *The International Archives of the Photogrammetry, Remote Sensing and Spatial Information Sciences* **2022**, *43*.
523. Zhang, D.; Wu, Z.; Shi, D.; Li, J.; Lu, Y. Integration of Terrestrial Laser Scanner (TLS) and Ground Penetrating Radar (GPR) to Characterize the Three-Dimensional (3D) Geometry of the Maoyaba Segment of the Litang Fault, Southeastern Tibetan Plateau. *Remote Sensing* **2022**, *14*, 6394.
524. Lv, P.; Xue, G.; Chen, W.; Song, W. Application of the transfer learning method in multisource geophysical data fusion. *Journal of Geophysics and Engineering* **2023**, *20*, 361-375.
525. Afshar, A.; Norouzi, G.; Moradzadeh, A.; Riahi, M.; Porkhial, S. Curie point depth, geothermal gradient and heat-flow estimation and geothermal anomaly exploration from integrated analysis of aeromagnetic and gravity data on the Sabalan Area, NW Iran. *Pure and Applied Geophysics* **2017**, *174*, 1133-1152.
526. Olierook, H.K.; Scalzo, R.; Kohn, D.; Chandra, R.; Farahbakhsh, E.; Clark, C.; Reddy, S.M.; Müller, R.D. Bayesian geological and geophysical data fusion for the construction and uncertainty quantification of 3D geological models. *Geoscience Frontiers* **2021**, *12*, 479-493.
527. Kuras, A.; Heincke, B.H.; Salehi, S.; Mielke, C.; Köllner, N.; Rogass, C.; Altenberger, U.; Burud, I. Integration of Hyperspectral and Magnetic Data for Geological Characterization of the Niaqornarssuit Ultramafic Complex in West-Greenland. *Remote Sensing* **2022**, *14*, 4877.
528. Leblanc, G.; Lee, M.; Morris, W. A simple adaptable data fusion methodology for geophysical exploration. *Exploration Geophysics* **2012**, *43*, 190-197.
529. Lamri, T.; Djemaï, S.; Hamoudi, M.; Zoheir, B.; Bendaoud, A.; Ouzegane, K.; Amara, M. Satellite imagery and airborne geophysics for geologic mapping of the Edembo area, Eastern Hoggar (Algerian Sahara). *Journal of African Earth Sciences* **2016**, *115*, 143-158.
530. Honarmand, M. Application of airborne geophysical and ASTER data for hydrothermal alteration mapping in the Sar-Kuh Porphyry Copper Area, Kerman Province, Iran. *Open Journal of Geology* **2016**, *6*, 1257-1268.
531. Agapiou, A.; Lysandrou, V.; Sarris, A.; Papadopoulos, N.; Hadjimitsis, D.G. Fusion of satellite multispectral images based on ground-penetrating radar (GPR) data for the investigation of buried concealed archaeological remains. *Geosciences* **2017**, *7*, 40.
532. Jackisch, R. Drone-based Integration of Hyperspectral Imaging and Magnetics for Mineral Exploration. **2022**.
533. Martelet, G.; Gloaguen, E.; Døssing, A.; Lima Simoes da Silva, E.; Linde, J.; Rasmussen, T.M. Airborne/UAV multisensor surveys enhance the geological mapping and 3d model of a pseudo-skarn deposit in Ploumanac'h, French Brittany. *Minerals* **2021**, *11*, 1259.
534. Ronchi, D.; Limongiello, M.; Demetrescu, E.; Ferdani, D. Multispectral UAV Data and GPR Survey for Archeological Anomaly Detection Supporting 3D Reconstruction. *Sensors* **2023**, *23*, 2769.
535. Lee, J.; Lee, H.; Ko, S.; Ji, D.; Hyeon, J. Modeling and Implementation of a Joint Airborne Ground Penetrating Radar and Magnetometer System for Landmine Detection. *Remote Sensing* **2023**, *15*, 3813.
536. Masini, N.; Sogliani, F.; Sileo, M.; Abate, N.; Danese, M.; Vitale, V.; Lasaponara, R.; Piro, S. Fusion and integration of heterogeneous close range remote sensing and geophysical data. The case of Grumentum. In Proceedings of the Journal of Physics: Conference Series, 2022; p. 012018.
537. Drone-Based Magnetic and Electromagnetic Measurements in Sweden: A Few Case Studies. Available online: https://seg.org/calendar_events/drone-based-magnetic-and-electromagnetic-measurements-in-sweden-a-few-case-studies/
538. Mu, Y.; Xie, W.; Zhang, X. The joint UAV-borne magnetic detection system and cart-mounted time domain electromagnetic system for UXO detection. *Remote Sensing* **2021**, *13*, 2343.
539. Šašak, J.; Gallay, M.; Kaňuk, J.; Hofierka, J.; Minár, J. Combined use of terrestrial laser scanning and UAV photogrammetry in mapping alpine terrain. *Remote Sensing* **2019**, *11*, 2154.
540. Mao, Z.; Hu, S.; Wang, N.; Long, Y. Precision evaluation and fusion of topographic data based on UAVs and TLS surveys of a loess landslide. *Frontiers in Earth Science* **2021**, *9*, 801293.
541. Sankey, J.B.; Sankey, T.T.; Li, J.; Ravi, S.; Wang, G.; Caster, J.; Kasprak, A. Quantifying plant-soil-nutrient dynamics in rangelands: Fusion of UAV hyperspectral-LiDAR, UAV multispectral-photogrammetry, and ground-based LiDAR-digital photography in a shrub-encroached desert grassland. *Remote Sensing of Environment* **2021**, *253*, 112223.
542. Guan, Y.; Grote, K. Assessing the Potential of UAV-Based Multispectral and Thermal Data to Estimate Soil Water Content Using Geophysical Methods. *Remote Sensing* **2023**, *16*, 61.

543. Blanco-Sacristán, J.; Panigada, C.; Gentili, R.; Tagliabue, G.; Garzonio, R.; Martín, M.P.; Ladron de Guevara, M.; Colombo, R.; Dowling, T.P.; Rossini, M. UAV RGB, thermal infrared and multispectral imagery used to investigate the control of terrain on the spatial distribution of dryland biocrust. *Earth Surface Processes and Landforms* **2021**, *46*, 2466-2484.
544. Laugier, E.J.; Casana, J. Integrating satellite, UAV, and ground-based remote sensing in archaeology: An exploration of pre-modern land use in Northeastern Iraq. *Remote Sensing* **2021**, *13*, 5119.